İlke Güntan

Characterisation of Circadian Dynamics of the Transcription Factor Zbtb14 in Naïve and Epileptic Mice

PhD thesis
Completed in the Laboratory of Epileptogenesis
of the Nencki Institute of Experimental Biology
Polish Academy of Sciences

SUPERVISOR:
Prof. dr hab. Katarzyna Łukasiuk

Warsaw, 2023

This study has received funding from the European Union's Horizon 2020 research and innovation programme under the Marie Skłodowska-Curie COFUND grant agreement no 665735 and Polish National Research Centre grant Harmonia agreement no UMO-2015/18/M/NZ3/00779.

ACKNOWLEDGEMENTS

First and foremost, I would like to thank my supervisor, prof. dr hab. Katarzyna Łukasiuk for her mentorship, support, and advice – this work would not have been possible to complete without her. I have learned a lot from her profound experiences on both academic and personal levels throughout my doctoral degree.

I would like to express my sincere thanks to Epileptogenesis lab members: dr Małgorzata Górniak-Walas, who taught the most techniques I used in this work; dr Anna Gręda, your friendship and moral and intellectual support meant the world to me; dr Kinga Szydłowska, thank you for the movie nights, good food and good science; dr Dorota Nowicka, her humor, cat support and expertise in immunofluorescence helped me and improved my work; dr Karolina Nizińska who shared her in silico results with me; MSc Kinga Nazaruk, thank you for being my friend and a colleague that I want to see every day; MSc Maciej Olszewski, thank you for your technical support when I need. I also thank dr Bernard Christophe and his team for providing epileptic animal tissue for this project.

I expand my thanks to TREND lab members who supported me last six months of my study: dr Ismail Gbadamosi, MSc Magdalena Gomółka, dr Izabela Lepiarz-Raba, MSc Weronika Tomaszewska, MSc Patrycja Rojek, MSc Taufik Hidayat, MSc Lena Majchrowicz, and finally head of the TREND lab dr Ali Jawaid. Your support, friendship, and warm smiles kept me going while writing this work.

I would like to thank my dear friends Sibel Sökel, Özlem Dinçsoy, Hanan Farahat, Zuhal Bektaş, Tuğba Duran, Alexandra Malatskovskaya, Maja Wieczorkowska, and Hafsa Jabeen for their great mental support, and encouragement.

Finally, I would like to thank my family: my parents, Fatma Yücel Güntan and Zafer Güntan, for supporting me in every way possible to achieve my dreams; my little sister Asli Güntan for always being there for me when I needed; my extended family Ewa Stańczyk, Paweł Stańczyk, Aleksandra Stańczyk, Sylwia Szwiec, Łukasz Szwiec, Jarosław Stańczyk, and Gabriela Stańczyk who supported me and welcomed me to their family; and lastly to my husband Przemysław Stańczyk, your support in every way possible meant everything to me.

October , 2023
İlke GÜNTAN

TABLE OF CONTENTS

LIST OF ABBREVIATIONS

Alv	Alveus of the hippocampus
BMAL1	Brain muscle aryl hydrocarbon receptor nuclear translocator-like 1
BTB/POZ	Broad-complex, tramtrack and bric-a-brac/poxvirus
CA	Cornu ammonis
CA1 Py	Pyramidal layer of CA1
CA2 Py	Pyramidal layer of CA2
CA3 Py	Pyramidal layer of CA3
cc	corpus callosum
CLOCK	Circadian locomotor output cycle kaput
CNS	Central nervous system
CRY 1/2	Cryptochrome 1/2
DG	Dentate gyrus
DNA	Deoxyribonucleic acid
DTT	Dithiothreitol
E-box	Enhancer box
ECL	Enhanced chemiluminescence
GABA	Gamma-aminobutyric acid
GFAP	Glial fibrillary acidic protein
GLUT4	Glucose transporter type 4
GrDG	Granular layer of the dentate gyrus
HC	Hippocampus
hDAT	Human dopamine transporter
hFMR1	Human fragile X messenger ribonucleoprotein 1
hLIF	Human leukemia inhibitory factor
HPA	Hypothalamic-pituitary-adrenal
IB	Immunoblot
IP	Immunoprecipitation
KEGG	Kyoto encyclopedia of genes and genomes
KPB	Potassium phosphate buffer
MBD3	Methyl-CpG binding domain protein 3
Mol	Molecular layer of the dentate gyrus
mRNA	Messenger RNA
mTLE	Medial temporal lobe epilepsy
NeuN	Hexaribonucleotide binding protein 3
NGS	Normal goat serum
NHS	Normal horse serum
NLS	Nuclear localisation complex

NMDA	N-methyl D-aspartate
NPC	Nuclear pore complex
NR1D1	Nuclear receptor subfamily 1 group D member 1
NR1D2	Nuclear receptor subfamily 1 group D member 2
Or	Oriens layer of the hippocampus
PB	Sodium phosphate buffer
PBS	Phosphate buffered saline
PER 1/2/3	Period 1/2/3
PFA	Paraformaldehyde
PMBCs	Peripheral blood mononuclear cells
Rad	Stratum radiatum of the hippocampus
RHT	Retinohypothalamic tract
RNA	Ribonucleic acid
RORα	Retinoic acid receptor-related orphan receptor alpha
RRE	REV response element
SCN	Suprachiasmatic nucleus
SDS-PAGE	Sodium dodecyl sulfate polyacrylamide gel
SGZ	Subgranular zone
shRNA	Short hairpin RNA
SLu	Stratum lucidum
SUMO	Small ubiquitin-related modifier
TCS	Tissue collection solution
TLE	Temporal lobe epilepsy
tRNA	Transfer RNA
TTFL	Transcriptional and translational feedback loops
WB	Western blot
WHO	World Health Organization
Zbtb	Broad-complex, tramtrack and bric-a-brac/poxvirus and zinc-finger
ZF	Zinc finger

ABSTRACT

While the relationship between epilepsy and circadian dysregulation is known, we know very little about circadian oscillations of the transcription factors which are responsible from modulating the gene expression in health and disease pathologies. This study aims to characterise circadian dynamics of one of the identified and prominent transcription factors in epilepsy – the Zbtb14.

In pursuit of this objective, protein rhythmicity of the Zbtb14 is observed in the ventral and dorsal hippocampus and the somatosensory cortex using immunochemistry, and in cytoplasmic and nuclear protein extracts of the hippocampus using western blot. The downregulated genes with ZF5 motif in their promoters identified in an in vitro model of epileptiform discharges is characterised. Zbtb14 protein expression is investigated in two time points in an *in vivo* model of epilepsy model.

The study showed that Zbtb14 protein only has a rhythmic expression in the ventral hippocampus but not in the dorsal hippocampus and the somatosensory cortex. Additionally, the cytoplasmic and nuclear dynamics of the Zbtb14 protein are different. I identified the downregulated genes in *in vitro* model of epileptiform discharges are mainly responsible from synaptic plasticity and transmission. Furthermore, the epilepsy pathology affected the Zbtb14 transcription factor expression in a time-dependent manner. My research shows that the studies on circadian regulations of the transcription factors can be beneficial target to unravel the disease pathologies and potential therapeutics.

Keywords: Zbtb14, epilepsy, hippocampus, circadian rhythm, chronotherapy

STRESZCZENIE

Chociaż związek między padaczką a deregulacją cyklu okołodobowego jest znany, wiemy bardzo niewiele o okołodobowych oscylacjach poziomów czynników transkrypcyjnych, które są odpowiedzialne za modulowanie ekspresji genów w padaczce. Niniejsze badanie miało na celu scharakteryzowanie dynamiki okołodobowej czynnika transkrypcyjnego Zbtb14, który był zidentyfikowany przez nas zespół jako potencjalnie ważny w patologii padaczki.

W ramach projektu zbadano poziomy i lokalizację białka Zbtb14 w brzusznym i grzbietowym hipokampie oraz korze somatosensorycznej przy użyciu immunohistochemii, a także poziomy Zbtb14 we frakcjach cytoplazmatycznej i jądrowej hipokampa przy użyciu Western blot. Scharakteryzowano in silico promotory genów o obniżonym poziomie ekspresji w modelu wyładowań padaczkowych *in vitro*. Ponadto zbadano ekspresję białka Zbtb14 w dwóch punktach czasowych w cyklu okołodobowym w modelu padaczki *in vivo*.

Badanie wykazało, że białko Zbtb14 wykazuje rytmiczną ekspresję tylko w hipokampie brzusznym, ale nie w hipokampie grzbietowym i korze somatosensorycznej. Dodatkowo, dynamika zmian poziomów białka Zbtb14 cytoplazmie i jądrze jest różna. Stwierdzono, że promotory genów o obniżonym poziomie ekspresji w modelu wyładowań padaczkowych *in vitro* charakteryzują się obecnością miejsca wiązania czynnika transkrypcyjnego Zbtb14, a ich produkty biorą udział w plastyczności i transmisji synaptycznej. Ponadto, padaczka wpływała na ekspresję czynnika transkrypcyjnego Zbtb14 w sposób zależny od cyklu okołodobowego. Moje badania pokazują, że badania okołodobowej regulacji czynników transkrypcyjnych mogą być wykorzystane w odkrywaniu mechanizmów choroby i potencjalnych celów terapeutycznych.

Słowa kluczowe: Zbtb14, padaczka, hipokamp, rytm okołodobowy, chronoterapia

CHAPTER 1

INTRODUCTION

1.1 Circadian rhythm

Life on Earth has evolved to follow the constantly repeating 24-hour day-night cycle called the circadian cycle. The name “circadian” originates from the Latin words “circa” and “diem” and means “about a day,” respectively (Vitaterna et al., 2001). The circadian cycle is crucial for the entrainment of the self-regulated endogenous clock of organisms, which creates the circadian rhythm within the organism. This entrainment occurs via cues called “zeitgebers,” a German word that translates to “time givers.” A zeitgeber can be a temperature change or an activity; however, the most robust zeitgeber is light (Redfern et al., 1991). The circadian rhythm plays an essential role in regulating the physiology and behaviour of organisms to adapt to the outside world (Hastings et al., 2018).

In mammals, the light cue entrains the central circadian rhythm regulator suprachiasmatic nucleus (SCN) through the retinohypothalamic tract (RHT) in the brain. The SCN attunes other brain areas, such as the hippocampus, hypothalamus, brain stem, and peripheral organs (Hastings et al., 2018; von Gall, 2022). Circadian rhythm regulation occurs via several transcriptional and translational feedback loops (TTFLs) of core clock genes. Simply, the core loop starts by heterodimerisation of brain muscle aryl hydrocarbon receptor nuclear translocator-like 1 (BMAL1 or ARNTL) and circadian locomotor output cycle kaput (CLOCK), and the BMAL1-CLOCK protein complex activates the transcription of other core clock genes, including *Per* and *Cry,* by binding their respective enhancer boxes (E-boxes). Period (PER 1/2/3) and cryptochrome (CRY 1/2) proteins form dimers and accumulate in the nucleus. When PER-CRY dimers reach a

certain threshold, they diminish their own transcription by disabling the BMAL1-CLOCK complex to bind their respective E-boxes. Inevitably, the reduction in PER and CRY protein level and the core loop start again. An additional TTFL controls the transcription of BMAL1. The BMAL1-CLOCK complex also activates the transcription of retinoic acid receptor-related orphan receptor alpha (*Rorα*), nuclear receptor subfamily 1 group d member 1 (*Nr1d1* or *Rev-Erbα*), and nuclear receptor subfamily 1 group d member 2 (*Nr1d2* or *Rev-Erb*β) by binding their respective E-boxes. While RORα is a positive regulator of *Bmal1* gene transcription, NR1D1 and NR1D2 suppress Bmal1 expression. RORα, NR1D1, and NR1D2 control Bmal1 expression by binding its REV response element (RRE) (Figure 1.1). These TTFLs of core clock genes regulate the expression of other clock-controlled genes and create a circadian rhythm that is approximately 24 hours within the brain and periphery (Hastings et al., 2018; Hetman et al., 2022; Leite Góes Gitai et al., 2019; Schurhoff & Toborek, 2023; Vitaterna et al., 2001; von Gall, 2022).

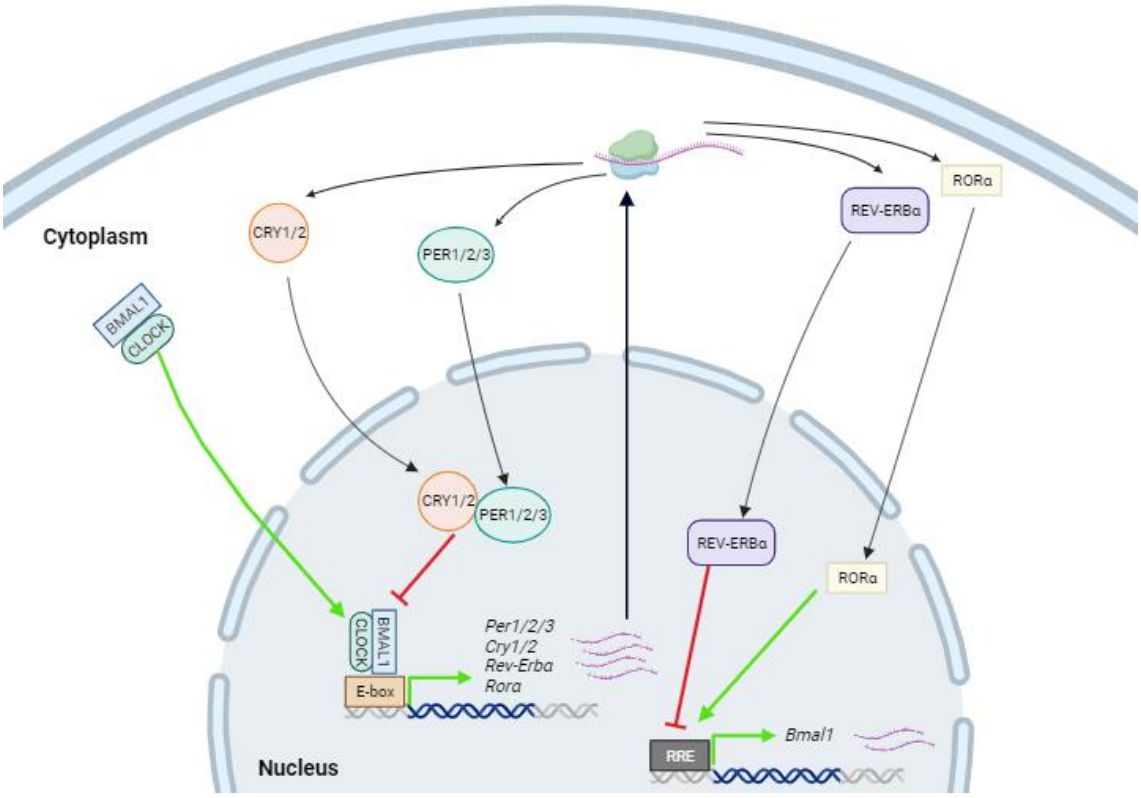

Figure 1.1 A general schematics of regulation of core clock genes and proteins. The cycle starts with binding of BMAL1 and CLOCK heterodimer to the E-box of *Per*, *Cry*, *Rev-Erbα* and *Rorα* genes. Translation of *Per*, *Cry*, *Rev-Erbα* and *Rorα* mRNAs creates a negative feedback loop on transcription of *Bmal1* gene and hence BMAL1 protein level decreases. Additionally, CRY and PER heterodimer represses the heterodimerisation of BMAL1 and

CLOCK proteins. In the scheme, the green arrows represent activation, the red lines represent inhibition and black arrows represents the direction of the proteins or mRNAs that are being translocated. BMAL1, brain muscle aryl hydrocarbon receptor nuclear translocator-like 1; CLOCK, circadian locomotor output cycle kaput; CRY, cryptochrome; E-box, enhancer box; PER, Period; REV-ERBα nuclear receptor subfamily 1 group d member 1; REV-ERBβ, nuclear receptor subfamily 1 group d member 2; RORα, retinoic acid receptor-related orphan receptor alpha; RRE, REV response element. Created in Biorender.com.

In a detailed circadian-regulated gene expression study (Mure et al., 2018), the researchers collected 64 tissue samples from a baboon species (*Papio anubis*) every two hours over the circadian cycle. They showed that more than 65% of all transcripts displayed a circadian rhythm of ~24 hours, and the transcriptome oscillations were tissue-specific, as observed in model organisms such as mice and fruit flies. Mure et al. (2018) reported that the expression of core clock genes (*Bmal1*, *Clock*, *Per1/2*, *Cry1-3*, *Rorα*, and *Nr1d1/2*) had a unique pattern depending on the baboon tissues, but they were expressed in all of the tissues collected.

Dysregulation in circadian-regulated genes depicts how interdependent the relationship between regulating circadian rhythm and human physiology is. There are numerous studies on disrupted circadian rhythm and its effect on various diseases ranging from sleep disorders (Hirano et al., 2016; Patke et al., 2017) and weak immune system (Edgar et al., 2016; Kiessling et al., 2017) to neurodegenerative diseases (Holth et al., 2019; Stevanovic et al., 2017) and epilepsies (Debski et al., 2020; Grigg-Damberger & Foldvary-Schaefer, 2021; Moore et al., 2021; Rocha et al., 2016; Roliz & Kothare, 2022). Shiftwork and jetlag illustrate how much, even as simple as light exposure at night, influences the transcription and translation of clock-controlled genes. For example, light exposure at night in shiftworkers has been shown to reduce melatonin levels (Razavi et al., 2019), and it has been reported that increased melatonin levels are associated with a rise in *Rorα* mRNA levels (Li et al., 2020). RORα is a core clock transcription factor that increases *Bmal1* expression, and BMAL1 increases *Per1* and *Per2* expression (Hastings et al., 2018; Leite Góes Gitai et al., 2019). Li and colleagues (2020) showed that a decrease in BMAL1 and PER1/2 levels diminished GLUT4 expression levels via the NAMPT/NAD^+/SIRT1 pathway and that a reduction in glucose transporter type 4 (GLUT4) can cause insulin resistance. Additionally, melatonin is responsible for browning white adipose tissue.

Hence, disruption in melatonin levels throughout the circadian cycle would increase insulin resistance and body weight (Cipolla-Neto et al., 2014).

The circadian-regulated gene expression study mentioned above by Mure et al. (2018) showed that the circadian rhythmicity pathway is the most common pathway detected for at least ten tissues out of 64 tissues investigated in the KEGG (Kyoto Encyclopedia of Genes and Genomes) biochemical pathway analysis from a baboon species, and other pathways that were enriched are related to DNA replication and repair, protein ubiquitination and energy metabolism-related pathways. Energy production in the brain is especially essential for neuronal activity. The literature shows that energy metabolism in the hippocampus changes in a time-of-day manner (Brancati et al., 2021; Debski et al., 2020) even within its own longitudinal axis (Brancati et al., 2021). Additionally, the same researchers revealed that the circadian rhythmicity of energy metabolism in the hippocampus was altered in an experimental epilepsy model (Brancati et al., 2021; Debski et al., 2020). These studies illustrate how essential circadian rhythmicity is to the well-being of organisms, from insects to humans. Arrhythmic circadian expression of genes and proteins affects disease pathologies, and disease pathologies affect the normal circadian rhythm.

1.2 Epilepsy

Epilepsy is one of the most prevalent neurological diseases in the world, with an estimated 50 million patients according to the World Health Organization (WHO). Epilepsy is not contagious and can affect people of all ages. Epilepsy can occur due to a concussion, inflammation of the brain, and brain malformations. Nevertheless, approximately half of the epilepsies have an unknown cause. However, there are several antiseizure medications available to control seizures, and approximately 30% of cases are refractory (https://www.who.int/news-room/fact-sheets/detail/epilepsy). Vagus nerve stimulation, dietary changes and surgery are among the treatment options for patients with drug-resistant epilepsies. However, they are not effective and available for all refractory epilepsy patients (Kossoff et al., 2015; Morris et al., 2013; Rugg-Gunn et al., 2020). Hence, there is an urgent need for new therapeutic strategies and agents.

Historically, epileptic seizures have been shown to follow a pattern rather than being random events by patient journals (Karoly et al., 2021). Recent technological advances have made tracking epileptic seizures easier, and the data are more available to researchers and healthcare providers. In a comprehensive study using two databases for human seizures by SeizureTracker and NeuroVista, the researchers found that 80% to 92% of the patients had 24-hour regulation of their seizures. While two-thirds of the NeuroVista had exactly a one-week cycle, one-sixth of the patients had biweekly cycles. Seven percent to 21% of SeizureTracker users displayed weekly rhythms, and 14% to 22% of the patients had seizure cycles that were longer than three weeks (Karoly et al., 2018). Additionally, it has been documented that the origin of seizures is correlated with a higher probability of seizure occurrence at certain times of the circadian cycle. For example, while focal seizures of the temporal lobe are associated with early morning and afternoon, focal seizures of the frontal lobe are linked to night hours (Re et al., 2020). In particular, juvenile myoclonic epilepsy, a genetically determined and common form of generalised epilepsy, and the sleep-wake cycle have been linked, and epileptic seizures frequently occur when transitioning into sleep or wakefulness in these patients (Gigli et al., 1992).

The clear connection between the daily, weekly, or even more extended periods of cycles in epileptic seizures opened a new area of research for scientists. Numerous studies on the core clock cycle and epilepsy support that they influence each other (Leite Góes Gitai et al., 2019; Li et al., 2017; Re et al., 2020; Rocha et al., 2016; Yue et al., 2020). Li and colleagues (2017) revealed that the CLOCK transcription factor is decreased in the brains of human patients with drug-resistant epilepsies. Researchers conditionally deleted the *Clock* gene in excitatory neurons of mice, and *Clock*-deficient neurons had defects in inhibition, increasing neuronal excitability (Li et al., 2017). Mechanistically, CLOCK binds to BMAL1 to start transcriptional and translational feedback loops of core clock genes. Another study demonstrated that *Bmal1*-knockout mice also have increased excitability in neurons and diminished seizure thresholds. They also showed that seizure thresholds changed in a time-of-day manner – higher at the first light-off time point – and that BMAL1 regulated seizure susceptibility at least partially (Gerstner et al., 2014). *RORα regulates bmal1 mRNA expression*, and Rocha et al. (2016) showed

that *Rorα* mRNA and protein levels were affected by the three phases of pilocarpine-induced temporal lobe epilepsy: acute [3 to 24 hours after status epilepticus (SE) induction], latent (5 days after SE), and chronic (2 months after SE). They observed that both mRNA and protein level of *Rorα* were significantly reduced in the hippocampus compared to control animals within the first 24 hours of SE induction, and in the latent phase, experimental animals continued to have lower mRNA and protein level of *Rorα* in the hippocampus (Rocha et al., 2016). Additionally, in the chronic phase, the authors observed that mRNA levels of *Rorα* did not change at any time point, and protein levels were affected only in the dentate gyrus of the hippocampus: the protein level of *Rorα* was increased at 10 pm (light off) compared to 10 am time-point (light on). When RORα protein level decreases, BMAL1 protein level also decreases. Hence, neuronal excitability increases, and the seizure threshold decreases (Gerstner et al., 2014). These results indicate the probable involvement of *Rorα* in epileptogenesis. (Rocha et al., 2016). In a different study, the authors reported that clock-regulated *Per1* mRNA and protein level were elevated in the hippocampus in response to the induction of acute seizures by kainic acid or electric convulsive shock (Eun et al., 2011). These studies emphasise that dysregulation of core clock genes alters seizure susceptibility in epilepsy by increasing excitability.

1.3 The role of the hippocampus in epilepsy and circadian rhythm

The hippocampus is a curved tube-shaped structure in the limbic lobe and a part of the medial temporal lobe (Pluta, 2021). Hippocampal formation includes the dentate gyrus, the cornu ammonis (CA; also known as the hippocampus proper), and the subiculum (Pluta, 2021; "StatPearls," 2023). Because the cornu ammonis and the dentate gyrus folded into each other halfway of their longitudinal axis during development, the cross-section of the hippocampus looks like a V-shaped structure hanging from the bottom of a C-shaped structure. The C-shaped structure is called the cornu ammonis and has three subfields: CA1, CA2, and CA3. CA1, CA2, and CA3 form a continuous pyramidal cell layer that follows the C-shape of the hippocampus proper. The principal cells in the cornu ammonis differ in soma size and connectivity depending on the subfield. The granular cell body layer folds around the CA3 subfield and creates the hanging V-shaped

structure: the dentate gyrus. The field between two blades of the granular cell layer is named the hilus (Figure 1.2) (Pluta, 2021; Spencer & Bland, 2019).

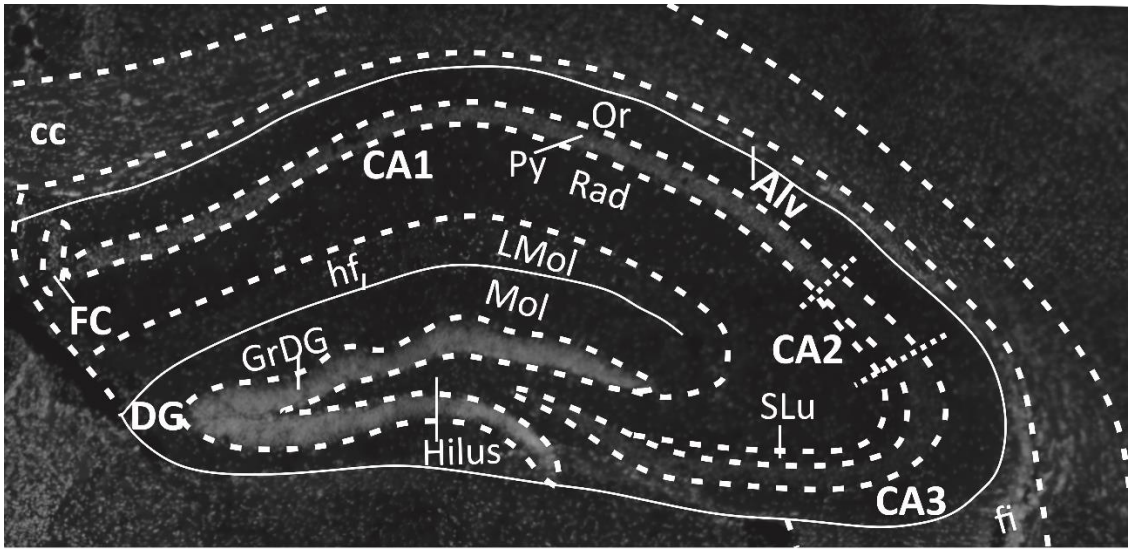

Figure 1.2 Anatomical features of the mice hippocampus. Alv, alveus of the hippocampus; CA1, field CA1 of hippocampus; CA2, field CA2 of hippocampus; CA3, field CA3 of hippocampus; cc, corpus callosum; DG, dentate gyrus; FC, fasciola cinereum; fi, fimbria of the hippocampus; GrDG, granular layer of the dentate gyrus; Hilus, also known as PoDG (polymorph layer of the dentate gyrus); LMol, lacunosum moleculare layer of the hippocampus; Mol, molecular layer of the dentate gyrus; Or, oriens layer of the hippocampus; Py, pyramidal cell layer of the hippocampus; Rad, stratum radiatum of the hippocampus; SLu, stratum lucidum, hippocampus (Franklin & Paxinos, 2008).

The hippocampus has been associated with memory, learning, and spatial navigation and has been linked to emotional and contextual memory and learning (Barr et al., 2017; Fanselow & Dong, 2010; Goosens, 2011; Moser & Moser, 1998; Scoville & Milner, 1957). Although there has been controversy over these seemingly two contradictory functions of the hippocampus, the recent literature has shown that cognitive- and affective-related functions of the hippocampus are a result of the heterogeneity of the hippocampus along its longitudinal axis (Barr et al., 2017; Bienkowski et al., 2018; Fanselow & Dong, 2010; Komorowski et al., 2013; Moser & Moser, 1998; O'Leary & Cryan, 2014). It has been shown that the dorsal pole of the hippocampus is differentially connected to the circuitry (Bienkowski et al., 2018), has different patterns of gene expression (Bienkowski et al., 2018), and has different neurotransmitter receptor expression patterns (Lothmann et al., 2021) than its ventral pole. The rodent dorsal

hippocampus corresponds to the human posterior hippocampus, and the rodent ventral hippocampus corresponds to the human anterior hippocampus (Barr et al., 2017). The dorsal part (human posterior) of the hippocampus and subiculum are connected with retrosplenial and anterior cingulate cortices. This network has been reported to play an essential role in cognitive processing, spatial learning, and navigation in rodents, monkeys, and humans (Bienkowski et al., 2018; Fanselow & Dong, 2010). The ventral part (human anterior) of the hippocampus and subiculum are connected with limbic structures, i.e., the hypothalamus and amygdala (Bienkowski et al., 2018; Fanselow & Dong, 2010; Moser & Moser, 1998). Herman and colleagues (1995) showed that rats with lesions in the ventral hippocampus and subiculum had stable and basal levels of corticosterone secretion at any given time. They reported that the ventral subiculum influences hypothalamic–pituitary–adrenal (HPA) activation (Herman et al., 1995). Activation of the HPA axis has been linked to temperamental behaviour in nonhuman primates (O'Leary & Cryan, 2014).

The link between the hippocampus and epilepsy is well-established in the literature (Chatzikonstantinou, 2014). Temporal lobe epilepsy – the most common type of epilepsy – has been known to cause neuronal loss, gliosis, neurogenesis, and mossy fiber spouting in the hippocampus (Aronica & Gorter, 2007; Jardim et al., 2021; Leite Góes Gitai et al., 2019; Noebels et al., 2012). Additionally, the influence of the ventral hippocampus on epileptic seizures was reported even as early as 1984. Bilateral ablation of the ventral hippocampus inhibited epileptic seizures in kindled rats (Yoshida, 1984). Toyoda and colleagues (2013) showed that the ventral hippocampus had the earliest seizure activity compared to the other structures observed in pilocarpine-treated rats. In line with their finding, King et al. (1997) previously suggested that the ictal onset site could be the anterior hippocampus (ventral hippocampus in rodents) in human epileptic patients. Last, Buckmaster et al. (2022) demonstrated that the ventral hippocampus is the primary ictal site in a pilocarpine model of temporal lobe epilepsy. They suppressed the activity of the ventral hippocampus bilaterally using a voltage-gated sodium channel blocker, tetradotoxin, in pilocarpine-treated rats. The inactivation of the ventral hippocampus resulted in seizure suppression (Buckmaster et al., 2022). Furthermore, Zeidler and colleagues (2018) showed that changing the kainic acid injection site from

the dorsal hippocampus to the ventral hippocampus resulted in temporal lobe epilepsy symptoms with additional affective traits in a modified intrahippocampal kainic acid model of epilepsy. They suggested that this modified model of epilepsy could be used to unfold molecular mechanisms that lead to depression as a comorbidity of epilepsy (Zeidler et al., 2018).

As mentioned at the beginning of the section, core clock genes affect excitability in the hippocampus, which can explain the 24-hour seizure pattern that has been observed in epileptic patients (Karoly et al., 2018; Karoly et al., 2021; Leite Góes Gitai et al., 2019). Brancati et al. (2021) presented the crosstalk between circadian rhythm, the hippocampus, and epilepsy in their study to untangle hippocampal energy metabolism in a time-of-day-dependent manner. They showed that the dorsal and ventral hippocampus have different energy needs depending on the time point in the circadian cycle. In addition, they demonstrated that hippocampal energy metabolism was disrupted in experimental epilepsy (Brancati et al., 2021). In a different study, Debski and colleagues (2020) reported that the control ventral hippocampus had over 1200 transcripts. The ventral hippocampus of epileptic mice in a pilocarpine model had over 1600 transcripts with oscillations over a circadian cycle. The researchers showed several changes to the gene expression introduced via epilepsy pathology: some genes gained a circadian oscillatory pattern. In contrast, others lost theirs, a subset of genes had alterations in their amplitude, and a cluster of the genes had a shift of several hours in their oscillations. The authors also reported that only 25% of the transcripts were common in epileptic and control animals. The functional enrichment analysis of the promoters of the transcripts with altered expression revealed several transcription factors. The most frequent motif belonged to the transcription factor ZF5 (Debski et al., 2020). These findings indicate that epilepsy pathology induces molecular remapping and that disturbed molecular oscillations can affect neuronal excitability, homeostasis, and/or mood, which can be targeted for future chronotherapeutics.

1.4 Zbtb14 protein

Zbtb14 (formerly known as Zfp161, Znf478, and Zf5) is a protein that belongs to the zinc finger and BTB/POZ (broad-complex, tramtrack, and bric-a-brac/poxvirus)-containing

protein family – one of the most prominent protein families in humans that controls transcriptional regulation (https://www.genecards.org/cgi-bin/carddisp.pl?gene=ZBTB14) (Donaldson et al., 2007; Liu et al., 2011). Zbtb14 has a BTB/POZ domain in its N-terminus, which is linked to protein-protein interactions, and it has five Cys_2–His_2 zinc finger motifs (also known as *Krüppel*-type zinc fingers) that are associated with DNA binding and interaction (Numoto et al., 1993). Numoto and colleagues (1999) showed that the BTB/POZ domain of the Zbtb14 protein affects the ability of the zinc finger domain to bind to DNA. Additionally, they revealed that the reverse effect was also present; the zinc finger domain was necessary for the BTB/POZ domain's protein binding ability (Numoto et al., 1999). Furthermore, zinc fingers 3 and 4 were demonstrated to be essential for the DNA binding feature of Zbtb14. Yokoro et al. (1998) revealed that BTB/POZ and zinc finger domains were highly conserved across several species, i.e., humans, mice, and chickens. Zbtb14 mRNA has been found in several mouse tissues, including the ovary, brain, heart, and lung (Numoto et al., 1997).

The first reports on the transcriptional activity of the Zbtb14 protein indicated that it has both transcriptional activator and repressor activity based on viral promoter studies (Numoto et al., 1993; Numoto et al., 1999). Kaplan and colleagues (1997) showed that the BTB/POZ domain was necessary for the transcriptional activity of Zbtb14. Obata et al. (1999) established the consensus binding site of the Zbtb14 protein as 5'- GSGCGCGR – 3' (S, G or C; R, A or G). Recent literature has elucidated that Zbtb14 is a positive regulator of human dopamine transporter (hDAT) (Lee et al., 2004) and a negative regulator of human fragile X messenger ribonucleoprotein 1 (hFMR1) (Gulyy et al., 2010; Orlov et al., 2007) and human leukemia inhibitory factor (hLIF) (Nylén et al., 2018). Zbtb14 was implicated in holoencephaly type 4 due to its chromosomal location (Sobek-Klocke et al., 1997).

The subcellular localisation of Zbtb14 was first reported in a study on COS7 (African green monkey kidney fibroblast-like cell line) cells that were transfected with HA-tagged human ZF5, and the researchers showed that the Zbtb14 protein had nuclear localisation (Sugiura et al., 1997). Bileck and colleagues (2017) revealed that the nuclear presence of the Zbtb14 protein was increased due to induced inflammation in PBMCs (peripheral blood mononuclear cells). In a zebrafish model, Deng et al. (2022) showed

that SUMOylated Zbtb14 at lysine 40 is responsible for transcriptional inhibition of the *pu.1* transcription factor, an essential transcription factor for the development of the immune system via regulation of the monocyte/macrophage lineage. In another study, the researchers elucidated that the ZF5 motif was overrepresented in the open chromatin regions isolated from the peripheral blood $CD4^+$ T cells of systemic lupus erythematosus patients (Wu et al., 2023). Furthermore, it has been reported that human sera collected from patients with immune disorders have autoantigenecity against the Zbtb14 protein (Yanagidani et al., 2000). Taken together, these results suggest that the Zbtb14 protein plays a role in the immune system in the periphery.

Other evidence on Zbtb14 protein function comes from two studies on *Xenopus* embryos. Takebayashi-Suzuki and colleagues (2018; 2022) showed that Zbtb14 modulates dorsal-ventral patterning and is crucial for neural development in *Xenopus*. In addition, Zbtb14 cooperates with the Zbtb21 protein to modulate anterior-posterior patterning in *Xenopus* embryos (Takebayashi-Suzuki et al., 2018; Takebayashi-Suzuki et al., 2022). The Zbtb21 protein was also previously reported to be a partner of the Zbtb14 protein by Wang and colleagues (2005). Additionally, Takebayashi-Suzuki et al. (2018) also elucidated that Zbtb14 abolishes BMP signalling by diminishing the phosphorylation of several SMAD proteins and elevates the Wnt pathway via the stabilisation of β-catenin.

A recent study in HCT116 (human colon cancer cell line) cells and mouse spleen tissue revealed that Zbtb14 regulates replication fork stability via recruitment of the RPA-ATR-ATRIP complex (Kim et al., 2019). In addition, in one extensive in silico analysis of clock-controlled genes from mammalian tissues, Bozek et al. (2009) reported that the promoters of clock-controlled genes are GC-rich and that the ZF5 motif was one of the enriched motifs that was identified in the heart liver, muscle and SCN.

Last, Debski and colleagues (2020) elucidated that the ZF5 motif was overrepresented in the promoter regions of genes with perturbed expression in the ventral hippocampus of pilocarpine-treated mice – a model of temporal lobe epilepsy. Nevertheless, aside from the Debski study and *Xenopus* studies, there are no studies on the function of the Zbtb14 protein in the brain, specifically the rodent brain as a model of human disease.

CHAPTER 2

AIM AND HYPOTHESIS

2.1 The aim of the thesis

In this Ph.D. study, my main aim was to characterise the protein level of a member of the Zbtb protein family, zinc finger and BTB domain containing 14 (Zbtb14), in the brains of naïve mice. Moreover, based on the findings of the abovementioned Debski et al. (2020) study, we endeavoured to decipher the circadian oscillatory pattern of the Zbtb14 protein in the hippocampus of naïve and epileptic mice. For this purpose, I utilised immunofluorescence, western blot, and immunoprecipitation techniques. Additionally, we employed in silico analysis to gain insight into the potential transcriptional targets of the Zbtb14 transcription factor. The present study aims to gain a better understanding of the function of the Zbtb14 protein in naïve and epileptic brains.

2.2 Hypothesis

This research was built around the following hypotheses:

i. As a transcription factor that is expected to regulate gene expression, Zbtb14 should have a nuclear presence.

ii. Based on previous findings, we expect oscillatory protein level of Zbtb14 over the circadian cycle in the mouse hippocampus.

iii. The oscillatory pattern of Zbtb14 is expected to be disrupted by epilepsy pathology.

CHAPTER 3

MATERIALS AND METHODS

3.1 Materials

3.1.1 Reagents, chemicals, enzymes, and materials

1X Phosphate Buffered Saline (PBS) (BioShop, Canada, #PBS404.100)

2-mercaptoethanol (Sigma-Aldrich, Saint Louis, MO, USA, #M3148)

6X Protein Assay Dye Reagent (Bio-Rad, Hercules, CA, USA, #500-0006)

96% Ethanol (Poch, Poland, #396420113)

Adhesion slides, Menzel Gläser, Polysine® (Thermo Fisher Scientific, Waltham, MA, USA, #J2800AMNZ)

Advanced PAP Pen (Merck KGaA, Darmstadt, Germany, #Z672548)

Ammonium persulfate (APS; Sigma-Aldrich, Saint Louis, MO, USA, #A9164 or Bio-Rad, Hercules, CA, USA, #1610700)

Bovine serum albumin (BSA; Sigma-Aldrich, Saint Louis, MO, USA, #A2153)

Bromophenol blue (Sigma-Aldrich, Saint Louis, MO, USA, #B5525)

Cresyl violet (Sigma-Aldrich, Saint Louis, MO, USA, #C5042)

DL-Dithiothreitol (DTT; Sigma-Aldrich, Saint Louis, MO, USA, #D9779)

DPX Mountant for Histology (Sigma-Aldrich, Saint Louis, MO, USA, #06522)

ECL Prime Western Blotting System (Cytiva, Marlborough, USA, #RPN2232)

ECL Western Blotting System (Cytiva, Marlborough, USA, #RPN2108)

ECL™ Blocking Agent (Cytiva, Marlborough, USA, #RPN2125)

Ethylene glycol (Chempur, Poland, #114466303)

Ethylene glycol-bis(2-aminoethyl ether)-N, N, N', N'-tetraacetic acid (EGTA; Sigma-Aldrich, Saint Louis, MO, USA, #E3889)

Gelatin (Sigma-Aldrich, Saint Louis, MO, USA, #G2500)

Glacial acetic acid (Chempur, Poland, #115687607)

Glycerol (Chempur, Poland, #114433204)

Glycine (Poch, Poland, #527560117)

Granulated skimmed milk powder (nonfat milk; SM Gostyń, Poland)

Hoechst 33342 (Thermo Fisher Scientific, Waltham, MA, USA, #62249)

Hydrochloric acid 35-38% (Chempur, Poland, #115752837)

KCl (Poch, Poland, #739740114)

$KCr(SO_4)_2$ (Poch, Poland, #249950113)

Medical X-ray Film (Carestream Health, Rochester, NY, USA, #7711468).

Methanol (Poch, Poland, #BA1990110)

$MgCl_2.6H_2O$ (Poch, Poland, #612050110)

Nitrocellulose blotting membrane (Cytiva, Marlborough, USA, #10600002)

Paraformaldehyde (Sigma-Aldrich, Saint Louis, MO, USA, #P6148)

Phenylmethasulfonyl fluoride (PMSF; Sigma-Aldrich, Saint Louis, MO, USA, #P7626)

PIPES (Sigma-Aldrich, Saint Louis, MO, USA, #P1851)

Ponceau S (Sigma-Aldrich, Saint Louis, MO, USA, #P3504)

Potassium phosphate, di-potassium salt (K_2HPO_4; Poch, Poland, #742100117)

Potassium phosphate, mono-potassium salt (KH_2PO_4; Poch, Poland, #742020112)

Protease inhibitor cocktail tablets (Roche Diagnostics, Switzerland, #11 697 498 001)

Recombinant human ZFP161 protein (Abcam, Cambridge, UK, #ab127611)

Sodium chloride (NaCl; Chempur, Poland, #117941206)

Sodium dodecyl sulfate (SDS; Sigma-Aldrich, USA, #L4509)

Sodium phosphate, disodium salt ($Na_2HPO_4.H_2O$; Poch, Poland, #799180111)

Sodium phosphate, mono-sodium salt ($NaH_2PO_4.12H_2O$; Poch, Poland, #799280115)

Sucrose (Chempur, Poland, #117720907)

The protein ladder (10 to 180 kDa) [molecular weight range in kDa (kilodalton)] (Thermo Fisher Scientific, Waltham, MA, USA, #26616)

Tissue freezing medium (Leica Biosystems, Germany, #14020108926)

Tris Base (Poch, Poland, #853470115)

Tris-HCl, pH 6.5 (Sigma-Aldrich, Saint Louis, MO, USA, #T3253)

Trisodium citrate (dihydrate) (Poch, Poland, #795780112)

Triton X-100 (Sigma-Aldrich, Saint Louis, MO, USA, #X100)

Tween 20 (Sigma-Aldrich, Saint Louis, MO, USA, #P7949)

VectaShield Mounting Medium (Vector Laboratories, Newark, CA, USA, #H-1000)

3.1.2 Kits

MOM Kit for Detecting Mouse Primary Antibodies on Mouse Tissue (Vector Laboratories, Newark, CA, USA, #BMK-2202)

NE-PER Nuclear and Cytoplasmic Extraction Kit (Thermo Fisher Scientific, Waltham, MA, USA, #78833)

Pierce™ Co-Immunoprecipitation (CoIP) Kit (Thermo Fisher Scientific, Waltham, MA, USA, #26149)

Zeba™ Spin Desalting Columns, 7K MWCO (Thermo Fisher Scientific, Waltham, MA, USA, #89882)

3.1.3. Antibodies, antigens and sera

Anti-ZBTB14 Antibody Produced in Rabbit (Atlas antibodies, Sweden, #HPA050758)

Anti-ZFP161 Antibody (Abcam, Cambridge, UK, #ab110904)

Anti-ZFP161 Antibody (C-4) (Santa Cruz Biotechnology, Santa Cruz, CA, USA, #sc-514298)

Anti-ZFP161 antibody Produced in Mouse (Sigma-Aldrich, Saint Louis, MO, USA, #SAB1400299)

Anti-ZFP161 Antibody Produced in Rabbit (Sigma-Aldrich, Saint Louis, MO, USA, #SAB2106303)

Anti-β-Actin–Peroxidase Antibody, Mouse Monoclonal (Sigma-Aldrich, Saint Louis, MO, USA, #A3854)

Blocking peptide for MBD3 (Santa Cruz Biotechnology, Santa Cruz, CA, USA, #sc-9402P)

Donkey anti-Mouse IgG (H+L) Highly Cross-Adsorbed Secondary Antibody, Alexa Fluor™ 568 (Invitrogen, Waltham, MA, USA, #A10037)

Donkey Anti-Mouse IgG Antibody, Biotin Conjugate, Species Adsorbed (Chemicon, Sigma-Aldrich, Saint Louis, MO, USA, #AP192B)

Fluorescein Avidin D, FITC (Vector Laboratories, Newark, CA, USA, Vector, #A-2001)

Goat Anti-Rabbit IgG Antibody (H+L), Biotinylated (Vector Laboratories, Newark, CA, USA, Vector Laboratories, #BA-1000)

Goat Anti-Rabbit IgG Antibody, Peroxidase Conjugated (Chemicon, Sigma-Aldrich, Saint Louis, MO, USA, #AP132P)

Monoclonal Anti-ZFP161 Antibody Produced in Mouse (Sigma-Aldrich, Saint Louis, MO, USA, #SAB1402396)

Mouse Anti-NeuN Antibody, Clone A60 (Sigma-Aldrich, Saint Louis, MO, USA, #MAB377)

Mouse IgG, HRP-linked whole Ab (from sheep; Cytiva, Marlborough, USA, #NA931)

Normal Donkey Serum (Jackson ImmunoResearch, #017-000-121)

Normal Goat Serum (Vector Laboratories, Newark, CA, USA, Vector, #S-1000)

Normal mouse IgG (Santa Cruz, CA, USA, Santa Cruz Biotechnology, #sc-2025)

Polyclonal Anti-ZBTB14 Antibody (Atlas antibodies, Sweden, #HPA070819)

PrEST Antigen ZBTB14 (Atlas Antibodies, Sweden, #APREST73794)

Rabbit IgG, HRP-linked whole Ab (from donkey; Cytiva, Marlborough, USA, #NA934)

Recombinant Human ZFP161 protein (Abcam, Cambridge, UK, #ab127611)

ZFP161 (Human) Recombinant Protein (P01) (Abnova™, Taipei, Taiwan, #H00007541-P01)

Zfp161 Antibody - Middle Region (Aviva Systems Biology, San Diego, CA, USA, #ARP33497_P050)

Zfp161 Antibody (Aviva Systems Biology, San Diego, CA, USA, #ARP38308_P050)

3.1.4. Equipment used in the experiments

Autoclave (Prestige Medical, Blackburn, UK)

CCD camera (Evolution VF, Media Cybernetics, Rockville, MD, USA)

Centrifuge 5804 R (Eppendorf, Hamburg, Germany)

Cryostat (CM1860, Leica, Wetzlar, Germany)

Developing machine (Optimax2010, Protec GmbH & Co., Germany)

Dounce Tissue Grinder, Glass 2 ml (Kimble Chase, Vineland, NJ, USA)

End-over-end rotator (Multi Bio RS-24, Biosan, Riga, Latvia)

GS-900 Calibrated Densitometer (Bio-Rad, Hercules, CA, USA)

Handheld rotor-stator homogeniser (TissueRuptor II, Qiagen, Hilde, Germany)

Heat block (TS-100C, Biosan, Riga, Latvia or Grant Instrumentals)

Magnetic stirrer (MR-3001, Heidolph, Germany or Variomag Mono, Komet, Germany)

Microcentrifuge Microspin 12 (Biosan, Riga, Latvia)

Microscope (Eclipse 80i, Nikon, Tokyo, Japan)

Mini-PROTEAN Tetra cell electrophoresis module (Bio-Rad, Hercules, CA, USA)

Multiskan EX Microplate Reader (Thermo Fisher Scientific, Waltham, MA, USA)

Objectives (10⁄0.30 DIC L⁄N1 or 20/0.50 DIC M/N2, Nikon, Tokyo, Japan)

Orbital shaker (TS-1000, ChemLand, Poland)

pH meter (SevenCompact S210, Mettler-Toledo, Columbus, OH, USA)

Scale (AD-200, Axis, Poland)

Spectrophotometer (DS-11, DeNovix, Wilmington, DE, USA)

Tetra Blotting Module (Bio-Rad, Hercules, CA, USA)

Ultrapure water system (Rephile, Boston, USA)

3.1.5. Solutions and buffers

All solutions and buffers were prepared with MilliQ water unless stated otherwise.

0.02 M Potassium Phosphate Buffer (KPB), pH 7.4

0.2 M KH_2PO_4

0.2 M K_2HPO_4

0.1 M Sodium Phosphate Buffer (PB), pH 7.4

0.2 M NaH_2PO_4

0.2 M Na_2HPO_4

10% Sucrose in KPB

10% Sucrose

0.02 M KPB, pH 7.4

10X Sodium Dodecyl Sulfate Polyacrylamide Gel (SDS-PAGE) Electrophoresis Buffer, pH 8.3

0.25 M Tris Base

1.92 M Glycine

1% SDS

10X Tris Buffered Saline (TBS), pH 8.0

1.5 M NaCl

100 mM Tris Base

1X TBS-T

1X TBS, pH 8.0

0.1% Tween 20

20% Sucrose in KPB

20% Sucrose

0.02 M KPB, pH 7.4

30% Sucrose in KPB

30 % Sucrose

0.02 M KPB, pH 7.4

3X Loading Buffer for SDS-PAGE with 2-mercaptoethanol

66 mM M Tris-HCl, pH 6.8

26% Glycerol

2.1% SDS

Bromophenol blue

1X 2-mercaptoethanol

4% Paraformaldehyde (PFA) Solution

8% PFA, pH 7.4

0.1 M PB, pH 7.4

4X Loading Buffer for SDS-PAGE with DTT

0.2 M Tris-HCl, pH 6.5

0.4 M DTT

Bromophenol blue (4 mg/ml)

SDS (80 mg/ml)

32% Glycerol

50% ethanol with acetic acid

50% Ethanol

1% Glacial acetic acid

Cresyl violet with acetic acid

0.1% Glacial acetic acid

3% Cresyl violet

Gelatin Solution

0.5% Gelatin

0.05% $KCr(SO_4)_2$

Lysis buffer for total protein isolation

0.5% Triton X-100

50 mM KCl

50 mM PIPES

2 mM $MgCl_2$

20 mM EGTA

0.1 mM PMSF

1 mM DTT

1X PIC

PBST

1X PBS

0.5% Triton X-100

Ponceau S Solution

0.1% Ponceau S

5% Glacial acetic acid

Separating Gel Buffer, pH 8.8

1.5 M Tris Base

Sodium citrate buffer, pH 6.0

10 mM sodium citrate

0.05% Tween 20

Stacking Gel Buffer, pH 6.8

0.5 M Tris Base

Stripping buffer, pH 3.0

93 mM Glycine

69 mM SDS

Tissue collection solution (TCS)

30% Ethylene glycol

25% Glycerol

9.5 mM NaH_2PO_4

9.5 mM Na_2HPO_4

Transfer Buffer

25 mM Tris Base

20% Methanol

192 mM Glycine

3.2 Methods

3.2.1 Animals and animal housing

All animal procedures followed European Council Directive 2010/63/EU and ARRIVE guidelines. For experiments performed in Poland, permission from the Warsaw Local Ethics Committee for Animal Experimentation was not needed. For experiments performed in France, permission from INSERM was obtained.

To optimise immunofluorescence, western blot and immunoprecipitation techniques, 9- to 11-week-old FVB male mice were obtained from the Nencki Institute Animal Facility (Polish Academy of Sciences, Warsaw, Poland). Mice were housed in a controlled environment (7:00 am/7:00 pm, light on/off) with water and food available *ad libitum*. The animals were kept together in groups (max. six animals per cage), and cardboard tunnels enriched their environment.

For the time-pointed tissue isolation performed at Nencki Institute of Experimental Biology, Poland, 4-week-old FVB male mice were obtained from the Nencki Institute Animal Facility (Polish Academy of Sciences, Warsaw, Poland). Mice were housed in a controlled environment (7:30 am/7:30 pm, light on/off) with water and food available *ad libitum*. During the dark phase, a red light while handling animals was used; any other light source was off to ensure that the circadian rhythm was unaffected. The animals were kept together in groups (max. six animals per cage), and cardboard tunnels and snacks enriched their environment. In addition, the same researchers took care of the animals to reduce external stressors.

For the time-pointed tissue isolation performed at INSERM, France, all procedures on control and epileptic animals were performed on FVB adult male mice following the INSERM procedures described in Debski et al. (2020). They were kept in a special in-house animal facility with strict control of light and temperature conditions (beginning of the light phase at 7:30 and beginning of the night phase at 19:30). Red light, which does not disrupt circadian rhythmicity, was present during the night phase to allow researchers to manipulate the animals. During the night phase, no external light could enter the room when opening the door. Mice were housed in groups of four to five to enable social interaction. Cages had an enriched environment. The same researcher

cared for the animals throughout the experimental procedure to limit external stressful factors.

3.2.2 Epilepsy induction

All epilepsy induction experiments were performed at INSERM, France.

Adult FVB mice were injected with methylscopolamine [1 mg/kg, intraperitoneally (i.p.)] 30 minutes before the pilocarpine injections. After that, pilocarpine was repeatedly injected (100 mg/kg, i.p.) every 20 minutes until status epilepticus (SE) was observed. After 90 minutes of SE, diazepam (10 mg/kg, i.p.) was injected to stop SE. All mice then received 0.5 ml of NaCl (0.9%) subcutaneously and again in the evening. If needed, mice were fed using a syringe during the following days. Control mice had the same treatment but were only injected with intraperitoneal NaCl (0.9%) instead of pilocarpine.

3.2.3 Tissue collection

3.2.3.1 Tissue collection by perfusion

To optimize immunofluorescence, 9- to 11-week-old FVB males were sacrificed. Adult FVB mice were injected intraperitoneally with a lethal dose of Morbital at a dose of 2 ml/kg of body weight. When the animal showed no response to paw pinch, the animal was placed on the operation table. A 5-6 cm lateral incision was made through the skin and abdominal muscle beneath the rib cage. Next, any tissue connected to the heart was trimmed. Next, a small incision was made to the right atrium using microspring scissors, and a needle attached to perfusion solutions was placed in the left ventricle. The animal was first perfused with ice-cold saline for 3 to 5 minutes. Afterward, it was replaced with 4% PFA, and the animal was perfused for 15 minutes.

After perfusion, the head was cut, and the brain was removed. Then, the brain was transferred into the PFA-filled vial and stored at 4°C. The next day, the PFA solution was changed to a 10% sucrose solution in KBP. The following day, the 10% sucrose solution in KBP was changed to a 20% sucrose solution in KBP. The following day, the 20% sucrose solution in KBP was changed to a 30% sucrose solution in KBP. Finally, after overnight

incubation in 30% sucrose solution in KBP, the brain was frozen on dry ice and stored at -80°C.

3.2.3.2 Fresh tissue collection

To optimize western blot and immunoprecipitation performed at the Nencki Institute of Experimental Biology, Poland, mice were anaesthetised with isoflurane. When they did not respond to the foot pinch, their head was removed to obtain the brain. The hippocampi and cortices were removed and quickly frozen on dry ice. Tissues were stored at -80°C.

For time-pointed tissue collection at the Nencki Institute of Experimental Biology, Poland, between the ages of 16 and 19 weeks, mice were anaesthetised with isoflurane at 11 am, 3 pm, 7 pm, 11 pm, 3 am, and 7 am. When they did not respond to the foot pinch, their head was removed to obtain the brain. First, the brain's left hemisphere was fresh-frozen on dry ice for immunofluorescence staining and stored at -80°C. Next, the right hippocampi were removed from the hemispheres and immediately used to extract nuclear and cytoplasmic protein extracts. Samples were stored at -80°C.

For time-pointed tissue collection in INSERM, France, three months after epilepsy induction, control, and epileptic animals were anaesthetised with isoflurane in the animal facility and were sacrificed at 3 pm and 11 pm. The hippocampus was removed in modified ice-cold artificial cerebrospinal fluid (ACSF). Both hippocampi from the same animal were quickly frozen and stored together at -80°C.

3.2.4 Tissue sectioning

3.2.4.1 Gelatin-Coated Slides

0.5% gelatin solution was heated and dissolved in a microwave and cooled. Microscope slides were placed in a microscope slide rack. The rack was put in MilliQ water for 1 minute and transferred into 0.5% gelatin solution for 30 seconds. All gelatin-coated slides were left to dry under a fume hood overnight. They were stored at 4°C.

3.2.4.2 Free-floating Sections Collected in Tissue Collection Solution (TCS)

The perfused brain was attached with tissue freezing medium to the holder perpendicularly. The left hemisphere of the animal was marked with a needle puncture on the left secondary visual cortex. Coronal sections with a thickness of 25 µm were cut with a cryostat starting from bregma 0.14 mm and collected on 24-well culture plates filled with TCS in a 4-in-1 series. A 4-in-1 series of plates was prepared for each brain. The plates were stored at -20°C. First, plates were used to perform NISSL staining. The rest of the plates were used to perform immunofluorescence with a standard protocol, mouse-on-mouse protocol, and antigen retrieval protocol.

3.2.4.3 Fresh-frozen Tissue Collected on Poly-L-Lysine Coated Microscope Slides

The left hemisphere of the brain was attached with tissue freezing medium to the holder perpendicularly. Sagittal sections with a thickness of 20 µm were cut and collected on poly-L-lysine-coated microscope slides. Slides were stored at -80°C. The sections were used for NISSL and fresh tissue immunofluorescence staining.

3.2.5 Tissue Staining Protocols and Analysis

3.2.5.1 NISSL Staining

The sections from the first series were washed three times with 1 ml PB per well for 10 minutes on an orbital shaker. The sections were mounted on gelatin-coated microscope slides with a paintbrush. The slices were dried overnight and NISSL-stained the next day.

The slides were immersed in 96% ethanol for 2 minutes, 70% ethanol for 2 minutes, and 50% ethanol for 2 minutes. Next, the slides were washed in MilliQ water for 2 minutes and immersed in 0.1% aqueous solution of cresyl violet with 3% acetic acid for 5-10 minutes. The slides were rinsed twice with MilliQ water. They were immersed in 50% ethanol for 2 minutes, 50% ethanol with 1% acetic acid for 30-60 seconds, 70% ethanol for 1-2 minutes, 96% ethanol for 1-2 minutes, and 100% ethanol for 2 minutes. Later, the slides were immersed in 1:1 ethanol:xylene for 2 minutes and xylene twice for 5 minutes. Finally, the slides were cover-slipped with DPX mounting resin and stored at room temperature after wholly drying.

3.2.5.2 Immunofluorescent Single Staining

The standard immunofluorescence staining of perfused tissue is explained in this paragraph. Any changes introduced to the immunofluorescence are explained in the results to avoid any possible confusion. The sections were washed in PBST thrice. Unspecific binding was blocked by incubation with 10% normal goat serum (NGS) or normal horse serum (NHS) diluted in PBST at room temperature. Next, the sections were incubated overnight with 1:500 primary antibody diluted in PBST at 4°C. The following day, the slices were washed in PBST three times and incubated with 1:1000 secondary antibody diluted in PBST at room temperature. Nuclei were stained with Hoechst dye. Finally, the slices were washed in PB or PBS, mounted on gelatine-coated microscope slides, and dried overnight. They were rinsed in cold tap water and were dried on a bench for 30 minutes. They were cover-slipped with VectaShield Mounting Medium and stored at 4°C. The omission of primary antibodies verified the specificity of the antibodies.

In the case of fresh-frozen tissue, sections were fixed in ice-cold 100% acetone for 10 minutes. Slides were washed in PBST thrice. Unspecific binding was blocked by incubation with 5% normal goat serum (NGS) or normal horse serum (NHS) diluted in PBST at room temperature. Next, the sections were incubated overnight with 1:100 primary antibody diluted in PBST at 4°C. The following day, the slides were washed in PBST three times and incubated with 1:200 secondary antibody diluted in PBST at room temperature. Nuclei were stained with Hoechst dye. Finally, the slides were washed in PBS thrice and rinsed in cold tap water. They were dried overnight and cover-slipped with VectaShield Mounting Medium the next day and stored at 4°C. The omission of primary antibodies verified the specificity of the antibodies.

3.2.5.3 Immunofluorescent Single Staining with Blocking Peptide

The perfused brain slices were washed in PBST three times. Unspecific binding was blocked by 10% NGS at room temperature. Identical sections were incubated with:

i. only recombinant Zbtb14 protein, 1:500 APREST73794 was prepared and stored for 2 hours,

ii. only with anti-Zbtb14 antibody, 1:500 HPA050758 was prepared and stored for 2 hours,

iii. HPA050758 (1:500) and APREST73794 (1:500) were prepared and stored together for 2 hours, and

iv. no primary and no recombinant protein solution, only PBST for 2 hours,

v. only recombinant Zbtb14 protein, 1:500 APREST73794 was prepared and stored overnight,

vi. only with anti-Zbtb14 antibody, 1:500 HPA050758 was prepared and stored overnight,

vii. HPA050758 (1:500) and APREST73794 (1:500) were prepared and stored together overnight,

viii. no primary and no recombinant protein solution, only PBST overnight.

The following day, the sections were incubated with the FITC-tagged anti-rabbit secondary antibody FI-1000 diluted to 1:1000 in PBST for 2 hours at room temperature. Nuclei were stained with Hoechst dye. Finally, the slices were washed in PBS three times. The slices were mounted on gelatine-coated microscope slides and dried overnight. They were rinsed in cold tap water and were dried on a bench for 30 minutes. They were cover-slipped with VectaShield Mounting Medium and stored at 4°C. The omission of primary antibodies verified the specificity of the antibodies. To check the effect of the blocking peptide on staining, a blocking peptide-only control was added.

3.2.5.4 Immunofluorescent Double Staining

In the case of Zbtb14 and NeuN double staining, sections were fixed in ice-cold 100% acetone for 10 min. Slides were washed in PBST thrice. A hydrophobic PAP pen was used to draw a rectangle around the tissue-mounted area. Unspecific binding was blocked by 5% NGS in PBST as the first blocking agent for 90 minutes at room temperature in a humid closed chamber. Next, the primary antibody against Zbtb14 HPA050758 was diluted to 1:100 in PBST and incubated overnight at 4°C in a humid closed chamber. The following day, the slides were washed in PBST three times, and the biotinylated anti-rabbit secondary antibody BA-1000 was diluted to 1:200 in PBST as the primary

secondary antibody solution and incubated for 2 hours at room temperature in a humid closed chamber. After washing, the sections were incubated with fluorescein Avidin D A-2001 at a 1:100 dilution in PBST for 20 minutes in a humid closed chamber. The sections were blocked with 2% NDS in PBST as the second blocking agent for 90 minutes in a humid closed chamber. Next, the sections were incubated overnight with a secondary antibody diluted in PBST at 4°C in a humid closed chamber. The following day, the secondary antibody against NeuN MAB377 was diluted to 1:1000 in PBST and incubated overnight at 4°C in a humid closed chamber. The Alexa Fluor 568-conjugated anti-mouse secondary antibody A10037 was diluted to 1:2000 in PBST as the secondary antibody solution and incubated for 2 hours at room temperature in a humid closed chamber. Nuclei were stained with Hoechst dye. Finally, the slides were washed in PBS thrice and rinsed in cold tap water. They were dried overnight and cover-slipped with VectaShield Mounting Medium the next day and stored at 4°C. The omission of primary antibodies verified the specificity of the antibodies.

In the case of Zbtb14 and GFAP double staining, sections were fixed in ice-cold 100% acetone for 10 min. Slides were washed in PBST thrice. A hydrophobic PAP pen was used to draw a rectangle around the tissue-mounted area. Unspecific binding was blocked by 5% NGS in PBST as the first blocking agent for 90 minutes at room temperature in a humid closed chamber. Next, the primary antibody against Zbtb14 HPA050758 was diluted to 1:100 in PBST and incubated overnight at 4°C in a humid closed chamber. The following day, the slides were washed in PBST three times, and the biotinylated anti-rabbit secondary antibody BA-1000 was diluted to 1:200 in PBST as the primary secondary antibody solution and incubated for 2 hours at room temperature in a humid closed chamber. After washing, the sections were incubated with fluorescein Avidin D A-2001 at a 1:100 dilution in PBST for 20 minutes in a humid closed chamber. The sections were blocked with 2% NHS in PBST as the second blocking agent for 90 minutes in a humid closed chamber. Next, the sections were incubated overnight with a secondary antibody diluted in PBST at 4°C in a humid closed chamber. The following day, the secondary antibody against GFAP MAB3402 was diluted to 1:1000 in PBST and incubated overnight at 4°C in a humid closed chamber. The Texas Red-conjugated anti-mouse secondary antibody TI-2000 was diluted to 1:2000 in PBST as the secondary

antibody solution and incubated for 2 hours at room temperature in a humid closed chamber. Nuclei were stained with Hoechst dye. Finally, the slides were washed in PBS thrice and rinsed in cold tap water. They were dried overnight and cover-slipped with VectaShield Mounting Medium the next day and stored at 4°C. The omission of primary antibodies verified the specificity of the antibodies.

3.2.5.5 MOM Staining

All immunofluorescence-related details are explained in the results to avoid any possible confusion. The following description gives a general outline of immunofluorescent single staining with the MOM kit for detecting mouse primary antibodies in mouse tissue (Vector Laboratories, Newark, CA, USA, #BMK-2202).

The MOM Kit was used according to the manufacturer's instructions. Shortly after, perfused free-floating brain slices were washed in MilliQ water for 5 minutes. A blocking solution was added, and the sections were incubated for 1 hour. The slices were washed for 2 minutes in PBS twice and incubated for 1 hour in a working solution of MOM Mouse IgG Blocking Reagent. The slices were washed for 2 minutes in PBS twice and incubated for 5 minutes in a working solution of MOM Diluent. The sections were incubated in primary antibody diluted in MOM Diluent for 30 minutes. The slices were washed for 2 minutes in PBS twice and incubated for 10 minutes in a working solution of MOM Biotinylated Anti-Mouse IgG Reagent. The slices were washed for 2 minutes in PBS twice and incubated in a secondary antibody solution for 2 hours at room temperature. The slices were washed for 15 minutes in PBS thrice, incubated with Avidin D solution, and incubated for 20 minutes. The slices were rinsed for 15 minutes with 500 µl PB three times. The sections were mounted on gelatine-coated glasses and dried overnight at room temperature. They were rinsed in cold tap water and were dried on a bench for 30 minutes. They were cover-slipped with VectaShield Mounting Medium and stored at 4°C.

3.2.5.6 Antigen Retrieval with Sodium Citrate

Free-floating sections were washed thrice for 15 minutes in PBS at room temperature. Next, sections were placed on a poly-L-lysine-coated microscope slide and dried

overnight. The next day, a vegetable steamer was set up at 95°C, and a Coplin jar containing sodium citrate buffer (pH 6.0) was preheated in the steamer. The slides were incubated in the buffer for 30 minutes at 95°C. The Coplin jar was removed from the steamer and cooled to room temperature. A hydrophobic PAP pen was used to draw a rectangle around the tissue-mounted area. The slides were washed thrice for 15 minutes with PBST, and immunofluorescence was performed as described above on microscope slides.

3.2.5.7 Quantification of the density of Zbtb14-positive cells

The fresh-frozen sections that were collected at specific time points were viewed with a Nikon Eclipse 80i microscope for double immunofluorescence with anti-ZBTB14 antibody produced in rabbit (Atlas antibodies, Sweden, #HPA050758) and NeuN antibodies.

The images were captured using a CCD camera (Evolution VF, MediaCybernetics) with a Nikon 10⁄0.30 DIC L⁄N1 or 20/0.50 DIC M/N2 objective. The wavelengths used to excite the fluorescent dyes were 465 – 495 nm for FITC, 540 – 580 nm for Texas Red and Alexa Fluor 568, and 340 – 380 nm for Hoechst. The emission ranges were 515 – 555, 600 – 660, and 435 – 485 nm, respectively.

Images were acquired for each area examined using the abovementioned filters for Alexa Fluor 568, FITC, and Hoechst and elaborated with Image-Pro Plus, version 5.0 for Windows (Media Cybernetics). The sections from 2.28 – 2.40 mm lateral from the midline (Franklin & Paxinos, 2008) were visually inspected under the microscope. All images were collected using the same exposure time, and then corresponding pictures were superimposed to visualise the colocalisation of the NeuN-stained neurons with Zbtb14 immunofluorescence.

The Zbtb14-positive cells were manually tagged and counted within the area of interest. The Zbtb14-positive cell numbers were collected from a manually delineated area covering the hilus (separately ventral and dorsal regions), CA3a area (averaged from two separate frames covering CA3a), and somatosensory cortex (-2 from bregma, same sections as for hilus). The hilus was distinguished according to Amaral et al. (2007). For the cortex, data were calculated from a 200 µm-wide profile of the somatosensory

cortex. The profile was divided into cortical layers II/III, layer IV, layer V and layer VI according to Hoechst staining. Only the cells with well-visible nucleoli (visualised with Hoechst staining) were included in the analysis. Expression for each marker was analysed as the number of immunopositive cells per mm^2.

In the ventral hilus, the numbers of NeuN/Zbtb14 double-stained cells were also recorded.

Figures were prepared using Adobe Photoshop CS2, CorelDraw X4 and CorelDraw 2018. Brightness and contrast were adjusted to regain the natural appearance of the sections.

3.2.6 Protein isolation and blotting protocols

3.2.6.1 Total Protein Isolation

All total protein isolation is explained in the results to avoid any possible confusion. The description below gives a general outline of the total protein extraction protocol.

Fresh-frozen brain tissues were homogenised with a handheld rotor-stator homogeniser in lysis buffer for total protein isolation. The tissue lysate was frozen for 20 minutes at -20°C. After thawing, the samples were centrifuged at 4°C; the supernatant was transferred into a clean tube and stored at -80°C. The concentration of the protein isolates was measured using Protein Assay Dye Reagent.

3.2.6.2 Nuclear and Cytoplasmic Protein Extraction

The right hippocampi from the time-pointed tissue collection were used for nuclear and cytoplasmic protein extraction. Nuclear and cytoplasmic protein extraction was performed using the NE-PER™ Nuclear and Cytoplasmic Extraction Reagents kit according to the manufacturer's instructions. The concentration of the protein extracts was measured using Protein Assay Dye Reagent.

3.2.6.3 Western blot

The standard western blot (WB) protocol is explained in this paragraph. Any changes introduced to the western blotting are explained in the results to avoid any possible confusion. 12% SDS–PAGE % Tris-glycine SDS–PAGE with Mini-PROTEAN Tetra cell

electrophoresis module (Bio-Rad, Hercules, CA, USA) and transferred to a nitrocellulose blotting membrane in transfer buffer for 90 minutes. Transfer efficiency was confirmed with Ponceau S staining. After removing Ponceau S staining, the membranes were blocked in 5% nonfat milk in TBS-T for 1 hour at room temperature. Next, they were incubated overnight with an anti-Zbtb14 primary antibody diluted to 1:500 in TBS-T at 4°C. Then, they were incubated for 2 hours with 1:5000 peroxidase-conjugated antibody, AP132P, diluted in TBS-T at room temperature. The signal was detected using the RPN2108 ECL system according to the manufacturer's instructions. The signal was captured on an X-ray film developed with an automatic film processor. After stripping, the membranes were reprobed with anti-β-actin−peroxidase antibody and mouse monoclonal diluted in TBS-T. X-ray films were scanned using a GS-900 Calibrated Densitometer, and optical density was measured by Image Lab Software version 5.2.1. GraphPad Prism version 5.01 was used for statistical analysis.

3.2.6.4 Stripping and reprobing

Separate incubation boxes were filled with stripping buffer. The membranes were transferred into stripping boxes and incubated for 30 minutes on a shaker. Next, the membranes were transferred into blotting boxes filled with TBS-T and washed three times for 5 minutes on a shaker. The membranes were blocked in 5% nonfat milk in TBS-T for 1 hour on a shaker. The membranes were washed three times with TBS-T for 5 minutes on a shaker. A primary antibody solution was added and incubated overnight in a cold room. The membranes were washed three times with TBS-T for 5 minutes on a shaker. A secondary antibody solution was added and incubated for 2 hours on a shaker. The membranes were washed six times with TTBS for 5 minutes on a shaker. The signal was detected using an ECL system according to the manufacturer's instructions. The signal was captured on an X-ray film developed with an automatic film processor. X-ray films were scanned using a GS-900 Calibrated Densitometer, and optical density was measured by Image Lab Software version 5.2.1. GraphPad Prism version 5.01 was used for statistical analysis.

3.2.6.5 Dot blotting

The nitrocellulose membrane was marked by pencil to indicate the sample spots. Next, the sample was spotted slowly below the pencil mark with a narrow-mouth pipette tip. Next, the membrane was dried. Nonspecific sites were blocked in 5% nonfat milk in TBS-T for 1 hour at room temperature. The membranes were incubated for 30 minutes in rabbit anti-ZBTB14 (1:1000; Atlas antibodies, Sweden, #HPA050758) or mouse anti-ZFP161 (1:2000; Santa Cruz Biotechnology, Santa Cruz, CA, USA, #sc-514298) diluted in TBS-T at room temperature. The membranes were washed with TBS-T three times for five minutes and incubated for 30 minutes in goat anti-rabbit IgG antibody, peroxidase-conjugated (1:20000; Sigma–Aldrich, Saint Louis, MO, USA, #AP132P) or peroxidase-labelled anti-mouse antibody (1:20000; Cytiva, Marlborough, USA #NA931) diluted in TBS-T at room temperature. The signal was detected using an ECL Prime Western Blotting System according to the manufacturer's instructions. The signal was captured on an X-ray film with an automatic film processor.

For each membrane, three samples were spotted: the human ZFP161 full-length ORF (NP_003400.2, 1 a.a. - 449 a.a.) recombinant protein with a GST tag at the N-terminus (Abnova™, Taipei, Taiwan, #H00007541-P01), the blocking peptide for MBD3 (Santa Cruz Biotechnology, Santa Cruz, CA, USA, #sc-9402P) that served as a negative control, the recombinant antigen that rabbit anti-ZBTB14 (Atlas antibodies, Sweden, #HPA050758) was produced against PrEST Antigen ZBTB14 (Atlas antibodies, Sweden, #APREST73794), and the recombinant antigen that rabbit anti-ZBTB14 (Atlas antibodies, Sweden, #HPA050758) was produced against PrEST Antigen ZBTB14 (Atlas antibodies, Sweden, #APREST73794).

3.2.7 Immunoprecipitation protocol

Total protein isolates pooled from six mouse hippocampi were used for immunoprecipitation. A Pierce Co-Immunoprecipitation (Co-IP) Kit was used with minor modifications according to the manufacturer's instructions. Briefly, the anti-Zbtb14 antibody sc-514298 was immobilised on the resin provided with the kit. After quenching and washing steps, protein isolate was added to the columns overnight incubation with gentle rocking at 4°C. The next day, the flowthrough was collected for further analysis,

and the resins were washed to remove nonspecific binding. The immunoprecipitates were collected after the elution step with the elution buffer provided with the kit.

Three independent immunoprecipitation replicates were performed. For each immunoprecipitation, one experimental column (with a primary antibody and protein isolate) and four control columns were prepared. The control columns were:

1. With primary antibody and without protein isolate
2. Without primary antibody and with protein isolate
3. With control antibody and with protein isolate
4. With primary antibody immobilised on control resin and with protein isolate

The presence of bait protein was verified with Western blotting. Western blot verification was performed with the anti-Zbtb14 antibodies sc-514298 and HPA050758.

SDS–PAGE (10%) was run with eluates, and proteins were transferred to a nitrocellulose membrane. Nonspecific sites were blocked with 5% nonfat milk in TBS-T for 1 hour at room temperature. The membranes were incubated overnight with anti-Zbtb14 antibody, 1:4000 sc-514298 diluted in TBS-T, at 4°C. The membranes were incubated for 2 hours with 1:40000 anti-mouse peroxidase conjugated antibody, NA931, diluted in TBS-T at room temperature. The signal was detected using the RPN2232 ECL system according to the manufacturer's instructions.

Immunoprecipitation with HPA050758 was impossible due to the low concentration (200 µg/mL) of the antibody. The IP blot was reprobed with the anti-Zbtb14 antibody HPA050758 at a dilution of 1:1000 in TBS-T at 4°C. The membranes were incubated for 2 hours with 1:20000 anti-rabbit peroxidase conjugated antibody AP132P in TBS-T at room temperature. The signal was detected using the RPN2232 ECL system according to the manufacturer's instructions.

3.2.8 Analysis of RNAseq data from an *in vitro* model of epileptiform discharge

Embryos at 18 days post-fertilization were used to establish primary cultures of cortical neurons (Xu et al., 2012). Isolated embryos were decapitated, and the skulls were placed in chilled HBSS buffer (Thermo Fisher, #14170-088). The brains of the embryos were

isolated under a binocular in HBSS buffer. Next, both hemispheres of the brain were isolated. The extracted cortex was transferred to a 15 ml tube containing fresh HBSS, washed twice with cold HBSS buffer and incubated at 37°C for 15 minutes with HBSS buffer containing 0.2% Trypsin (Thermo Fisher, #27250-0180) and 0.15 mg/ml DNase (Sigma-Aldrich, #DN-25). The solution was then removed and warm 10% FBS (Thermo Fisher, #10106-151) diluted in HBSS was added. After washing the tissue twice with fresh, warm HBSS without FBS, the buffer was drawn off and 2 ml of warm medium containing: 1x B-27, 10% FBS, 10 mg/ml Gentamycin, 0.5 mM Glutamax in Neurobasal Medium was added, and then pipetted several times. The number and viability of cells were measured in 0.4% Trypan Blue using a Neubauer chamber (Marienfeld). 200000 cells per well were seeded into the wells of a 12-well plate pre-coated with poly-D-lysine (poly-D-lysine, 5 µg/ml in 0.1 M borate buffer, Sigma-Aldrich, #P7280). Cultures were grown in an incubator, under conditions: 37°C and 5% CO_2. 50% of the medium was exchanged for FBS serum-free medium (1X B-27, 10 mg/ml Gentamycin, 0.5 Mm Glutamax in Neurobasal Medium) on days 2 and 6.

Epileptiform discharges in vitro were induced as previously described by Jiang et al. (2010) with some modification. Briefly, cultures were incubated for 3 hours in pBRS buffer without magnesium (145 mM NaCl, 2.5 mM KCl, 10 mM HEPES, 2 mM $CaCl_2$, 10 mM glucose, 0.002 mM glycine, pH 7.3) . The control cultures were incubated in pBRS buffer with magnesium (145 mM NaCl, 2.5 mM KCl, 10 mM HEPES, 2 mM $CaCl_2$, 10 mM glucose, 0.002 mM glycine, 1mM $MgCl_2$, pH 7.3). At the end of the incubation, the pBRS buffer was replaced with fresh, warmed, serum-free culture medium (37°C). Material for further studies was collected 24 hours after induction of epileptiform discharges.

To isolate RNA from the cell culture, the plate was washed twice with sterile, cold PBS buffer. After the buffer was drawn off, 400 µl of Qiazole (Qiagen, #79306) was added to the well of a plate and incubated 5 minutes at room temperature with shaking. Next, the homogenate was pipetted several times and transferred to new tubes. 80 µl of chloroform (Sigma, #C0549-1PT) was added to the homogenate. The samples were vortexed and incubated 10-15 minutes at room temperature until phase separation. The upper phase was used for further RNA isolation, which was performed according to the protocol of the RNA isolation kit: RNeasy Mini Kit (Qiagen, #74104). The RNA was

measured on a Nanodrop Spectrophotometer (DS-11 Spectrophotometer, DeNovix) at λ= 260 nm and 280 nm. The isolated RNA was stored at -80°C.

RNAseq libraries were prepared by KAPA Stranded mRNA Sample Preparation Kit according to the manufacturer's protocol (Kapa Biosystems, MA, USA) as previously described (Grabowska et al., 2022). Transcriptomic data analysis was done as follows: fastq files were aligned to rn6 rat reference genome with STAR program (Dobin et al., 2013), reads were counted to genes using feature Counts algorithm (Liao et al., 2014). Gene counts were normalized with FPKM method and differential analysis was performed by DESeq2 (Love et al., 2014). Genes were considered to be differentially expressed (DE) with adjusted p value 0.05 (Yu et al., 2012).

Analysis of overrepresentation of transcription factor binding motifs in groups of genes was performed using g:Profiler (https://biit.cs.ut.ee/gprofiler/gost).

In vitro experiments and RNA extraction was performed by dr Karolina Nizińska and dr Kinga Szydłowska. Next-generation sequencing and Basic RNAseq analysis were performed by Laboratory of Sequencing at the Nencki Institute (Nizińska et al.). I characterised the genes that had a ZF5 motif (GSGCGCGR; TF: M00716_1) in their promoters and investigated their potential role in epilepsy pathology.

CHAPTER 4

RESULTS

4.1 Antibody optimisation

Since my goal was to characterise the Zbtb14 protein using immunofluorescence and western blot, I tested nine antibodies available on the market produced against the Zbtb14 protein: ab110904, ARP33497_P050, SAB2106303, SAB1400299, ARP38308_P050, SAB1402396, HPA070819, sc-514298, and HPA050758. Here, I present the results obtained using each antibody in a separate subsection.

4.1.1 Abcam, #ab110904, anti-ZFP161 antibody

ab110904 is a rabbit polyclonal antibody. A recombinant human antigen (Abcam, Cambridge, UK, #ab127611), amino acids 151-427 of human Zbtb14, was used to generate the antibody. This antibody was discontinued during my PhD study.

4.1.1.1 Immunofluorescence

For the standard immunofluorescence protocol, all steps were performed on the free-floating sections. The sections were washed in 300 µl of PBST or PB for 10 minutes. The slices were blocked with 10% NGS in PBST for 2 hours. The primary antibody against Zbtb14 ab110904 was diluted to 1:500 in PBST and incubated overnight at 4°C. The biotinylated anti-rabbit secondary antibody BA-1000 was diluted to 1:1000 in PBST and incubated for 2 hours at room temperature. The sections were incubated with fluorescein Avidin D A-2001 at a 1:1000 dilution in PBST for 20 minutes (Figure 4.1 A-iv).

The staining has a low background and low intensity. In the CA1 and CA3 subfields, the cells have evident nuclear staining and morphologically resemble neurons. In the subfield granular cell layer of the dentate gyrus, the background-to-staining ratio was higher, and it was impossible to discern cytoplasmic and nuclear staining due to the densely packed granular cell layer. Additionally, the staining had unspecific binding to what resembles the astrocytic process in the alveus and corpus callosum (Figure 4.1 A-i-iii).

The washing volume and time were increased in the following staining to improve the staining-to-background ratio (Figure 4.1 B). All steps were performed on the free-floating sections. The sections were washed in 500 µl of PBST or PB for 15 minutes. Blocking solution, primary and secondary antibody volumes, dilutions, and incubation times were the same as the standard staining (Table 4.1 B-iv). This washing volume and time-optimised staining had a worse staining-to-background intensity ratio than the initial staining (Figure 4.1 A and B). In the CA1 and CA3 subfields, the cells have apparent nuclear staining and morphologically resemble neurons. Astrocytic processes are also stained in the alveus of the hippocampus. Because the background staining is higher in this staining, the cells in the DG subfield are not distinguished from the background (Figure 4.1 B-i-iii).

The staining protocol with a FITC-tagged secondary antibody was performed to eliminate the multiple steps needed by the streptavidin–biotin complex staining procedure. I used the same washing steps as the washing volume and time-optimised staining protocol. The blocking solution, primary antibody volumes, dilutions and incubation times were the same as those for standard staining. The FITC-tagged secondary antibody, FI-1000, was diluted to 1:1000 in PBST and incubated for 2 hours at room temperature (Figure 4.1 C-iv). The staining with FITC-tagged secondary antibody also has evident nuclear staining. The cells that are Zbtb14-positive morphologically resemble neurons. The background-to-signal ratio is similar to what is observed in the standard staining images. The astrocytic process is also observed in this staining. Therefore, I concluded that it was a characteristic of the primary antibody used. The staining pattern in the dentate gyrus, except for some cells in the hilus, is also

indistinguishable from the background staining in this staining. Moreover, this staining has a dotty pattern across the tissue (Figure 4.1 C-i-iii).

A. Standard Staining Protocol

i. 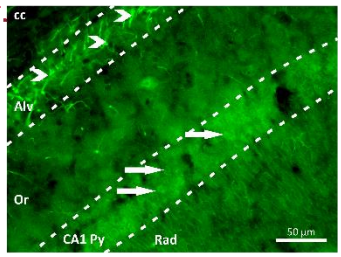

ii. 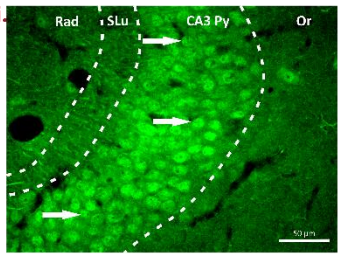

iii. 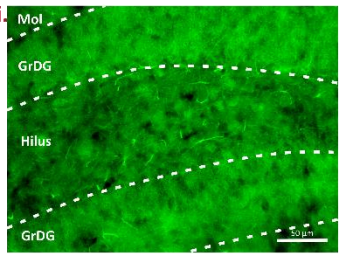

iv.

Steps	Solutions/Reagents	Time (min)	Volume (per well)	Temp
Wash	PBST	10 x 3	300 µl	RT
Blocking	10% NGS	120	300 µl	RT
Primary antibody	1:500 ab110904	Overnight	300 µl	4°C
Wash	PBST	10 x 3	300 µl	RT
Secondary antibody	1:1000 BA-1000	120	300 µl	RT
Wash	PBST	10 x 3	300 µl	RT
Fluorescein Avidin D	1:1000 A-2001	20	300 µl	RT
Wash	PB	10 x 3	300 µl	RT

B. Washing Volume and Time Optimised Protocol

i. 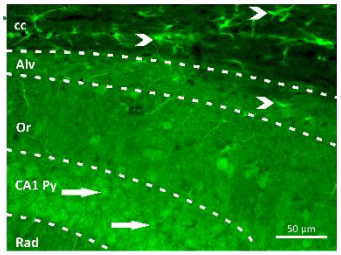

ii. 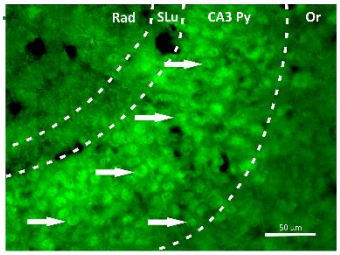

iii. 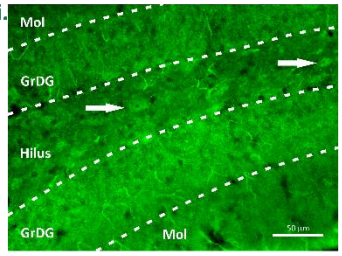

iv.

Steps	Solutions/Reagents	Time (min)	Volume (per well)	Temp
Wash	PBST	15 x 3	500 µl	RT
Blocking	10% NGS	120	300 µl	RT
Primary antibody	1:500 ab110904	Overnight	300 µl	4°C
Wash	PBST	15 x 3	500 µl	RT
Secondary antibody	1:1000 BA-1000	120	300 µl	RT
Wash	PBST	15 x 3	500 µl	RT
Fluorescein Avidin D	1:1000 A-2001	20	300 µl	RT
Wash	PB	15 x 3	500 µl	RT

C. Staining Protocol with an FITC-Tagged Secondary Antibody

i. 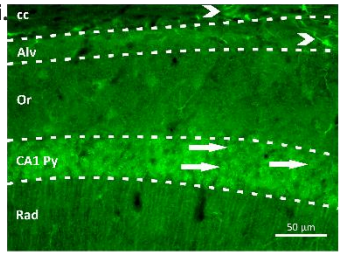

ii. 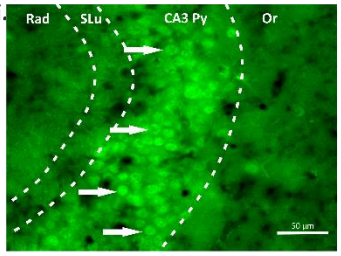

iii. 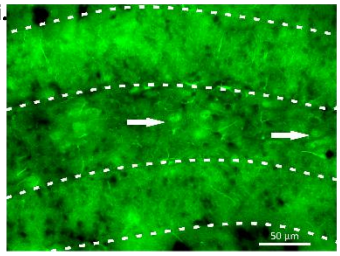

iv.

Steps	Solutions/Reagents	Time (min)	Volume (per well)	Temp
Wash	PBST	15 x 3	500 µl	RT
Blocking	10% NGS	120	300 µl	RT
Primary antibody	1:500 ab110904	Overnight	300 µl	4°C
Wash	PBST	15 x 3	500 µl	RT
Secondary antibody	1:1000 FI-1000	120	300 µl	RT
Wash	PB	15 x 3	500 µl	RT

Figure 4.1 Images of the hippocampal sections with different staining protocols using the anti-Zbtb14 antibody ab110904. The CA1 (A-i), CA3 (A-ii), and DG (A-iii) of the hippocampus are shown with the standard staining protocol. The standard protocol is a table under the images (A-iv). The CA1 (B-i), CA3 (B-ii), and DG (B-iii) of the hippocampus are shown with the washing volume- and time-optimised protocol. The washing volume and time optimised protocol are given as a table under the images (B-iv). The CA1 (C-i), CA3 (C-ii), and DG (C-iii) of the hippocampus are shown with the staining protocol with a FITC-tagged secondary antibody. The staining protocol with a FITC-tagged secondary antibody is given as a table under the images (C-iv). The white arrows indicate Zbtb14-stained nuclei. The white arrowheads indicate the Zbtb14-stained astrocytic processes. Alv, alveus; CA2 Py, pyramidal layer of CA2 field; CA3 Py, pyramidal layer of CA3 field; cc, corpus callosum; GrDG, granular layer of the dentate gyrus; Mol, molecular layer of the dentate gyrus; Or, oriens layer of the hippocampus; Rad, stratum radiatum of the hippocampus; S1, primary somatosensory cortex; SLu, stratum lucidum.

4.1.1.2. Western blot

The predicted molecular weight of the Zbtb14 protein is approximately 51 kDa, and the Abcam datasheet for ab110904 had a western blot image with a 51 kDa band. Heart total protein isolate served as a positive control.

For the standard WB protocol, 12% SDS–PAGE was run, and proteins were transferred to a nitrocellulose membrane. Nonspecific sites were blocked with 5% nonfat milk in TBS-T for 1 hour at room temperature. The membranes were incubated overnight with anti-Zbtb14 antibody ab110904 at a dilution of 1:500 in TBS-T, 4°C and then for 2 hours with 1:5000 anti-rabbit peroxidase-conjugated antibody, AP132P, diluted in TBS-T at room temperature. The signal was detected using the RPN2108 ECL system (Figure 4.2 A-ii). The image of the standard WB membrane has several unspecific bands in both tissue extracts, contrary to the Abcam datasheet image (Figure 4.2 A-i).

To distinguish the Zbtb14 band from unspecific bands, the recombinant protein used for antibody production was used as a sponge in the primary antibody solution. The anti-Zbtb14 antibody, ab110904, and recombinant Zbtb14 protein, ab127611, were incubated together before incubation with the membrane. Next, the identical membranes were incubated with (Figure 4.2 B-v-viii):

i. only recombinant Zbtb14 protein, 1:500 ab127611,

ii. only with anti-Zbtb14 antibody, 1:500 ab110904,

iii. 1:500 ab110904 and 1:500 ab127611 were incubated together for 2 hours, and

iv. Then, 1:500 ab110904 and 1:500 ab127611 were incubated together overnight.

The disappearance of a band at approximately 51 kDa on the membrane would show us which band is specific to the Zbtb14 protein. However, I identified that the pattern observed in the standard blot protocol did not change, and incubation with ab110904 and/or ab127611 resulted in unspecific binding to the ladder (Figure 4.2 B-i-iv).

A. Standard WB Protocol

i.

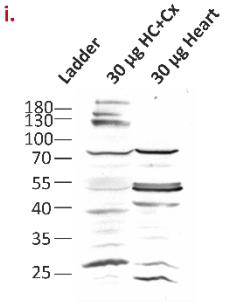

ii.

Western Blot Parameters	Solutions/Reagents	Time (min)	Volume (per membrane)	Temp
Blocking	5% nonfat milk	60	25 ml	RT
Primary antibody	1:500 ab110904	Overnight	6 ml	4 °C
Secondary antibody	1:5000 AP132P	120	6 ml	RT
ECL reagent	RPN2108	2	2 ml	RT

B. WB Protocols with Recombinant Protein

i.

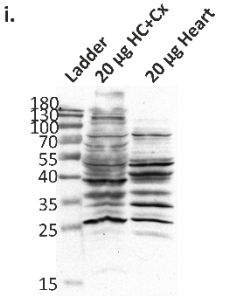

v.

Western Blot Parameters	Solutions/Reagents		Time (min)	Volume (per membrane)	Temp
Blocking	5% nonfat milk		60	25 ml	RT
Primary antibody	+ab110904 +ab127611 2 hours incubation	1:500 ab110904 and 1:500 ab127611 mixed and stored together for two hours at 4°C before the overnight incubation with the membrane	Overnight	6 ml	4°C
Secondary antibody	1:5000 AP132P		120	6 ml	RT
ECL reagent	RPN2108		2	2 ml	RT

ii.

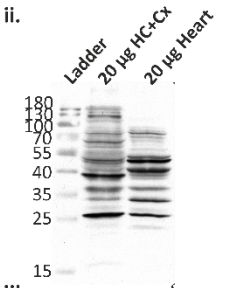

vi.

Western Blot Parameters	Solutions/Reagents		Time (min)	Volume (per membrane)	Temp
Blocking	5% nonfat milk		60	25 ml	RT
Primary antibody	+ab110904 +ab127611 Overnight incubation	1:500ab110904 and 1:500 ab127611 mixed and stored together overnight before the overnight incubation with the membrane	Overnight	6 ml	4°C
Secondary antibody	1:5000 AP132P		120	6 ml	RT
ECL reagent	RPN2108		2	2 ml	RT

iii.

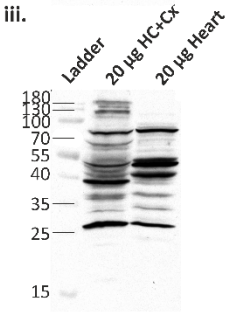

vii.

Western Blot Parameters	Solutions/Reagents		Time (min)	Volume (per membrane)	Temp
Blocking	5% nonfat milk		60	25 ml	RT
Primary antibody	-ab110904 +ab127611 Overnight incubation	1:500 ab127611 stored at 4°C overnight before the overnight incubation with the membrane	Overnight	6 ml	4°C
Secondary antibody	1:5000 AP132P		120	6 ml	RT
ECL reagent	RPN2108		2	2 ml	RT

iv.

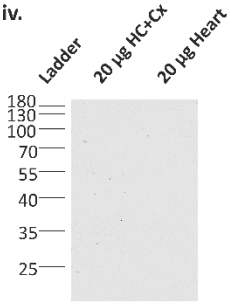

viii.

Western Blot Parameters	Solutions/Reagents		Time (min)	Volume (per membrane)	Temp
Blocking	5% nonfat milk		60	25 ml	RT
Primary antibody	+ab110904 -ab127611 Overnight incubation	1:500 ab110904 stored at 4°C overnight before the overnight incubation with the membrane	Overnight	6 ml	4°C
Secondary antibody	1:5000 AP132P		120	6 ml	RT
ECL reagent	RPN2108		2	2 ml	RT

Figure 4.2 Results of western blots probed against Zbtb14 with ab110904 using a standard protocol and protocols with recombinant protein. The anti-Zbtb14 antibody ab110904 was utilised in the standard WB protocol **(A)** and WB protocol with recombinant protein ab127611 as a competitor **(B)**. The standard WB protocol **(A-ii)** and the WB protocols with recombinant

protein **(B-v-viii)** are given in a table next to the images. HC+Cx: hippocampus and cortex; Temp: temperature.

4.1.2 Aviva systems biology, #ARP33497_P050, Zfp161 antibody - middle region

ARP33497_P050 is a rabbit polyclonal antibody produced with a synthetic peptide: DDDVEEIGDQDDSPSDDTVEGTPPSQEDGKSPTTTLRVQEAILKELGSEE (https://www.avivasysbio.com/sd/tds/html_datasheet.php?sku=ARP33497_P050).

For the standard immunofluorescence with ARP33497 (Figure 4.3 A-iv), the staining has a low background but no specificity. All granular, hilar and pyramidal cells had empty nuclei (Figure 4.3 A-i-iii).

The antigen retrieval staining protocol was applied to reveal any potentially masked antigenic sites of the Zbtb14 protein. After incubation with sodium citrate buffer on microscope slides, the standard staining protocol steps were carried out as described in the standard protocol (Figure 4.3 B-iv and B-viii). The staining of the hippocampus after the antigen retrieval immunofluorescence protocol did not show nuclear staining in the pyramidal cells of the CA1 and CA3 fields or granular cells of the dentate gyrus, similar to the initial staining. In the CA1 and CA3 pyramidal cells, cytoplasmic staining was observed; however, nonspecific binding of the secondary antibody was observed (Figure 4.3 B-i-iii) because the same pattern was also present in the primary antibody-omitted staining (Figure 4.3 B-v-vii).

A. Standard Staining Protocol

i. 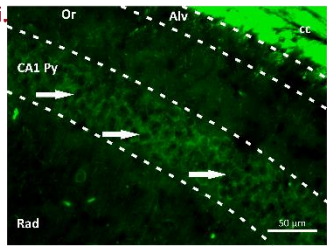

ii. 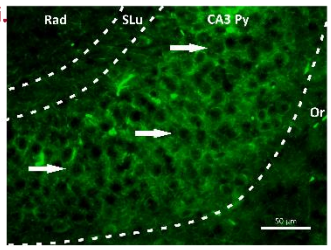

iii. 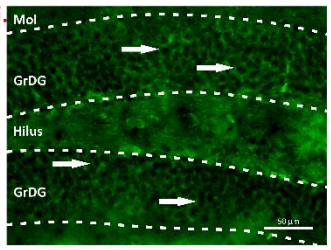

iv.

Steps	Solutions/Reagents	Time (min)	Volume (per well)	Temp
Wash	PBST	15 x 3	500 µl	RT
Blocking	10% NGS	120	300 µl	RT
Primary antibody	1:500 ARP33497	Overnight	300 µl	4°C
Wash	PBST	15 x 3	500 µl	RT
Secondary antibody	1:1000 FI-1000	120	300 µl	RT
Wash	PB	15 x 3	500 µl	RT

B. Antigen Retrieval Staining Protocol

Primary antibody-included images

i. 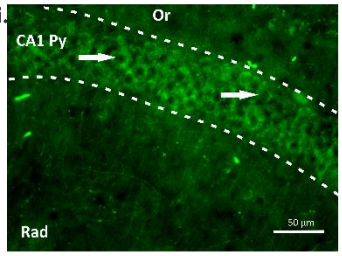

ii. 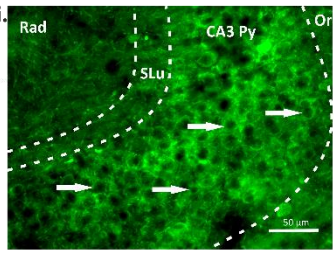

iii. 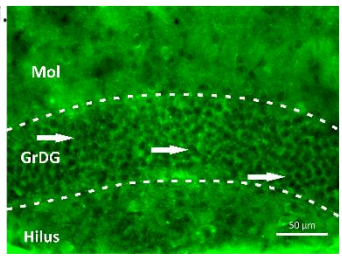

iv.

Steps	Solutions/Reagents	Time (min)	Volume (per slide)	Temp
Antigen retrieval	Sodium citrate buffer	30	-	95°C
Wash	PBST	15 x 3	-	RT
Blocking	10% NGS	120	200 µl	RT
Primary antibody	1:500 ARP33497	Overnight	200 µl	4°C
Wash	PBST	15 x 3	-	RT
Secondary antibody	1:1000 FI-1000	120	200 µl	RT
Wash	PB	15 x 3	-	RT

Primary antibody-omitted images

v. 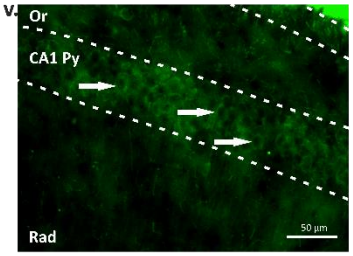

vi. 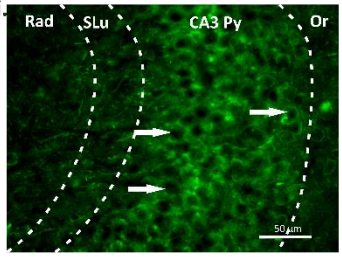

vii. 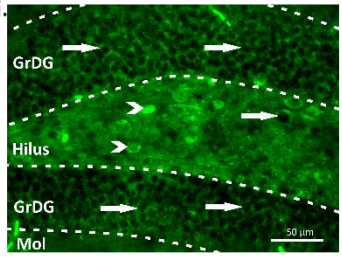

viii.

Steps	Solutions/Reagents	Time (min)	Volume (per slide)	Temp
Antigen retrieval	Sodium citrate buffer	30	-	95°C
Wash	PBST	15 x 3	-	RT
Blocking	10% NGS	120	200 µl	RT
Primary antibody	No primary	Overnight	200 µl	4°C
Wash	PBST	15 x 3	-	RT
Secondary antibody	1:1000 FI-1000	120	200 µl	RT
Wash	PB	15 x 3	-	RT

Figure 4.3 Images of the hippocampal sections after standard and antigen retrieval staining protocols using the anti-Zbtb14 antibody ARP33497. The CA1 **(A-i)**, CA3 **(A-ii)** and dentate gyrus **(A-iii)** of the hippocampus are shown with the standard staining protocol. The standard protocol is given as a table under the image **(A-iv)**. The CA1 **(B-i)**, CA3 **(B-ii)** and dentate gyrus **(B-iii)** of the hippocampus are shown under the antigen retrieval staining protocol. The primary antibody-

omitted staining images with the antigen retrieval protocol of the CA1 **(B-v)**, CA3 **(B-vi)** and dentate gyrus **(B-vii)** of the hippocampus are included. The antigen retrieval staining protocols are given as a table under the images **(B-iv and B-viii)**. The white arrows indicate Zbtb14-stained nuclei. The white arrowheads indicate the Zbtb14-stained astrocytic processes. CA1 Py, pyramidal layer of CA1 field; CA3 Py, pyramidal layer of CA3 field; GrDG, granular layer of the dentate gyrus; Mol, molecular layer of the dentate gyrus; Or, oriens layer of the hippocampus; Rad, stratum radiatum of the hippocampus; SLu, stratum lucidum.

4.1.2.2. Western blot

For the standard WB protocol (Figure 4.4 A-ii), no band was observed at the level of 51 kDa in either the brain or heart extracts. In the heart extracts, two faint bands are observed at 35 and 40 kDa (Figure 4.4 A-i).

The Aviva Systems Biology Company recommended a protocol for WB for ARP33497 antibody, which was performed next (Figure 4.4 B-ii). The Aviva WB protocol changed the following compared to the standard WB protocol:

i. Blocking with 3% nonfat milk in TBS-T for 30-45 minutes,

ii. Incubation with a 1:1000 dilution of the anti-Zbtb14 antibody ARP33497 for 4 hours at room temperature and

iii. The cells were incubated with a 1:10000 dilution of HRP secondary antibody for 45 minutes at room temperature.

No bands were observed in any extracts used. This suggests that the ARP33497 antibody does not detect the Zbtb14 protein in our extracts (Figure 4.4 B-i).

A. Standard WB Protocol

i.

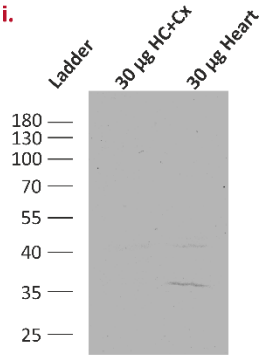

ii.

Western Blot Parameters	Solutions/Reagents	Time (min)	Volume (per membrane)	Temp
Blocking	5% nonfat milk	60	25 ml	RT
Primary antibody	1:500 ARP33497	Overnight	6 ml	4°C
Secondary antibody	1:5000 AP132P	120	6 ml	RT
ECL reagent	RPN2108	2	2 ml	RT

B. Aviva WB Protocol

i.

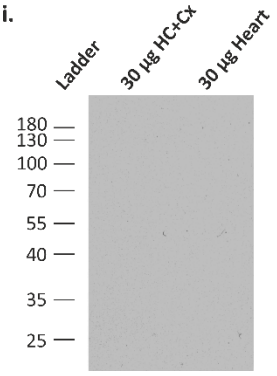

ii.

Western Blot Parameters	Solutions/Reagents	Time (min)	Volume (per membrane)	Temp
Blocking	3% nonfat milk	30-45	25 ml	RT
Primary antibody	1:1000 ARP33497	240	6 ml	RT
Secondary antibody	1:10000 AP132P	45	6 ml	RT
ECL reagent	RPN2108	2	2 ml	RT

Figure 4.4 Results of the western blots probed against Zbtb14 with ARP33497 antibody using standard and Aviva protocols. The anti-Zbtb14 antibody ARP33497 was utilised in standard WB **(A)** and Aviva WB **(B)** protocols. The standard WB protocol **(A-ii)** and the Aviva WB protocol **(B-ii)** are given as a table next to the images. HC+Cx: hippocampus and cortex; Temp: temperature.

4.1.3 Aviva systems biology, #ARP38308_P050, Zfp161 antibody

ARP38308_P050 is a rabbit polyclonal antibody produced with a synthetic peptide: TKAFAKASDLKRHENNMHSERKQVTPSAIQSETEQLQAAAMAAEAEQQLE. This antibody was discontinued during my PhD study.

4.1.3.1 Immunofluorescence

For the standard staining protocol of ARP38308, a dilution of 1:2000 in PBST was used for the primary antibody, and 1:4000 in PBST was used for the secondary antibody, FI-1000 (Figure 4.5 A-v). The staining has a high background and high intensity. In the CA1 subfield, the cells have clear cytoplasmic staining with empty nuclei. In the CA2 subfield, the cells have cytoplasmic staining, and most of the nuclei are also stained. In the CA3 subfield, most cells are not stained, but some cells have strong nuclear staining. In the

DG, similar to the CA3 subfield, half of the granular cells were not stained, but the other half had cytoplasmic staining. All cells that are stained morphologically resemble neurons. This antibody also stained some neuronal processes (Figure 4.5 A-i-iv).

For the protocol with increased antibody dilutions, the primary antibody was diluted to 1:5000 to improve the staining-to-background ratio. The FITC-tagged anti-rabbit secondary antibody FI-1000 was diluted to 1:10000 in PBST and incubated for 2 hours at room temperature (Figure 4.5 B-v). The staining has a high background but no distinguishable specific staining. The cells had empty nuclei across the hippocampus. Additionally, neuronal processes that we observed in the previous staining protocol disappeared in this staining (Figure 4.5 B-i-iv).

The two-day primary antibody incubation protocol aimed to increase the binding of the primary antibody by two-day incubation with the primary antibody at a cold temperature. The sections were incubated with the primary antibody ARP38308 diluted to 1:2000 in PBST for two days at 4°C to increase its binding to its antigen. The FITC-tagged anti-rabbit secondary antibody FI-1000 was diluted to 1:4000 in PBST and incubated for 2 hours at room temperature (Figure 4.5 C-v). This staining has a low staining-to-background ratio compared to standard staining. Zbtb14-stained cytoplasm and nuclei were observed in the CA2 and CA3 pyramidal cell layers, but not all cells were stained (Figure 4.5 C-i-iv).

A. Standard Staining Protocol

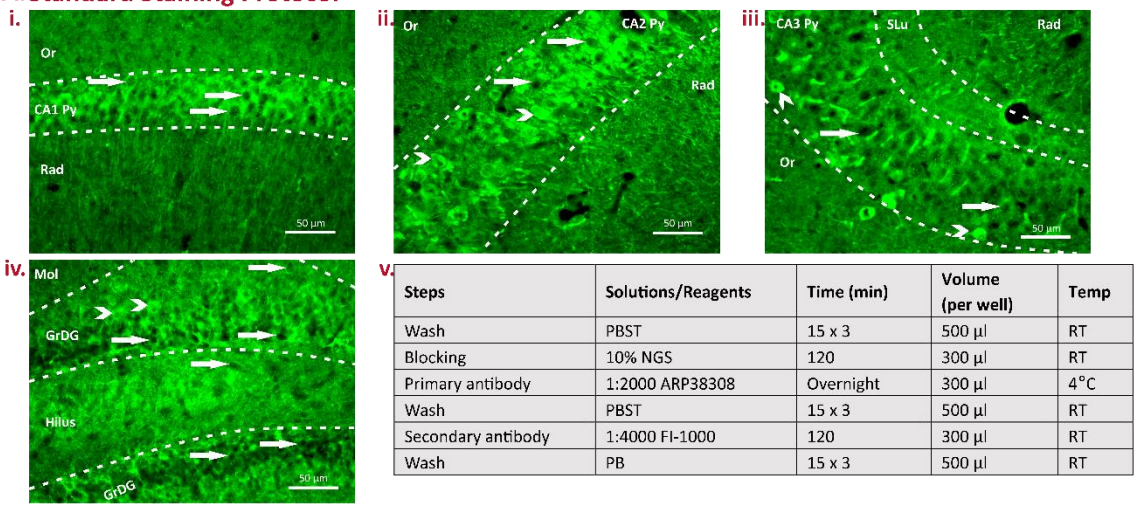

v.

Steps	Solutions/Reagents	Time (min)	Volume (per well)	Temp
Wash	PBST	15 x 3	500 µl	RT
Blocking	10% NGS	120	300 µl	RT
Primary antibody	1:2000 ARP38308	Overnight	300 µl	4°C
Wash	PBST	15 x 3	500 µl	RT
Secondary antibody	1:4000 FI-1000	120	300 µl	RT
Wash	PB	15 x 3	500 µl	RT

B. The Protocol with Increased Antibody Dilutions

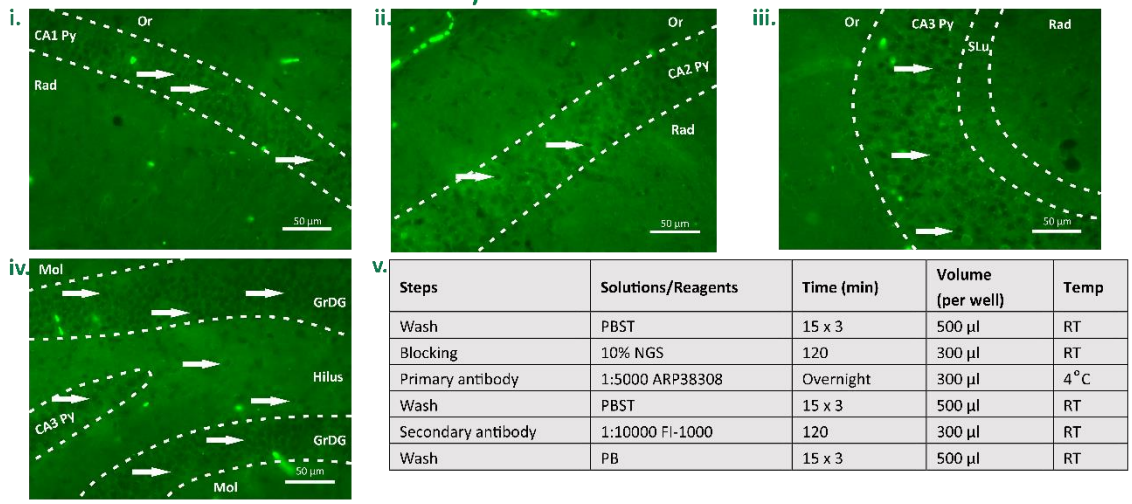

v.

Steps	Solutions/Reagents	Time (min)	Volume (per well)	Temp
Wash	PBST	15 x 3	500 µl	RT
Blocking	10% NGS	120	300 µl	RT
Primary antibody	1:5000 ARP38308	Overnight	300 µl	4°C
Wash	PBST	15 x 3	500 µl	RT
Secondary antibody	1:10000 FI-1000	120	300 µl	RT
Wash	PB	15 x 3	500 µl	RT

C. Two-Day Primary Antibody Incubation Protocol

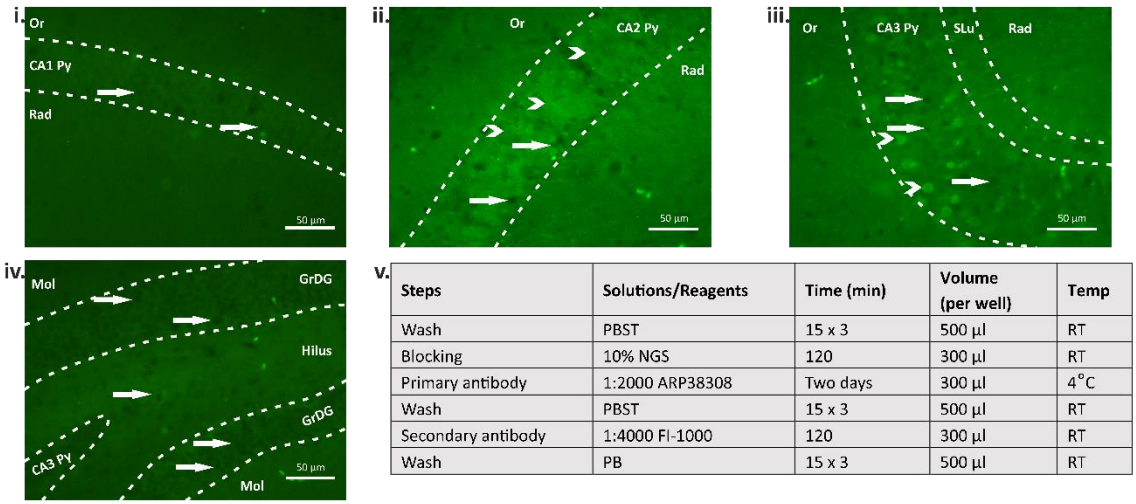

v.

Steps	Solutions/Reagents	Time (min)	Volume (per well)	Temp
Wash	PBST	15 x 3	500 µl	RT
Blocking	10% NGS	120	300 µl	RT
Primary antibody	1:2000 ARP38308	Two days	300 µl	4°C
Wash	PBST	15 x 3	500 µl	RT
Secondary antibody	1:4000 FI-1000	120	300 µl	RT
Wash	PB	15 x 3	500 µl	RT

Figure 4.5 Images of the hippocampal sections after the standard protocol, the protocol with increased antibody dilutions, and the two-day primary antibody incubation protocol using the anti-Zbtb14 antibody ARP38308. The CA1 **(A-i)**, CA2 **(A-ii)**, CA3 **(A-iii),** and dentate gyrus **(A-iv)** of the hippocampus are shown with the standard staining protocol. The standard protocol is a table following the image **(A-v)**. The CA1 **(B-i)**, CA2 **(B-ii)**, CA3 **(B-iii),** and dentate gyrus **(B-iv)** of

the hippocampus are shown under the protocol with increased antibody dilutions. The protocol with increased antibody dilutions is given as a table next to the images **(B-v)**. The CA1 **(C-i)**, CA2 **(C-ii)**, CA3 **(C-iii),** and dentate gyrus **(C-iv)** of the hippocampus are shown under the two-day primary antibody incubation protocol. The two-day primary antibody incubation protocol is given as a table next to the images **(C-v)**. The white arrows indicate Zbtb14-stained nuclei. The white arrowheads indicate the Zbtb14-stained astrocytic processes. CA1 Py, pyramidal layer of CA1 field; CA2 Py, pyramidal layer of CA2 field; CA3 Py, pyramidal layer of CA3 field; GrDG, granular layer of the dentate gyrus; Mol, molecular layer of the dentate gyrus; Or, oriens layer of the hippocampus; Rad, stratum radiatum of the hippocampus; SLu, stratum lucidum.

The antigen retrieval protocol was applied to reveal any potentially masked antigenic sites of the Zbtb14 protein that the ARP38308 antibody recognises. After incubation with sodium citrate buffer was performed on microscope slides, the standard staining protocol steps were carried out (Figure 4.6 B-v). The antigen retrieval protocol did not improve the staining quality compared to the standard staining protocol. The staining-to-background ratio was low, and the sections were damaged because of treatment with sodium citrate buffer at a high temperature. Hence, the images that are taken have a blurry appearance. Across the pyramidal cell layers and the DG granular layer of the hippocampus, the staining resembles cytoplasmic staining with empty nuclei. However, it is hard to interpret because of the damaged tissue due to the antigen retrieval method (Figure 4.6 B-i-iv).

A. Standard Staining Protocol

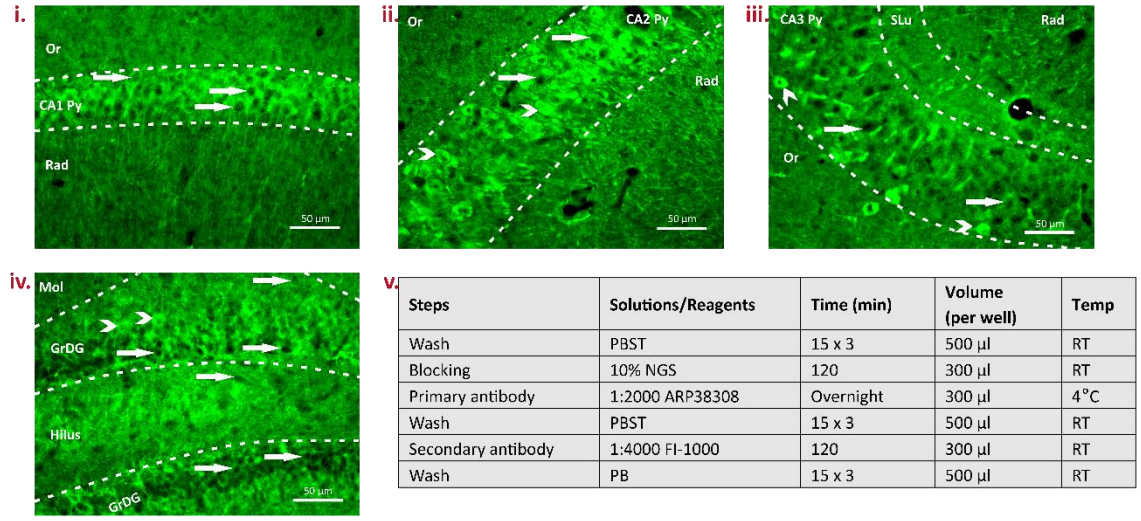

v.

Steps	Solutions/Reagents	Time (min)	Volume (per well)	Temp
Wash	PBST	15 x 3	500 µl	RT
Blocking	10% NGS	120	300 µl	RT
Primary antibody	1:2000 ARP38308	Overnight	300 µl	4°C
Wash	PBST	15 x 3	500 µl	RT
Secondary antibody	1:4000 FI-1000	120	300 µl	RT
Wash	PB	15 x 3	500 µl	RT

B. The Antigen Retrieval Staining Protocol

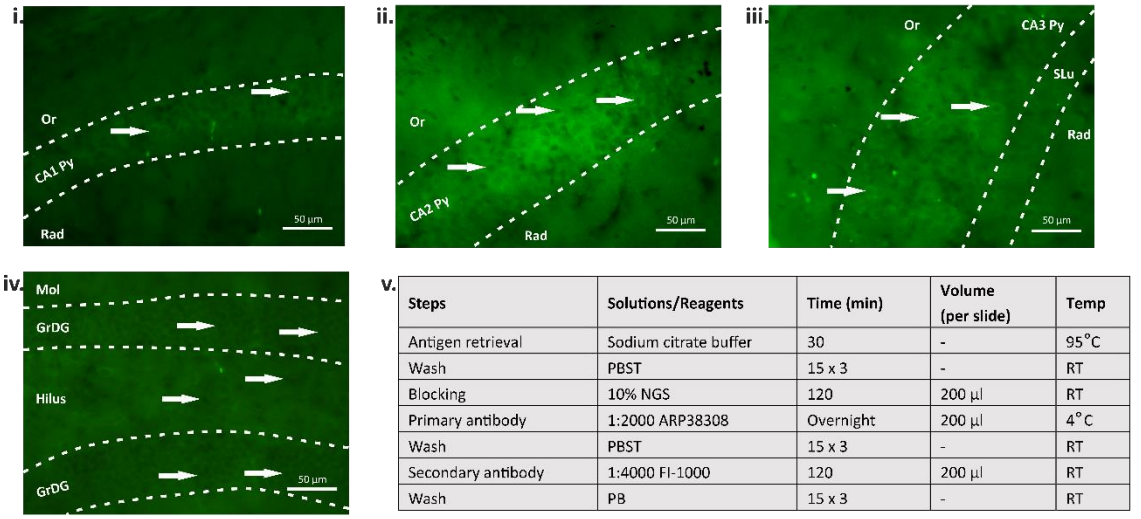

v.

Steps	Solutions/Reagents	Time (min)	Volume (per slide)	Temp
Antigen retrieval	Sodium citrate buffer	30	-	95°C
Wash	PBST	15 x 3	-	RT
Blocking	10% NGS	120	200 µl	RT
Primary antibody	1:2000 ARP38308	Overnight	200 µl	4°C
Wash	PBST	15 x 3	-	RT
Secondary antibody	1:4000 FI-1000	120	200 µl	RT
Wash	PB	15 x 3	-	RT

Figure 4.6 Images of the hippocampal sections after standard and antigen retrieval staining protocols using the anti-Zbtb14 antibody ARP38308. The CA1 **(A-i)**, CA2 **(A-ii)**, CA3 **(A-iii),** and dentate gyrus **(A-iv)** of the hippocampus are shown with the standard staining protocol. The standard protocol is a table following the image **(A-v)**. The CA1 **(B-i)**, CA2 **(B-ii)**, CA3 **(B-iii),** and dentate gyrus **(B-iv)** of the hippocampus are shown under the antigen retrieval staining protocol. The antigen retrieval staining protocol is a table following the image **(B-v)**. The white arrows indicate Zbtb14-stained nuclei. The white arrowheads indicate the Zbtb14-stained astrocytic processes. CA1 Py, pyramidal layer of CA1 field; CA2 Py, pyramidal layer of CA2 field; CA3 Py, pyramidal layer of CA3 field; GrDG, granular layer of the dentate gyrus; Mol, molecular layer of the dentate gyrus; Or, oriens layer of the hippocampus; Rad, stratum radiatum of the hippocampus; SLu, stratum lucidum.

4.1.3.2. Western blot

For the standard WB protocol (Figure 4.7 A-ii), the image of the membrane has several unspecific bands in both tissue extracts, contrary to the datasheet image provided by Aviva Systems Biology (Figure 4.7 A-i).

To reduce or eliminate the unspecific bands, the antibody solutions were prepared in TBS-T containing nonfat milk. The antibody solutions prepared in only TBS-T served as a control. The membranes were incubated overnight with the anti-Zbtb14 antibody ARP38308 at a dilution of 1:2000 in TBS-T or 5% nonfat milk in TBS-T at 4°C. The membranes were incubated for 2 hours with 1:10000 anti-rabbit peroxidase conjugated antibody, AP132P, diluted in TBS-T or 5% nonfat milk in TBS-T at room temperature (Figure 4.7 B-ii and B-iv). Images from Figure 4.7 B-i and B-iii were taken on the same film and exposure. While the membrane incubated with antibody solutions in TBS-T alone had strong bands, the antibody solutions in 5% nonfat milk reduced the signal strength at the same exposure time. However, preparing antibody solutions in 5% nonfat milk in TBS-T did not eliminate all the unspecific bands observed in the brain extracts, but it changed the pattern (Figure 4.7 B-i and B-iii).

For the WB protocol with the ECL reagent RPN2232, the same percentage of gel and transfer method was used as the standard WB protocol. The ECL reagent RPN2232 has increased sensitivity when using higher antibody dilutions, according to the manufacturer's manual. Hence, I reduced the antibody concentration twice for primary and secondary antibody solutions compared to the previous WB protocol. The membranes were incubated overnight with the anti-Zbtb14 antibody ARP38308 at a dilution of 1:4000 in TBS-T at 4°C. The membranes were incubated for 2 hours with 1:40000 anti-rabbit peroxidase conjugated antibody, NA934, diluted in TBS-T at room temperature. The signal was detected using the RPN2232 ECL system (Figure 4.7 C-ii). The changed parameters in the WB protocol with the ECL reagent RPN2232 helped to reduce the number of unspecific bands in the blot image. Nevertheless, I did not observe a 51 kDa band for the Zbtb14 protein in either lane. In the brain extracts two bands were detected, one at 40 kDa and the other above 180 kDa. In the heart extracts, two bands were observed, one between 70 kDa and 100 kDa and the other between 40 kDa and 55 kDa (Figure 4.7 C-i).

A. Standard WB Protocol

i.

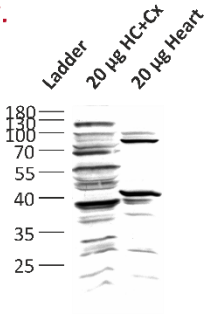

ii.

Western Blot Parameters	Solutions/Reagents	Time (min)	Volume (per membrane)	Temp
Blocking	5% nonfat milk	60	25 ml	RT
Primary antibody	1:500 ARP38308	Overnight	6 ml	4°C
Secondary antibody	1:5000 AP132P	120	6 ml	RT
ECL reagent	RPN2108	2	2 ml	RT

B. The WB Protocol to Compare Antibody Solutions in Nonfat Milk in TBS-T or Only-TBS-T

Antibody Solutions in Only-TBS-T

i.

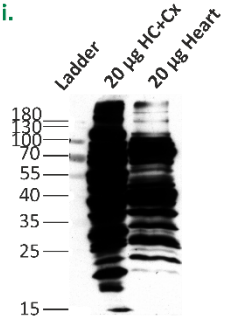

ii.

Western Blot Parameters	Solutions/Reagents	Time (min)	Volume (per membrane)	Temp
Blocking	5% nonfat milk	60	25 ml	RT
Primary antibody	1:2000 ARP38308	Overnight	6 ml	4°C
Secondary antibody	1:10000 ARP38308	120	6 ml	RT
ECL reagent	RPN2108	2	2 ml	RT

Antibody Solutions in Milk in TBS-T

iii.

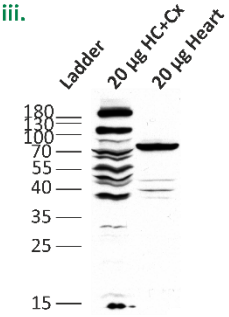

iv.

Western Blot Parameters	Solutions/Reagents	Time (min)	Volume (per membrane)	Temp
Blocking	5% nonfat milk	60	25 ml	RT
Primary antibody	1:2000 ARP38308 in 5% nonfat milk in TBS-T	Overnight	6 ml	4°C
Secondary antibody	1:10000 AP132P in 5% nonfat milk in TBS-T	120	6 ml	RT
ECL reagent	RPN2108	2	2 ml	RT

C. WB Protocol with ECL Reagent RPN2232

i.

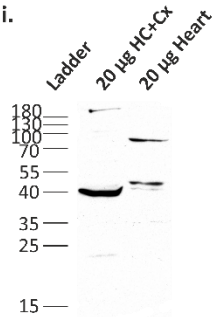

ii.

Western Blot Parameters	Solutions/Reagents	Time (min)	Volume (per membrane)	Temp
Blocking	5% nonfat milk	60	25 ml	RT
Primary antibody	1:4000 ARP38308	Overnight	6 ml	4°C
Secondary antibody	1:40000 NA934	120	6 ml	RT
ECL reagent	RPN2232	2	2 ml	RT

Figure 4.7 Results of the western blots probed against Zbtb14 with ARP38308 antibody using the standard protocol, the protocol to compare antibody solutions in nonfat milk in TBS-T or only TBS-T, and the protocol with the ECL reagent RPN2232. The anti-Zbtb14 antibody ARP38308 was utilised in the standard WB protocol **(A)**, the WB protocol to compare antibody solutions in nonfat milk in TBS-T or only TBS-T **(B)**, and the WB protocol with the ECL reagent RPN2232 **(C)**. The standard WB protocol **(A-ii)**, the WB protocol to compare antibody solutions in milk in TBS-

T or only TBS-T **(B-ii and B-iv)**, and the WB protocol with ECL reagent RPN2232 **(C-ii)** are given in a table next to the images. HC+Cx: hippocampus and cortex; Temp: temperature.

For the WB protocol with the blocking agent RPN2125, the same percentage of gel and transfer method was used as the standard WB protocol. The aim was to check the efficiency of blocking with milk and compare its effect on the blotting pattern to that of the blocking agent RPN2125. Nonspecific sites were blocked with 5% RPN2125 in TBS-T for 1 hour at room temperature. The membranes were incubated overnight with the anti-Zbtb14 antibody ARP38308 at a dilution of 1:4000 in TBS-T at 4°C. The membranes were incubated for 2 hours with 1:40000 anti-rabbit peroxidase conjugated antibody, NA934, diluted in TBS-T at room temperature. The signal was detected using an RPN2232 ECL system (Figure 4.8 B-ii and B-iv). Changing the blocking agent did not improve the blotting. The band at 40 kDa is also present in the primary antibody omitted membrane, which means that this band is an unspecific band due to secondary antibody. In the brain extracts, there were four bands at 40, 55, 70 and 100 kDa. In the heart extracts, there is only one band between 70 and 100 kDa (Figure 4.8 B-i and B-iii).

A. Standard WB Protocol

i.

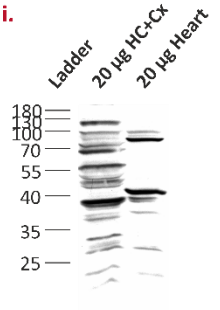

ii.

Western Blot Parameters	Solutions/Reagents	Time (min)	Volume (per membrane)	Temp
Blocking	5% nonfat milk	60	25 ml	RT
Primary antibody	1:500 ARP38308	Overnight	6 ml	4°C
Secondary antibody	1:5000 AP132P	120	6 ml	RT
ECL reagent	RPN2108	2	2 ml	RT

B. WB Protocol with The Blocking Agent RPN2125

i.

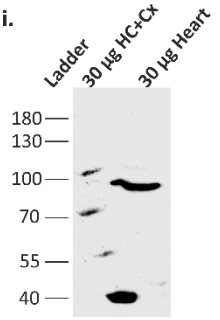

ii.

Western Blot Parameters	Solutions/Reagents	Time (min)	Volume (per membrane)	Temp
Blocking	5% RPN2125 blocking agent	60	25 ml	RT
Primary antibody	1:4000 ARP38308	Overnight	6 ml	4°C
Secondary antibody	1:40000 NA934	120	6 ml	RT
ECL reagent	RPN2232	2	2 ml	RT

iii.

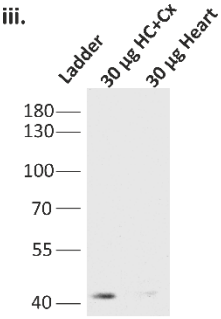

iv.

Western Blot Parameters	Solutions/Reagents	Time (min)	Volume (per membrane)	Temp
Blocking	5% RPN2125 blocking agent	60	25 ml	RT
Primary antibody	No primary	Overnight	6 ml	4°C
Secondary antibody	1:40000 NA934	120	6 ml	RT
ECL reagent	RPN2232	2	2 ml	RT

Figure 4.8 Results of the western blots probed against Zbtb14 with ARP38308 antibody using the standard protocol and protocol with the blocking agent RPN2125. The anti-Zbtb14 antibody ARP38308 was utilised in the standard WB protocol **(A)** and WB protocol with the blocking agent RPN2125 **(B)**. The standard WB protocol **(A-ii)** and the WB protocol with the blocking agent RPN2125 **(B-ii and B-iv)** are given as a table next to the images. HC+Cx: hippocampus and cortex; Temp: temperature.

4.1.4 Sigma-Aldrich, #SAB2106303, anti-ZFP161 antibody produced in rabbit

SAB2106303 is a rabbit polyclonal antibody produced with a synthetic peptide: DDDVEEIGDQDDSPSDDTVEGTPPSQEDGKSPTTTLRVQEAILKELGSEE. This antibody was discontinued during my PhD study.

4.1.4.1 Immunofluorescence

For the standard staining protocol with SAB2106303, a dilution of 1:200 in PBST was used for the primary antibody, and 1:500 in PBST was used for the secondary antibody, FI-1000 (Figure 4.9 A-iv). The standard staining images show that the anti-Zbtb14 antibody SAB2106303 did not give any specific staining. In the CA1 and CA3 pyramidal cell layers, the granular cell layer of dentate gyrus had empty nuclei of cells that morphologically resembled neurons (Figure 4.9 A-i-iii).

Increased primary antibody dilution (1:500) was used to improve the staining-to-background ratio. The FITC-tagged anti-rabbit secondary antibody FI-1000 was diluted to 1:1000 in PBST and incubated for 2 hours at room temperature (Figure 4.9 B-iv). Similar to the standard staining images, I did not observe specific staining. In the CA1 and CA3 pyramidal cell layers, the cells have empty nuclei and morphologically resemble neurons. In addition, the staining had an unspecific dotty pattern across all tissues (Figure 4.9 B-i-iii).

For the antigen retrieval staining protocol, after incubation with sodium citrate buffer on microscope slides, the protocol with increased antibody dilution steps was performed (Figure 4.9 C-iv). The antigen retrieval protocol changed the pattern of staining compared to previous protocols. Cytoplasmic staining was observed in the CA1 and CA3 pyramidal cell layers and the granular cell layer of dentate gyrus. In the hilus, the cells have both nuclear and cytoplasmic staining. These cells morphologically resemble neurons. However, because the antigen retrieval method is damaging the tissue, it was impossible to obtain clear and focused images. I concluded that it is not feasible to use the SAB2106303 antibody to characterise Zbtb14 localisation in the brain.

A. Standard Staining Protocol

i. ii. iii.

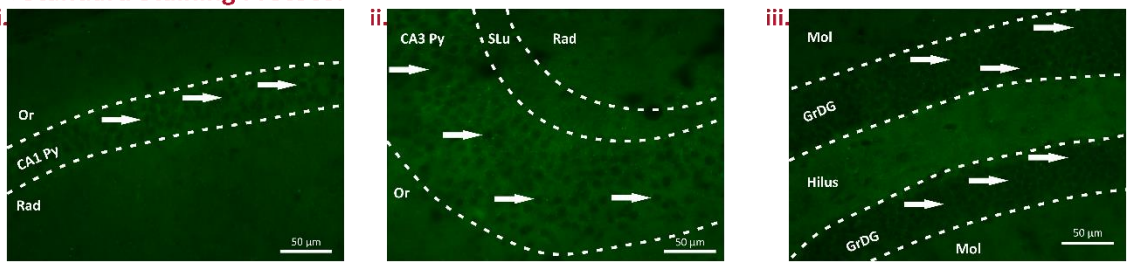

iv.

Steps	Solutions/Reagents	Time (min)	Volume (per well)	Temp
Wash	PBST	15 x 3	500 µl	RT
Blocking	10% NGS	120	300 µl	RT
Primary antibody	1:200 SAB2106303	Overnight	300 µl	4°C
Wash	PBST	15 x 3	500 µl	RT
Secondary antibody	1:500 FI-1000	120	300 µl	RT
Wash	PB	15 x 3	500 µl	RT

B. The Protocol with Increased Antibody Dilutions

i. ii. iii.

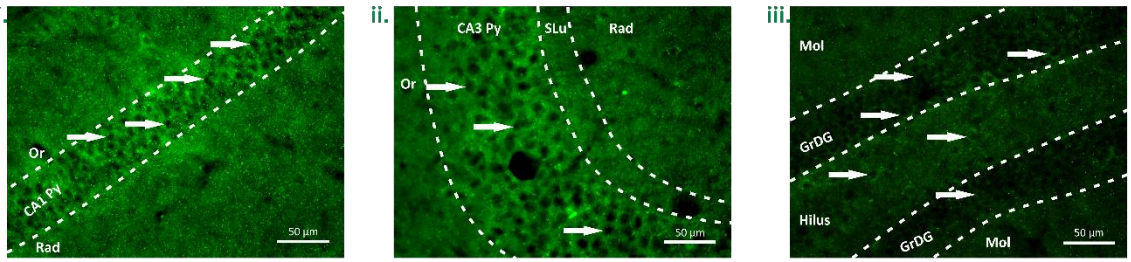

iv.

Steps	Solutions/Reagents	Time (min)	Volume (per well)	Temp
Wash	PBST	15 x 3	500 µl	RT
Blocking	10% NGS	120	300 µl	RT
Primary antibody	1:500 SAB2106303	Overnight	300 µl	4°C
Wash	PBST	15 x 3	500 µl	RT
Secondary antibody	1:1000 FI-1000	120	300 µl	RT
Wash	PB	15 x 3	500 µl	RT

C. The Antigen Retrieval Staining Protocol

i. ii. iii.

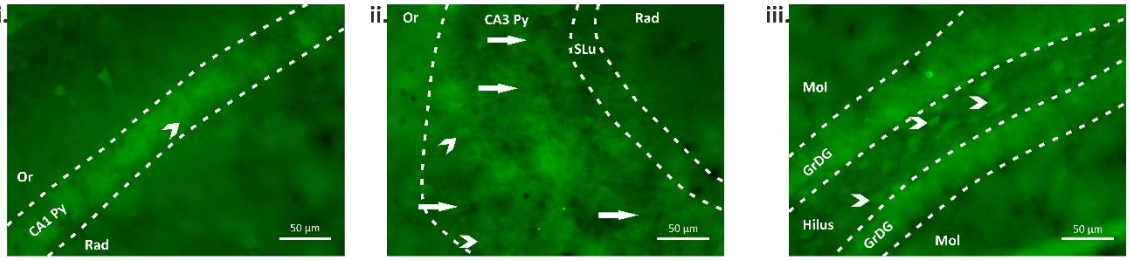

iv.

Steps	Solutions/Reagents	Time (min)	Volume (per slide)	Temp
Antigen retrieval	Sodium citrate buffer	30	-	95°C
Wash	PBST	15 x 3	-	RT
Blocking	10% NGS	120	200 µl	RT
Primary antibody	1:500 SAB2106303	Overnight	200 µl	4°C
Wash	PBST	15 x 3	-	RT
Secondary antibody	1:1000 FI-1000	120	200 µl	RT
Wash	PB	15 x 3	-	RT

Figure 4.9 Images of the hippocampal sections after the standard staining protocol, the protocol with increased antibody dilutions, and the antigen retrieval staining protocol using the anti-Zbtb14 antibody SAB2106303. The CA1 **(A-i)**, CA3 **(A-ii)**, and dentate gyrus **(A-iii)** of the

hippocampus are shown with the standard staining protocol. The standard protocol is a table under the image **(A-iv)**. The CA1 **(B-i)**, CA3 **(B-ii)**, and dentate gyrus **(B-iii)** of the hippocampus are shown under the protocol with increased antibody dilutions. The protocol with increased antibody dilutions is given as a table under the images **(B-iv)**. The CA1 **(C-i)**, CA3 **(C-ii)**, and dentate gyrus **(C-iii)** of the hippocampus are shown under the antigen retrieval staining protocol. The antigen retrieval staining protocol is given as a table under the images **(C-iv)**. The white arrows indicate the empty nuclei of the principal cells. The white arrowheads indicate Zbtb14-positive cells. CA1 Py, pyramidal layer of CA1 field; CA3 Py, pyramidal layer of CA3 field; GrDG, granular layer of the dentate gyrus; Mol, molecular layer of the dentate gyrus; Or, oriens layer of the hippocampus; Rad, stratum radiatum of the hippocampus; SLu, stratum lucidum.

4.1.4.2. Western blot

For the standard WB protocol (Figure 4.10 A-ii), in the heart extracts several bands between 25 and 55 kDa were detected. In the brain extracts, bands between 25 and 70 kDa were observed. I assumed that the faint band below the level of 55 kDa could be the Zbtb14 protein (Figure 4.10 A-i).

For the WB protocol with the ECL reagent RPN2232, the ECL system changed to RPN2232 from RPN2108. The same percentage of gel and transfer method was used as the standard WB protocol. The ECL reagent RPN2232 has increased sensitivity when using higher antibody dilutions according to the manufacturer's manual. Hence, I reduced the antibody concentration by four times for primary and secondary antibody solutions compared to the standard WB protocol. The dilution of the primary antibody was increased to 1:2000 in TBS-T, and the dilution of the secondary antibody was increased to 1:20000 in TBS-T. Primary antibody-omitted control was added to observe any unspecific bands resulting from the secondary antibody (Figure 4.10 B-ii-iv). The changes introduced to the WB revealed that the observed bands were due to secondary antibodies, and SAB2106303 did not detect the Zbtb14 protein.

A. Standard WB Protocol

i.

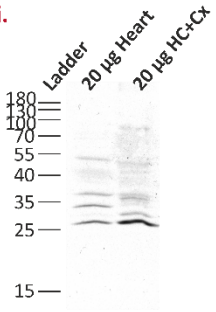

ii.

Western Blot Parameters	Solutions/Reagents	Time (min)	Volume (per membrane)	Temp
Blocking	5% nonfat milk	60	25 ml	RT
Primary antibody	1:500 SAB2106303	Overnight	6 ml	4°C
Secondary antibody	1:5000 AP132P	120	6 ml	RT
ECL reagent	RPN2108	2	2 ml	RT

B. WB Protocol with ECL Reagent RPN2232

Primary antibody-included membrane

i.

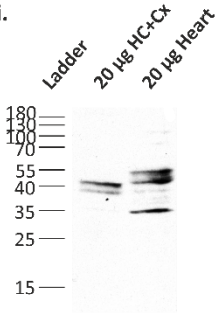

ii.

Western Blot Parameters	Solutions/Reagents	Time (min)	Volume (per membrane)	Temp
Blocking	5% nonfat milk	60	25 ml	RT
Primary antibody	1:2000 SAB2106303	Overnight	6 ml	4°C
Secondary antibody	1:20000 NA934	120	6 ml	RT
ECL reagent	RPN2232	2	2 ml	RT

Primary antibody-omitted membrane

iii.

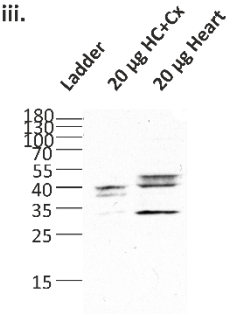

iv.

Western Blot Parameters	Solutions/Reagents	Time (min)	Volume (per membrane)	Temp
Blocking	5% nonfat milk	60	25 ml	RT
Primary antibody	No primary	Overnight	6 ml	4°C
Secondary antibody	1:20000 NA934	120	6 ml	RT
ECL reagent	RPN2232	2	2 ml	RT

Figure 4.10 Results of the western blots probed against Zbtb14 with SAB2106303 antibody using the standard protocol and protocol with the ECL reagent RPN2232. The anti-Zbtb14 antibody SAB2106303 was utilised in the standard WB protocol **(A)** and the WB protocol with the ECL reagent RPN2232 **(B)**. The standard WB protocol **(A-ii)** and the WB protocol with ECL reagent RPN2232 **(B-ii and B-iv)** are given as a table next to the images. HC+Cx: hippocampus and cortex; Temp: temperature.

4.1.5 Atlas antibodies, #HPA070819, polyclonal anti-ZBTB14 antibody

HPA070819 is a rabbit polyclonal antibody produced with a recombinant protein epitope signature tag (PrEST) antigen sequence: DMKFEYLLYGHHREQIACQACGKTFSDEG RLRKHEKLHTADRPCVCEMCTKGFTTQAHLKEH (https://www.atlasantibodies.com/products/antibodies/primary-antibodies/triple-a-polyclonals/zbtb14-antibody-hpa070819/).

3.1.5.1 Immunofluorescence

The standard staining protocol (Figure 4.11 iv) did not give any specific staining and had a high background. The cells that resemble neurons have empty nuclei in the CA1 and CA3 pyramidal cell layers and the granular cell layer of dentate gyrus (Figure 4.11 i-iii).

Standard Staining Protocol

i.

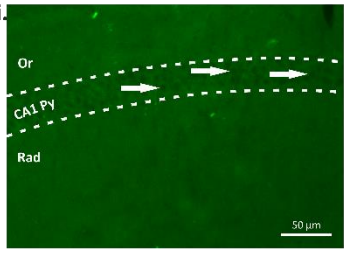

ii.

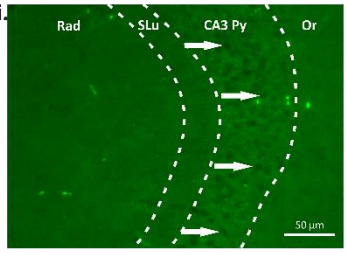

iii.

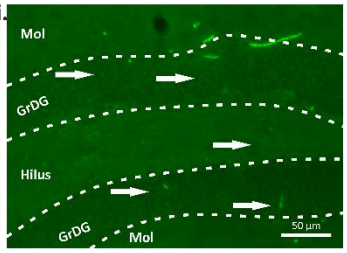

iv.

Steps	Solutions/Reagents	Time (min)	Volume (per well)	Temp
Wash	PBST	15 x 3	500 µl	RT
Blocking	10% NGS	120	300 µl	RT
Primary antibody	1:500 HPA070819	Overnight	300 µl	4°C
Wash	PBST	15 x 3	500 µl	RT
Secondary antibody	1:1000 FI-1000	120	300 µl	RT
Wash	PB	15 x 3	500 µl	RT

Figure 4.11 Images of the hippocampal sections after the standard staining protocol using the anti-Zbtb14 antibody HPA0701819. The CA1 (**i**), CA3 **(ii),** and DG **(iii)** of the hippocampus are shown with the standard staining protocol. The standard protocol is a table under the images **(iv)**. The white arrows indicate the empty nuclei of the principal cells. CA1 Py, pyramidal layer of CA1 field; CA3 Py, pyramidal layer of CA3 field; GrDG, granular layer of the dentate gyrus; Mol, molecular layer of the dentate gyrus; Or, oriens layer of the hippocampus; Rad, stratum radiatum of the hippocampus; SLu, stratum lucidum.

4.1.5.2. Western Blot

For the standard WB protocol, the membranes were incubated overnight with the anti-Zbtb14 antibody HPA070819 at a dilution of 1:2000 in TBS-T at 4°C. The membranes were incubated for 2 hours with 1:20000 anti-rabbit peroxidase conjugated antibody, NA934, diluted in TBS-T at room temperature. The signal was detected using an RPN2232 ECL system (Figure 4.12 A-ii and A-iv). The standard WB membrane image shows that in the brain extracts bands between 35 and 55 kDa and in the heart extracts bands between 35 and 100 kDa were detected. Because the bands between 40 and 55 kDa on the primary antibody-included membrane are also on the primary antibody-omitted membrane, I concluded this is an inconclusive result (Figure 4.12 A-i and A-iii).

For the WB protocol with the blocking agent RPN2125, 5% RPN2125 blocking agent was used instead of 5% nonfat milk to check the efficiency of the blocking. Afterward, the same parameters were used as the standard WB protocol for HPA070819 (Figure 4.12 B-ii and B-iv). The WB protocol with the blocking agent RPN2125 revealed a 100 kDa band in the brain extracts and a 40 kDa band in the heart extracts (Figure 4.12 B-ii and B-iii). When I considered every result from HPA070819, I concluded that the antibody was not detecting Zbtb14 protein in our extracts.

A. Standard WB Protocol

Primary antibody-included membrane

i.

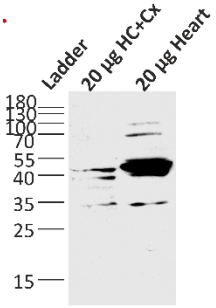

ii.

Western Blot Parameters	Solutions/Reagents	Time (min)	Volume (per membrane)	Temp
Blocking	5% nonfat milk	60	25 ml	RT
Primary antibody	1:2000 HPA070819	Overnight	6 ml	4°C
Secondary antibody	1:20000 NA934	120	6 ml	RT
ECL reagent	RPN2232	2	2 ml	RT

Primary antibody-omitted membrane

iii.

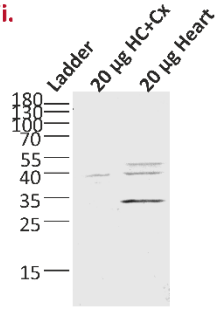

iv.

Western Blot Parameters	Solutions/Reagents	Time (min)	Volume (per membrane)	Temp
Blocking	5% nonfat milk	60	25 ml	RT
Primary antibody	No primary	Overnight	6 ml	4°C
Secondary antibody	1:20000 NA934	120	6 ml	RT
ECL reagent	RPN2232	2	2 ml	RT

B. WB Protocol with Blocking Agent RPN2125

Primary antibody-included membrane

i.

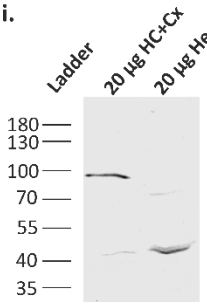

ii.

Western Blot Parameters	Solutions/Reagents	Time (min)	Volume (per membrane)	Temp
Blocking	5% RPN2125	60	25 ml	RT
Primary antibody	1:2000 HPA070819	Overnight	6 ml	4°C
Secondary antibody	1:20000 NA934	120	6 ml	RT
ECL reagent	RPN2232	2	2 ml	RT

Primary antibody-omitted membrane

iii.

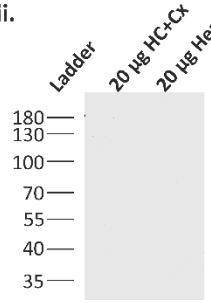

iv.

Western Blot Parameters	Solutions/Reagents	Time (min)	Volume (per membrane)	Temp
Blocking	5% RPN2125	60	25 ml	RT
Primary antibody	No primary	Overnight	6 ml	4°C
Secondary antibody	1:20000 NA934	120	6 ml	RT
ECL reagent	RPN2232	2	2 ml	RT

Figure 4.12 Results of the blots probed against Zbtb14 with HPA070819 antibody using the standard protocol and protocol with the blocking agent RPN2125. The anti-Zbtb14 antibody HPA070819 was utilised in the standard WB protocol **(A)** and WB protocol with the blocking agent RPN2125 **(B)**. The standard WB protocol **(A-ii and A-iv)** and the WB protocol with the

blocking agent RPN2125 **(B-ii and B-iv)** are given as a table next to the images. HC+Cx: hippocampus and cortex; Temp: temperature.

4.1.6 Sigma-Aldrich, #SAB1400299, anti-ZFP161 antibody produced in mouse

SAB1400299 is a mouse polyclonal antibody produced against full-length human protein (NP_003400.2, 1 a.a. ~ 449 a.a.): MEFFISMSETIKYNDDDHKTLFLKTLNEQRLEGEFCDIAIV VEDVKFRAHRCVLAACSTYFKKLFKKLEVDSSSVIEIDFLRSDIFEEVLNYMYTAKISVKKEDVNLMM SSGQILGIRFLDKLCSQKRDVSSPDENNGQSKSKYCLKINRPIGDAADTQDDDVEEIGDQDDSPSD DTVEGTPPSQEDGKSPTTTLRVQEAILKELGSEEVRKVNCYGQEVESMETPESKDLGSQTPQALTF NDGMSEVKDEQTPGWTTAASDMKFEYLLYGHHREQIACQACGKTFSDEGRLRKHEKLHTADRPF VCEMCTKGFTTQAHLKEHLKIHTGYKPYSCEVCGKSFIRAPDLKKHERVHSNERPFACHMCDKAFK HKSHLKDHERRHRGEKPFVCGSCTKAFAKASDLKRHENNHSERKQVTPSAIQSETEQLQAAAMA AEAEQQLETIACS. This antibody was discontinued during my PhD study (https://www.sigma aldrich.com/PL/pl/product/sigma/sab1400299).

3.1.6.1 Immunofluorescence

For the standard staining protocol (Figure 4.13 A-iv), images show that the anti-Zbtb14 antibody did not give any specific staining with a high background. The cells that resemble neurons have empty nuclei in the CA1 and CA3 pyramidal cell layers and the granular cell layer of dentate gyrus (Figure 4.13 A-i-iii).

A mouse-on-mouse (MOM) staining kit was used to reduce background and increase specific binding of anti-mouse primary antibody to the mouse tissue. All steps were performed on the free-floating sections. The sections were washed in 500 µl of PBS. The sections were blocked with 10% NHS in PBS for 1 hour. The primary antibody against Zbtb14 SAB1400299 was diluted to 1:250 in MOM Diluent Working Solution and incubated for 30 minutes at room temperature. The biotinylated anti-mouse secondary antibody BA-2001 was diluted to 1:500 in PBS and incubated for 2 hours at room temperature. The sections were incubated with fluorescein Avidin D A-2001 at a 1:500 dilution in PBS for 20 minutes (Figure 4.13 B-iv). The MOM staining protocol did not improve the staining with SAB1400299. Similar to standard staining with SAB1400299, there was no specific staining, and in the CA1 and CA3 pyramidal cell layers, the granular cell layer of the dentate gyrus had empty nuclei (Figure 4.13 B-i-iii).

For the antigen retrieval staining protocol, after incubation with sodium citrate buffer on microscope slides, the standard staining protocol steps were performed (Figure 4.13 C-iv). The antigen retrieval method did not improve the staining with SAB1400299, and the damage to the tissue due to antigen retrieval made it impossible to obtain a focused and clear image. The cells that resemble neurons have empty nuclei in the CA1 and CA3 pyramidal cell layers and the granular cell layer of dentate gyrus (Figure 4.13 C-i-iii).

A. Standard Staining Protocol

i. 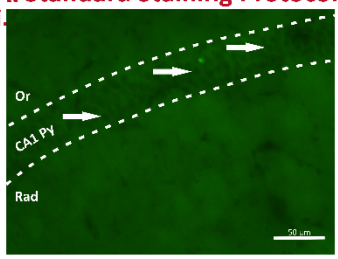

ii. 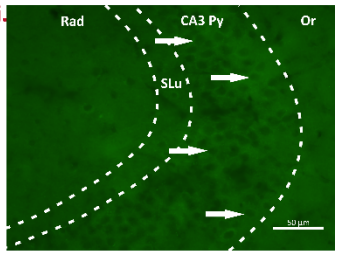

iii. 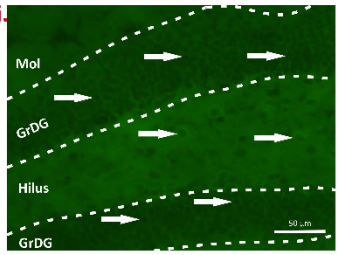

iv.

Steps	Solutions/Reagents	Time (min)	Volume (per well)	Temp
Wash	PBST	15 x 3	500 µl	RT
Blocking	10% NHS	120	300 µl	RT
Primary antibody	1:500 SAB1400299	Overnight	300 µl	4°C
Wash	PBST	15 x 3	500 µl	RT
Secondary antibody	1:1000 BA-2001	120	300 µl	RT
Wash	PBST	15 x 3	500 µl	RT
Fluorescein Avidin D	1:1000 A-2001	20	300 µl	RT
Wash	PB	15 x 3	500 µl	RT

B. The Mouse-on-Mouse (MOM) Kit Staining Protocol

i. 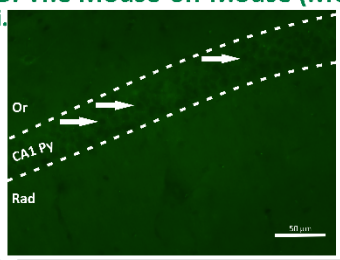

ii. 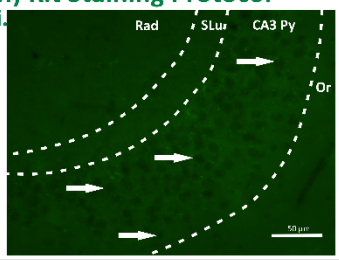

iii. 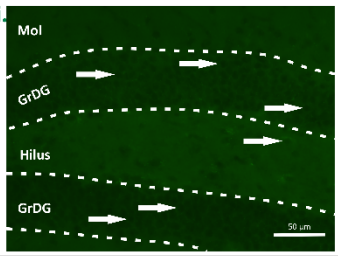

iv.

Steps	Solutions/Reagents	Time (min)	Volume (per well)	Temp
Wash	PBS	15 x 3	500 µl	RT
Blocking	10% NHS	60	300 µl	RT
Wash	PBS	2 x 2	500 µl	RT
MOM Mouse IgG Blocking Reagent	2 drops in 2.5 ml PBS	60	500 µl	RT
Wash	PBS	2 x 2	500 µl	RT
MOM Diluent	600 µl protein concentrate stock solution in 7.5 ml PBS	5	500 µl	RT
Primary antibody	1:250 SAB1400299 in MOM Diluent	30	300 µl	RT
Wash	PBS	2 x 2	500 µl	RT
MOM Biotinylated Anti-Mouse IgG Reagent	10 µl of stock solution in 2.5 ml MOM Diluent	10	500 µl	RT
Wash	PBS	2 x 2	500 µl	RT
Secondary antibody	1:500 BA-2001	120	300 µl	RT
Wash	PBS	15 x 3	500 µl	RT
Fluorescein Avidin D	1:500 A-2001	20	300 µl	RT
Wash	PB	15 x 3	500 µl	RT

C. The Antigen Retrieval Staining Protocol

i. 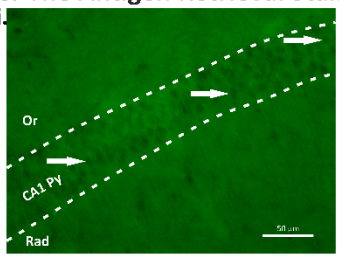

ii. 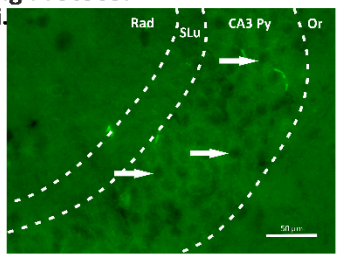

iii. 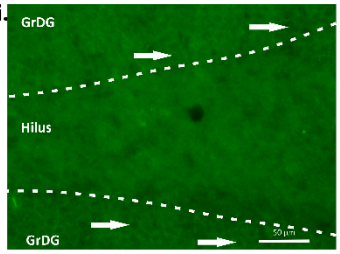

iv.

Steps	Solutions/Reagents	Time (min)	Volume (per slide)	Temp
Antigen retrieval	Sodium citrate buffer	30	-	95°C
Wash	PBST	15 x 3	-	RT
Blocking	10% NHS	120	200 µl	RT
Primary antibody	1:500 SAB2106303	Overnight	200 µl	4°C
Wash	PBST	15 x 3	-	RT
Secondary antibody	1:1000 BA-2001	120	200 µl	RT
Wash	PBST	15 x 3	-	RT
Fluorescein Avidin D	1:1000 A-2001	20	200 µl	RT
Wash	PB	15 x 3	-	RT

Figure 4.13 Images of the hippocampal sections after standard staining, mouse-on-mouse kit staining, and antigen retrieval staining protocol using the anti-Zbtb14 antibody SAB1400299. The CA1 **(A-i)**, CA3 **(A-ii),** and DG **(A-iii)** of the hippocampus are shown with the standard staining protocol. The standard protocol is a table under the images **(A-iv)**. The CA1 **(B-i)**, CA3 **(B-ii),** and

DG **(B-iii)** of the hippocampus are shown with the mouse-on-mouse kit staining protocol. The mouse-on-mouse kit staining protocol is given as a table under the images **(B-iv)**. The CA1 **(C-i)**, CA3 **(C-ii),** and DG **(C-iii)** of the hippocampus are shown with the antigen retrieval staining protocol. The antigen retrieval staining protocol is given as a table under the images **(C-iv)**. The white arrows show some of the empty nuclei of the principal cells in the hippocampal structures, as an example. CA1 Py, pyramidal layer of CA1 field; CA3 Py, pyramidal layer of CA3 field; GrDG, granular layer of the dentate gyrus; Mol, molecular layer of the dentate gyrus; Or, oriens layer of the hippocampus; Rad, stratum radiatum of the hippocampus; SLu, stratum lucidum.

3.1.6.2. Western blot

For the standard WB protocol (Figure 4.14 A-ii), the image shows that both in the brain and heart extracts several bands between 25 and 100 kDa were detected. There is a strong band between 40 and 55 kDa, which can be the Zbtb14 protein (Figure 4.14 A-i).

In the following approach, blocking the nonspecific sites with 5% nonfat milk in TBS-T was compared to 5% blocking reagent RPN2125 in TBS-T. The membranes were incubated overnight with anti-Zbtb14 antibody SAB1400299 at a dilution of 1:4000 in TBS-T at 4°C. The membranes were incubated for 2 hours with 1:40000 anti-mouse peroxidase conjugated antibody, NA931, diluted in TBS-T at room temperature. The signal was detected using an RPN22232 ECL system. A primary antibody-omitted control was added to observe any unspecific bands resulting from the secondary antibody (Figure 4.14 B-ii, B-iv, B-vi, and B-viii). The WB images of nonfat milk as a blocking agent showed that primary antibody-incubated and primary antibody-omitted membranes had the same bands in the brain and heart extracts. This means that the bands observed are not specific to the Zbtb14 antigen. Similarly, the WB images of RPN2125 as a blocking agent did not contain a band at the level of 51 kDa (Figure 4.14 B-i, B-iii, B-v and B-vii). Taken together, I concluded that SAB1400299 does not detect the Zbtb14 protein in our extracts.

A. Standard WB Protocol

i.

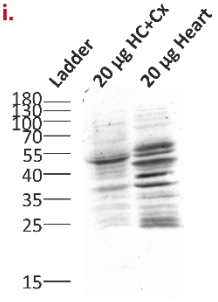

ii.

Western Blot Parameters	Solutions/Reagents	Time (min)	Volume (per membrane)	Temp
Blocking	5% nonfat milk	60	25 ml	RT
Primary antibody	1:500 SAB1400299	Overnight	6 ml	4°C
Secondary antibody	1:5000 PI-2000	120	6 ml	RT
ECL reagent	RPN2108	2	2 ml	RT

B. WB Protocol to Compare 5% nonfat milk and 5% RPN2125 as Blocking Agents

i.

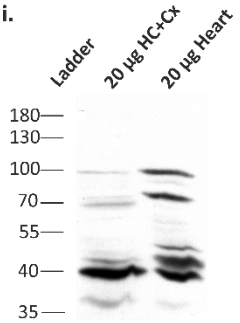

ii.

Western Blot Parameters	Solutions/Reagents	Time (min)	Volume (per membrane)	Temp
Blocking	5% nonfat milk	60	25 ml	RT
Primary antibody	1:4000 SAB1400299	Overnight	6 ml	4°C
Secondary antibody	1:40000 NA931	120	6 ml	RT
ECL reagent	RPN2232	2	2 ml	RT

iii.

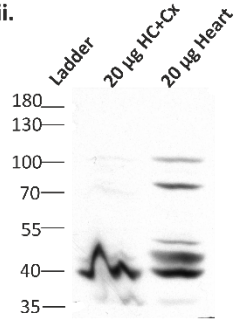

iv.

Western Blot Parameters	Solutions/Reagents	Time (min)	Volume (per membrane)	Temp
Blocking	5% nonfat milk	60	25 ml	RT
Primary antibody	No primary	Overnight	6 ml	4°C
Secondary antibody	1:40000 NA931	120	6 ml	RT
ECL reagent	RPN2232	2	2 ml	RT

v.

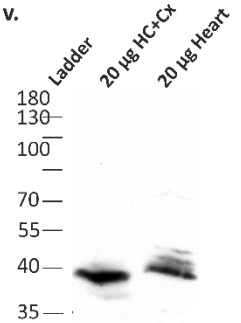

vi.

Western Blot Parameters	Solutions/Reagents	Time (min)	Volume (per membrane)	Temp
Blocking	5% RPN2125	60	25 ml	RT
Primary antibody	1:4000 SAB1400299	Overnight	6 ml	4°C
Secondary antibody	1:40000 NA931	120	6 ml	RT
ECL reagent	RPN2232	2	2 ml	RT

vii.

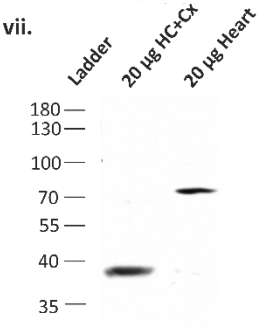

viii.

Western Blot Parameters	Solutions/Reagents	Time (min)	Volume (per membrane)	Temp
Blocking	5% RPN2125	60	25 ml	RT
Primary antibody	No primary	Overnight	6 ml	4°C
Secondary antibody	1:40000 NA931	120	6 ml	RT
ECL reagent	RPN2232	2	2 ml	RT

Figure 4.14 Results of the western blots probed against Zbtb14 with SAB1400299 antibody using the standard protocol and protocol to compare 5% nonfat milk and 5% RPN2125 as blocking agents. The anti-Zbtb14 antibody SAB1400299 was utilised in the standard WB protocol **(A)** and WB protocol to compare 5% nonfat milk and 5% RPN2125 as blocking agents **(B)**. The standard

WB protocol **(A-ii and A-iv)** and the WB protocol to compare 5% nonfat milk and 5% RPN2125 as blocking agents **(B-ii, B-iv, B-vi, and B-viii)** are given in a table following the WB images. HC+Cx: hippocampus and cortex; Temp: temperature.

4.1.7 Sigma–Aldrich, #SAB1402396, monoclonal anti-ZFP161 antibody produced in mice

SAB1402396 is a mouse monoclonal antibody produced in mouse clone 4F7 using a partial recombinant protein with a GST tag (NP_003400.2, 311 a.a. ~ 420 a.a.). The molecular weight of the GST tag alone is 26 kDa. The sequence of the partial recombinant protein was TKGFTTQAHLKEHLKIHTGYKPYSCEVCGKSFIRAPDLKKHERVHSN ERPFACHMCDKAFKHKSHLKDHERHRGEKPFVCGSCTKAFAKASDLKRHENNMHSERKQVTP. This antibody was discontinued during my PhD study (https://www.sigmaaldrich.com/PL/pl/product/sigma/sab1402396).

4.1.7.1 Immunofluorescence

For the standard staining protocol, all steps were performed on the free-floating sections. The primary antibody against Zbtb14 SAB1402396 was diluted to 1:250 in PBST and incubated overnight at 4°C. The biotinylated anti-mouse secondary antibody BA-2001 was diluted to 1:500 in PBST and incubated for 2 hours at room temperature (Figure 4.15 A-iv). The standard staining with SAB1402396 shows that the anti-Zbtb14 antibody did not give any specific staining and had a high background. Empty nuclei of the cells were observed in the CA1 and CA3 pyramidal cell layers and the granular cell layer of dentate gyrus (Figure 4.15 A-i-iii).

A mouse-on-mouse (MOM) staining kit was used to reduce background and increase specific binding of anti-mouse primary antibody to the mouse tissue. All steps were performed on the free-floating sections. The sections were washed in 500 µl of PBS. The sections were blocked with 10% NHS in PBS for 1 hour. The primary antibody against Zbtb14 SAB1402396 was diluted to 1:250 in MOM Diluent Working Solution and incubated for 30 minutes at room temperature. The biotinylated anti-mouse secondary antibody BA-2001 was diluted to 1:500 in PBS and incubated for 2 hours at room temperature. The sections were incubated with fluorescein Avidin D A-2001 at a 1:500 dilution in PBS for 20 minutes (Figure 4.15 B-iv). The MOM staining protocol did not

improve the staining with SAB1402396. Similar to the standard staining with SAB1402396, there was no specific staining in the CA1 and CA3 pyramidal cell layers or the DG granular cell layer. The empty nuclei of the cells are observed on the hippocampal structures (Figure 4.15 B-i-iii).

For the antigen retrieval staining protocol, after incubation with sodium citrate buffer on microscope slides, the sections were blocked with 10% NHS in PBST for 2 hours. The primary antibody against Zbtb14 SAB1402396 was diluted to 1:500 in PBST and incubated overnight at 4°C. The biotinylated anti-mouse secondary antibody BA-2001 was diluted to 1:1000 in PBST and incubated for 2 hours at room temperature. The sections were incubated with fluorescein Avidin D A-2001 at a 1:1000 dilution in PBST for 20 minutes (Figure 4.15 C-iv). The antigen retrieval method did not improve the staining with SAB1402396, and the damage to tissue due to antigen retrieval made it impossible to obtain a focused and clear image (Figure 4.15 C-i-iii).

A. Standard Staining Protocol

i. ii. iii.

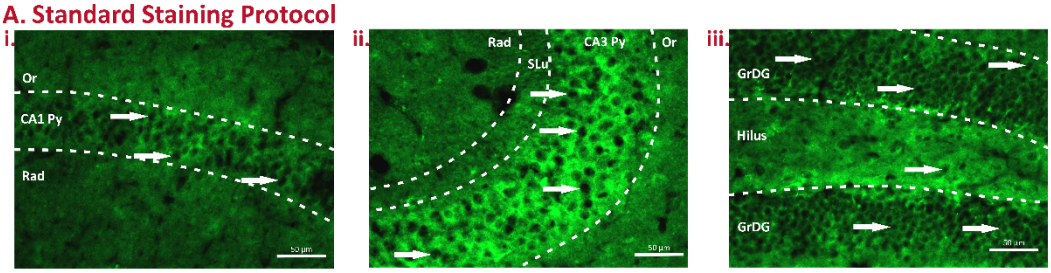

iv.

Steps	Solutions/Reagents	Time (min)	Volume (per well)	Temp
Wash	PBST	15 x 3	500 µl	RT
Blocking	10% NHS	120	300 µl	RT
Primary antibody	1:250 SAB1402396	Overnight	300 µl	4°C
Wash	PBST	15 x 3	500 µl	RT
Secondary antibody	1:500 BA-2001	120	300 µl	RT
Wash	PBST	15 x 3	500 µl	RT
Fluorescein Avidin D	1:500 A-2001	20	300 µl	RT
Wash	PB	15 x 3	500 µl	RT

B. The Mouse-on-Mouse (MOM) Kit Staining Protocol

i. ii. iii.

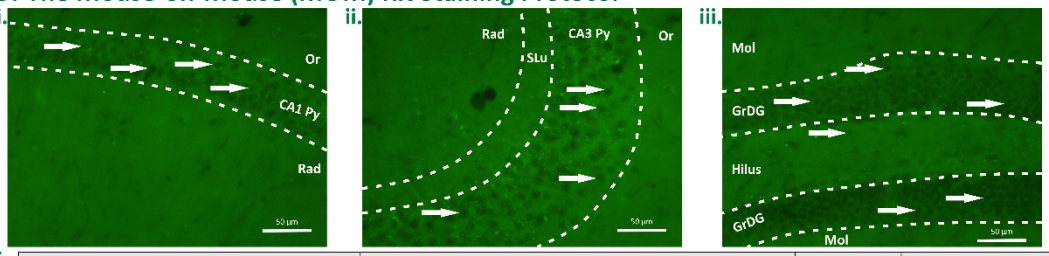

iv.

Steps	Solutions/Reagents	Time (min)	Volume (per well)	Temp
Wash	PBS	15 x 3	500 µl	RT
Blocking	10% NHS	60	300 µl	RT
Wash	PBS	2 x 2	500 µl	RT
MOM Mouse IgG Blocking Reagent	2 drops in 2.5 ml PBS	60	500 µl	RT
Wash	PBS	2 x 2	500 µl	RT
MOM Diluent	600 µl protein concentrate stock solution in 7.5 ml PBS	5	500 µl	RT
Primary antibody	1:250 SAB1402396 in MOM Diluent	30	300 µl	RT
Wash	PBS	2 x 2	500 µl	RT
MOM Biotinylated Anti-Mouse IgG Reagent	10 µl of stock solution in 2.5 ml MOM Diluent	10	500 µl	RT
Wash	PBS	2 x 2	500 µl	RT
Secondary antibody	1:500 BA-2001	120	300 µl	RT
Wash	PBS	15 x 3	500 µl	RT
Fluorescein Avidin D	1:500 A-2001	20	300 µl	RT
Wash	PB	15 x 3	500 µl	RT

C. The Antigen Retrieval Staining Protocol

i. ii. iii.

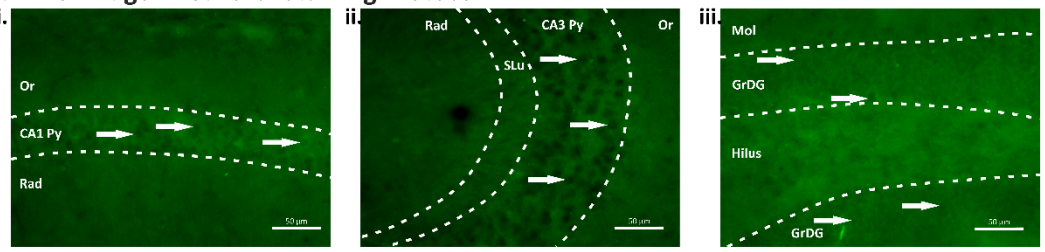

iv.

Steps	Solutions/Reagents	Time (min)	Volume (per slide)	Temp
Antigen retrieval	Sodium citrate buffer	30	-	95°C
Wash	PBST	15 x 3	-	RT
Blocking	10% NHS	120	200 µl	RT
Primary antibody	1:500 SAB1402396	Overnight	200 µl	4°C
Wash	PBST	15 x 3	-	RT
Secondary antibody	1:1000 BA-2001	120	200 µl	RT
Wash	PBST	15 x 3	-	RT
Fluorescein Avidin D	1:1000 A-2001	20	200 µl	RT
Wash	PB	15 x 3	-	RT

Figure 4.15 Images of the hippocampal sections after standard staining, mouse-on-mouse kit staining, and antigen retrieval staining protocol using the anti-Zbtb14 antibody SAB1402396. The CA1 **(A-i)**, CA3 **(A-ii),** and DG **(A-iii)** of the hippocampus are shown with the standard staining protocol. The standard protocol is a table under the images **(A-iv)**. The CA1 **(B-i)**, CA3 **(B-ii),** and DG **(B-iii)** of the hippocampus are shown with the mouse-on-mouse kit staining protocol. The

mouse-on-mouse kit staining protocol is given as a table under the images **(B-iv)**. The CA1 **(C-i)**, CA3 **(C-ii),** and DG **(C-iii)** of the hippocampus are shown with the antigen retrieval staining protocol. The antigen retrieval staining protocol is given as a table under the images **(C-iv)**. The white arrows show some of the empty nuclei of the principal cells in the hippocampal structures, as an example. CA1 Py, pyramidal layer of CA1 field; CA3 Py, pyramidal layer of CA3 field; GrDG, granular layer of the dentate gyrus; Mol, molecular layer of the dentate gyrus; Or, oriens layer of the hippocampus; Rad, stratum radiatum of the hippocampus; SLu, stratum lucidum.

4.1.7.2. Western blot

The standard WB protocol (Figure 4.16 A-ii) membrane image shows that both the brain and heart extracts several bands between 25 and 100 kDa were detected. There are bands between 40 and 55 kDa, which might be the Zbtb14 protein (Figure 4.16 A-i).

In the following approach, to reduce nonspecific binding, 5% nonfat milk in TBS-T was used in the antibody solutions. The antibody solutions prepared in only TBS-T served as a control. The membranes were incubated overnight with the anti-Zbtb14 antibody SAB1402396 at a dilution of 1:2000 in TBS-T or 5% nonfat milk in TBS-T at 4°C. The membranes were incubated for 2 hours with 1:10000 anti-mouse peroxidase conjugated antibody, PI-2000, diluted in TBS-T or 5% nonfat milk in TBS-T at room temperature (Figure 4.16 B-ii and B-iv). Images from Figure 4.16 B-i and B-iii were taken on the same film and exposure. While the membrane incubated with antibody solutions in only TBS-T had strong bands, the preparation of antibody solutions in 5% nonfat milk had no signal at the same exposure time (Figure 4.16 B-i and B-iii).

A. Standard WB Protocol

i.

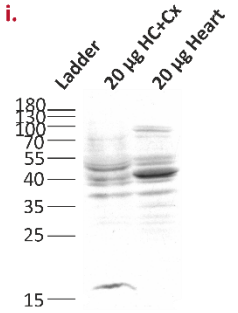

ii.

Western Blot Parameters	Solutions/Reagents	Time (min)	Volume (per membrane)	Temp
Blocking	5% nonfat milk	60	25 ml	RT
Primary antibody	1:500 SAB1402396	Overnight	6 ml	4°C
Secondary antibody	1:5000 PI-2000	120	6 ml	RT
ECL reagent	RPN2108	2	2 ml	RT

B. The WB Protocol to Compare Antibody Solutions in Nonfat Milk in TBS-T or Only-TBS-T

Antibody Solutions in Only-TBS-T

i.

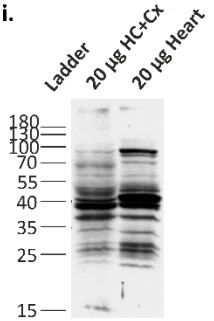

ii.

Western Blot Parameters	Solutions/Reagents	Time (min)	Volume (per membrane)	Temp
Blocking	5% nonfat milk	60	25 ml	RT
Primary antibody	1:2000 SAB1402396	Overnight	6 ml	4°C
Secondary antibody	1:10000 PI-2000	120	6 ml	RT
ECL reagent	RPN2108	2	2 ml	RT

Antibody Solutions in Milk in TBS-T

iii.

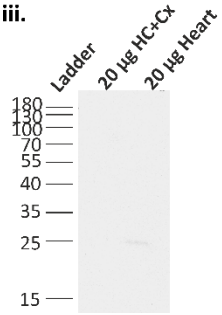

iv.

Western Blot Parameters	Solutions/Reagents	Time (min)	Volume (per membrane)	Temp
Blocking	5% nonfat milk	60	25 ml	RT
Primary antibody	1:2000 SAB1402396 in 5% nonfat milk	Overnight	6 ml	4°C
Secondary antibody	1:10000 PI-2000 in 5% nonfat milk	120	6 ml	RT
ECL reagent	RPN2108	2	2 ml	RT

Figure 4.16 Results of the western blots probed against Zbtb14 with SAB1402396 antibody using the standard protocol and protocol to compare antibody solutions in nonfat milk in TBS-T or only TBS-T. The anti-Zbtb14 antibody SAB1402396 was utilised in the standard WB protocol **(A)** and WB protocol to compare antibody solutions in nonfat milk in TBS-T or only TBS-T **(B)**. The standard WB protocol **(A-ii and A-iv)** and the WB protocol to compare antibody solutions in nonfat milk in TBS-T or only TBS-T **(B-ii and B-iv)** are given as a table following the WB images. HC+Cx: hippocampus and cortex; Temp: temperature.

Next, the efficiency of blocking with 5% nonfat milk was compared to that of blocking with 5% RPN2125. Nonspecific sites were blocked with 5% nonfat milk in TBS-T or 5% blocking reagent RPN2125 in TBS-T for 1 hour at room temperature. The membranes were incubated overnight with the anti-Zbtb14 antibody SAB1402396 at a dilution of 1:4000 in TBS-T at 4°C. The membranes were incubated for 2 hours with 1:40000 anti-

mouse peroxidase conjugated antibody, NA931, diluted in TBS-T at room temperature. The signal was detected using an RPN22232 ECL system. A primary antibody-omitted control was added to observe any unspecific bands resulting from the secondary antibody (Figure 4.17 B-ii, B-iv, B-vi, and B-viii). The WB images of nonfat milk as a blocking agent showed that primary antibody-incubated and primary antibody-omitted membranes had the same bands on the brain and heart extracts. This means that the bands observed are not specific to the Zbtb14 antigen. Similarly, in the WB images of RPN2125 as a blocking agent, I did not observe a band at the level of 51 kDa (Figure 4.17 B-i, B-iii, B-v and B-vii). Taken together, I concluded that SAB1402396 does not detect the Zbtb14 protein in our extracts.

A. Standard WB Protocol

i.

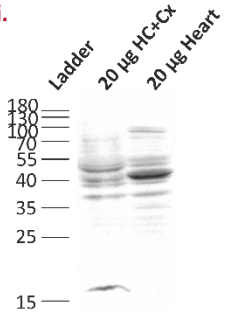

ii.

Western Blot Parameters	Solutions/Reagents	Time (min)	Volume (per membrane)	Temp
Blocking	5% nonfat milk	60	25 ml	RT
Primary antibody	1:500 SAB1402396	Overnight	6 ml	4°C
Secondary antibody	1:5000 PI-2000	120	6 ml	RT
ECL reagent	RPN2108	2	2 ml	RT

B. WB Protocol to Compare 5% nonfat milk and 5% RPN2125 as Blocking Agents

i.

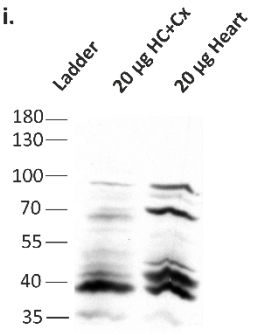

ii.

Western Blot Parameters	Solutions/Reagents	Time (min)	Volume (per membrane)	Temp
Blocking	5% nonfat milk	60	25 ml	RT
Primary antibody	1:4000 SAB1402396	Overnight	6 ml	4°C
Secondary antibody	1:40000 NA931	120	6 ml	RT
ECL reagent	RPN2232	2	2 ml	RT

iii.

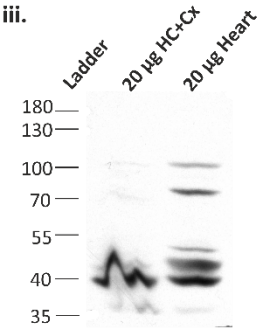

iv.

Western Blot Parameters	Solutions/Reagents	Time (min)	Volume (per membrane)	Temp
Blocking	5% nonfat milk	60	25 ml	RT
Primary antibody	No primary	Overnight	6 ml	4°C
Secondary antibody	1:40000 NA931	120	6 ml	RT
ECL reagent	RPN2232	2	2 ml	RT

v.

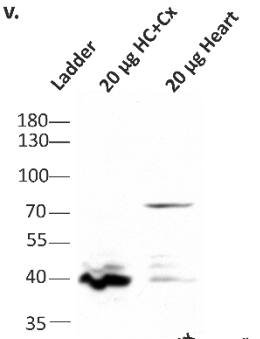

vi.

Western Blot Parameters	Solutions/Reagents	Time (min)	Volume (per membrane)	Temp
Blocking	5% RPN2125	60	25 ml	RT
Primary antibody	1:4000 SAB1402396	Overnight	6 ml	4°C
Secondary antibody	1:40000 NA931	120	6 ml	RT
ECL reagent	RPN2232	2	2 ml	RT

vii.

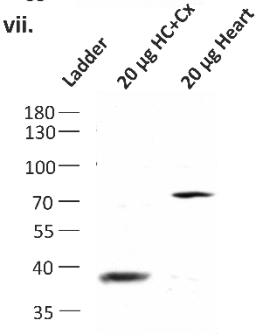

viii.

Western Blot Parameters	Solutions/Reagents	Time (min)	Volume (per membrane)	Temp
Blocking	5% RPN2125	60	25 ml	RT
Primary antibody	No primary	Overnight	6 ml	4°C
Secondary antibody	1:40000 NA931	120	6 ml	RT
ECL reagent	RPN2232	2	2 ml	RT

Figure 4.17 Results of the western blots probed against Zbtb14 with SAB1402396 antibody using a standard protocol and a protocol to compare 5% nonfat milk and 5% RPN2125 as blocking

agents. The anti-Zbtb14 antibody SAB1402396 was utilised in the standard WB protocol **(A)** and WB protocol to compare 5% nonfat milk and 5% RPN2125 as blocking agents **(B)**. The standard WB protocol **(A-ii and A-iv)** and the WB protocol to compare 5% nonfat milk and 5% RPN2125 as blocking agents **(B-ii, B-iv, B-vi, and B-viii)** are given in a table following the WB images. HC+Cx: hippocampus and cortex; Temp: temperature.

4.1.8 Santa cruz biotechnology, #sc-514298, anti-ZFP161 antibody (C-4)

sc-514298 (C-4) is a mouse monoclonal antibody raised against amino acids 150-449 mapping at the C-terminus of ZFP161 of human origin (https://www.scbt.com/p/zfp161-antibody-c-4).

4.1.8.1 Immunofluorescence

A mouse-on-mouse (MOM) staining kit was used to reduce background and increase specific binding of anti-mouse primary antibody to the mouse tissue. All steps were performed on the free-floating sections. The sections were washed in 500 µl of PBS. The sections were blocked with 10% NHS in PBS for 1 hour. The primary antibody against Zbtb14 sc-514298 was diluted to 1:500 in MOM Diluent Working Solution and incubated for 30 minutes at room temperature. The biotinylated anti-mouse secondary antibody BA-2001 was diluted to 1:1000 in PBS and incubated for 2 hours at room temperature. The sections were incubated with fluorescein Avidin D A-2001 at a 1:1000 dilution in PBS for 20 minutes (Figure 4.18 A-iv). The MOM staining protocol with sc-514298 gave no specific staining in the CA1 and CA3 pyramidal cell layers and the granular cell layer of dentate gyrus. The empty nuclei of the cells are observed on the hippocampal structures (Figure 4.18 A-i-iii).

For the antigen retrieval staining protocol, after incubation with sodium citrate buffer on microscope slides, staining with sc-514298 was carried out with the same blocking, primary and secondary antibody dilutions (Figure 4.18 B-iv). The antigen retrieval method improved the staining with sc-514298. Nuclear staining was observed in the CA1 pyramidal cell layer and the granular cell layer of dentate gyrus. Nevertheless, the antigen retrieval protocol caused significant damage to the tissue that can be seen in the CA3 subfield of the hippocampus, making it impossible to obtain a focused and clear image of the staining (Figure 4.18 B-i-iii).

For the staining protocol with fresh tissue following acetone fixation, the sections were fixed with ice-cold acetone for 10 minutes and blocked with 10% NHS in PBST for 90 minutes on microscope slides. The primary antibody against Zbtb14 sc-514298 was diluted to 1:100 in PBST and incubated overnight at 4°C. The biotinylated anti-mouse secondary antibody AP192P was diluted to 1:200 in PBST and incubated for 2 hours at room temperature. The sections were incubated with fluorescein Avidin D A-2001 at a 1:100 dilution in PBST for 20 minutes (Figure 4.18 C-iv). The images from the fresh frozen tissue staining method have nuclear staining with sc-514298 in the CA1, CA3 and DG of the hippocampus. (Figure 4.18 C-i-iii).

A. The Staining Protocol with Mouse-on-Mouse (MOM) Kit

i. ii. iii.

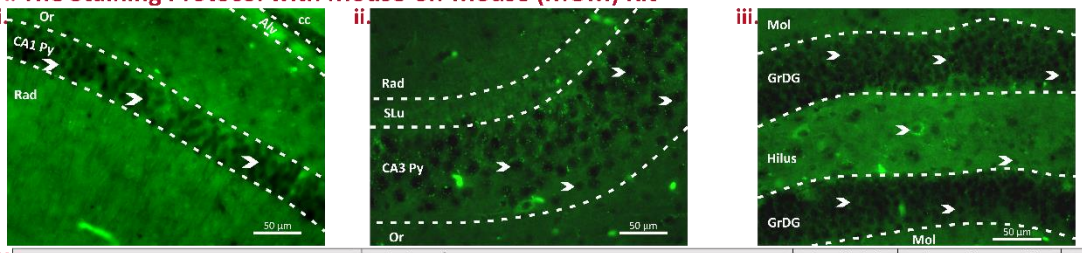

iv.

Steps	Solutions/Reagents	Time (min)	Volume (per well)	Temp
Wash	PBS	15 x 3	500 µl	RT
Blocking	10% NHS	60	300 µl	RT
Wash	PBS	2 x 2	500 µl	RT
MOM Mouse IgG Blocking Reagent	2 drops in 2.5 ml PBS	60	500 µl	RT
Wash	PBS	2 x 2	500 µl	RT
MOM Diluent	600 µl protein concentrate stock solution in 7.5 ml PBS	5	500 µl	RT
Primary antibody	1:500 sc-514298 in MOM Diluent	30	300 µl	RT
Wash	PBS	2 x 2	500 µl	RT
MOM Biotinylated Anti -Mouse IgG Reagent	10 µl of stock solution in 2.5 ml MOM Diluent	10	500 µl	RT
Wash	PBS	2 x 2	500 µl	RT
Secondary antibody	1:1000 BA-2001	120	300 µl	RT
Wash	PBS	15 x 3	500 µl	RT
Fluorescein Avidin D	1:1000 A-2001	20	300 µl	RT
Wash	PB	15 x 3	500 µl	RT

B. The Antigen Retrieval Staining Protocol

i. ii. iii.

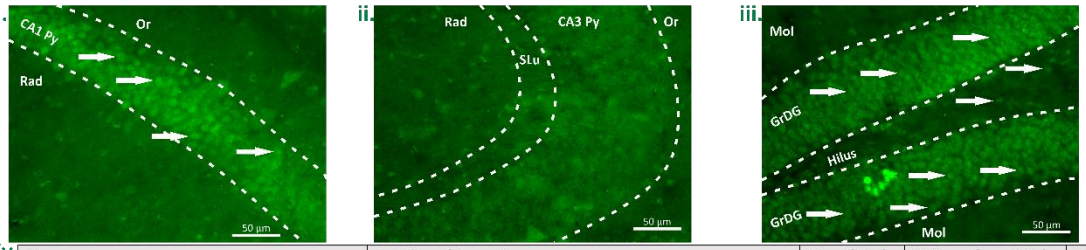

iv.

Steps	Solutions/Reagents	Time (min)	Volume (per slide)	Temp
Antigen retrieval	Sodium citrate buffer	30	-	95°C
Wash	PBST	15 x 3	-	RT
Blocking	10% NHS	120	200 µl	RT
Primary antibody	1:500 sc-514298	Overnight	200 µl	4°C
Wash	PBST	15 x 3	-	RT
Secondary antibody	1:1000 BA-2001	120	200 µl	RT
Wash	PBST	15 x 3	-	RT
Fluorescein Avidin D	1:1000 A-2001	20	200 µl	RT
Wash	PB	15 x 3	-	RT

C. The Staining Protocol with Fresh Tissue Following Acetone Fixation

i. ii. iii.

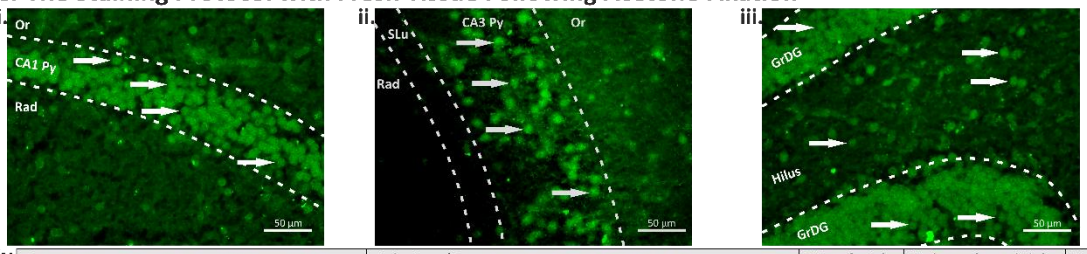

iv.

Steps	Solutions/Reagents	Time (min)	Volume (per slide)	Temp
Fixation	Acetone pure	10	-	4°C
Wash	PBST	5 x 3	-	RT
Blocking	10% NDS	90	200 µl	RT
Primary antibody	1:100 sc-514298	Overnight	200 µl	4°C
Wash	PBST	5 x 3	-	RT
Secondary antibody	1:200 AP192P	120	200 µl	RT
Wash	PBST	5 x 3	-	RT
Fluorescein Avidin D	1:100 A-2001	20	200 µl	RT
Wash	PBS	5 x 3	-	RT

Figure 4.18 Images of the hippocampal sections after the mouse-on-mouse kit staining protocol, the antigen retrieval staining protocol, and the staining protocol with fresh tissue following acetone fixation using anti-Zbtb14 antibody, sc-514298. The CA1 **(A-i)**, CA3 **(A-ii),** and DG **(A-iii)** of the hippocampus are shown with the mouse-on-mouse kit staining protocol. The mouse-on-mouse kit staining protocol is given as a table under the images **(A-iv)**. The CA1 **(B-i)**, CA3 **(B-ii),**

and DG **(B-iii)** of the hippocampus are shown with the antigen retrieval staining protocol. The antigen retrieval staining protocol is given as a table under the images **(B-iv)**. The CA1 **(C-i)**, CA3 **(C-ii),** and DG **(C-iii)** of the hippocampus are shown with the staining protocol with fresh tissue following acetone fixation. The staining protocol with fresh tissue following acetone fixation is given as a table under the images **(C-iv)**. The white arrows indicate Zbtb14-positive cells. The white arrowheads indicate the empty nuclei of the principal cells. Alv, alveus; CA1 Py, pyramidal layer of CA1 field; CA3 Py, pyramidal layer of CA3 field; cc, corpus callosum; GrDG, granular layer of the dentate gyrus; Mol, molecular layer of the dentate gyrus; Or, oriens layer of the hippocampus; Rad, stratum radiatum of the hippocampus; SLu, stratum lucidum.

4.1.8.2. Western blot

For the standard WB protocol (Figure 4.19 A-ii), the membrane image shows that both in the brain and heart extracts several bands between 35 and 55 kDa were observed. In the brain extracts a strong ~55 kDa band was detected, which might be the Zbtb14 protein, and in the heart extracts the same band was also detected but the band was fainter (Figure 4.19 A-i).

The aim was to reduce or eliminate the unspecific bands by preparing antibody solutions in milk in TBS-T for the WB protocol to compare antibody solutions in nonfat milk in TBS-T or only TBS-T. The antibody solutions prepared in only TBS-T served as a control. The membranes were incubated overnight with the anti-Zbtb14 antibody sc-514298 at a dilution of 1:4000 in TBS-T or 1:2000 in 5% nonfat milk in TBS-T at 4°C. The membranes were incubated for 2 hours with 1:40000 anti-mouse peroxidase conjugated antibody, NA931, diluted in TBS-T or 1:20000 anti-mouse peroxidase conjugated antibody, NA931, diluted in 5% nonfat milk in TBS-T at room temperature. The signal was detected using an RPN2232 ECL system (Figure 4.19 B-ii and B-iv). All images from Figure 4.19 B were taken on the same film and exposure. The primary antibody-containing membrane with antibody solutions prepared in TBS-T alone has similar bands, a ~55 kDa band that is Zbtb14 specific and a 40 kDa band that does not specifically bind the secondary antibody. However, the membranes with antibody solutions prepared in nonfat milk in TBS-T showed no bands. The preparation of antibody solutions did not improve the images but blocked all the signals (Figure 4.19 B-i and B-iii). Hence, I can conclude that nonfat milk in antibody solutions blocks antibody binding to the membranes.

A. Standard WB Protocol

i.

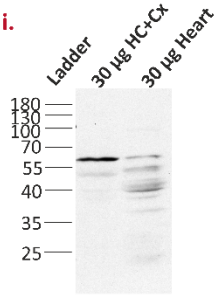

ii.

Western Blot Parameters	Solutions/Reagents	Time (min)	Volume (per membrane)	Temp
Blocking	5% nonfat milk	60	25 ml	RT
Primary antibody	1:500 sc-514298	Overnight	6 ml	4°C
Secondary antibody	1:5000 PI-2000	120	6 ml	RT
ECL reagent	RPN2108	2	2 ml	RT

B. The WB Protocol to Compare Antibody Solutions in Nonfat Milk in TBS-T or Only-TBS-T

i.

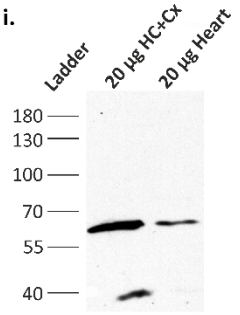

ii.

Western Blot Parameters	Solutions/Reagents	Time (min)	Volume (per membrane)	Temp
Blocking	5% nonfat milk	60	25 ml	RT
Primary antibody	1:4000 sc-514298	Overnight	6 ml	4°C
Secondary antibody	1:40000 NA931	120	6 ml	RT
ECL reagent	RPN2232	2	2 ml	RT

iii.

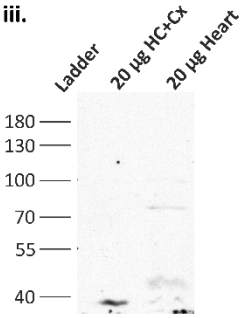

iv.

Western Blot Parameters	Solutions/Reagents	Time (min)	Volume (per membrane)	Temp
Blocking	5% nonfat milk	60	25 ml	RT
Primary antibody	No primary	Overnight	6 ml	4°C
Secondary antibody	1:40000 NA931	120	6 ml	RT
ECL reagent	RPN2232	2	2 ml	RT

v.

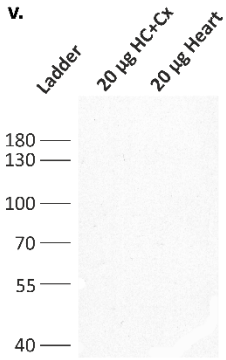

vi.

Western Blot Parameters	Solutions/Reagents	Time (min)	Volume (per membrane)	Temp
Blocking	5% nonfat milk	60	25 ml	RT
Primary antibody	1:2000 sc-514298 in 5% nonfat milk	Overnight	6 ml	4°C
Secondary antibody	1:20000 NA931 in 5% nonfat milk	120	6 ml	RT
ECL reagent	RPN2232	2	2 ml	RT

vii.

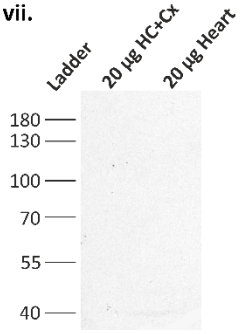

viii.

Western Blot Parameters	Solutions/Reagents	Time (min)	Volume (per membrane)	Temp
Blocking	5% nonfat milk	60	25 ml	RT
Primary antibody	No primary	Overnight	6 ml	4°C
Secondary antibody	1:20000 NA931 in 5% nonfat milk	120	6 ml	RT
ECL reagent	RPN2232	2	2 ml	RT

Figure 4.19 Results of the western blots probed against Zbtb14 with sc-514298 antibody using the standard protocol and protocol to compare antibody solutions in nonfat milk in TBS-T or only TBS-T. The anti-Zbtb14 antibody sc-514298 was utilised in the standard WB protocol **(A)** and WB

protocol to compare antibody solutions in nonfat milk in TBS-T or only TBS-T **(B)**. The standard WB protocol **(A-ii and A-iv)** and the WB protocol to compare antibody solutions in nonfat milk in TBS-T or only TBS-T **(B-ii, B-iv, B-vi, and B-viii)** are given in a table following the WB images. HC+Cx: hippocampus and cortex; Temp: temperature.

For the WB protocol with the blocking agent RPN2125, 5% RPN2125 blocking agent was used instead of 5% nonfat milk to improve the blocking efficiency. The membranes were incubated overnight with the anti-Zbtb14 antibody sc-514298 at a dilution of 1:4000 in TBS-T at 4°C. The membranes were incubated for 2 hours with 1:40000 anti-mouse peroxidase conjugated antibody, NA931, diluted in TBS-T at room temperature. (Figure 4.20 B-ii, B-iv, B-vi and B-viii). The WB images of nonfat milk as a blocking agent showed that the primary antibody-omitted membrane had the same bands in the brain and heart extracts – between the 35 and 40 kDa levels. This means that the bands observed are not specific to the Zbtb14 antigen but are specific to the secondary antibody. The primary antibody-containing membrane with nonfat milk blocking had a band just above 55 kDa that was Zbtb14 protein-specific and was present in both tissue extracts. Similarly, in the WB images of RPN2125 as a blocking agent, I observed a similar pattern on the primary antibody-omitted membrane and the primary antibody-included membrane. The 40 kDa and lower bands result from the nonspecific binding of the secondary antibody (Figure 4.20 B-i, B-iii, B-v, and B-vii). When all blot results for sc-514298 are taken together, I concluded that sc-514298 is a specific Zbtb14 protein and gives a band just above 55 kDa, higher than expected.

A. Standard WB Protocol

i.

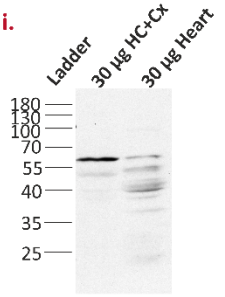

ii.

Western Blot Parameters	Solutions/Reagents	Time (min)	Volume (per membrane)	Temp
Blocking	5% nonfat milk	60	25 ml	RT
Primary antibody	1:500 sc-514298	Overnight	6 ml	4°C
Secondary antibody	1:5000 PI-2000	120	6 ml	RT
ECL reagent	RPN2108	2	2 ml	RT

B. WB Protocol to Compare 5% nonfat milk and 5% RPN2125 as Blocking Agents

i.

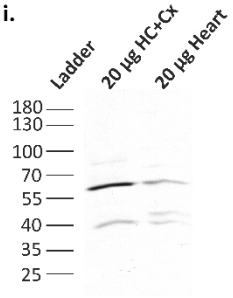

ii.

Western Blot Parameters	Solutions/Reagents	Time (min)	Volume (per membrane)	Temp
Blocking	5% nonfat milk	60	25 ml	RT
Primary antibody	1:4000 sc-514298	Overnight	6 ml	4°C
Secondary antibody	1:40000 NA931	120	6 ml	RT
ECL reagent	RPN2232	2	2 ml	RT

iii.

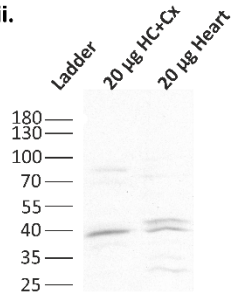

iv.

Western Blot Parameters	Solutions/Reagents	Time (min)	Volume (per membrane)	Temp
Blocking	5% nonfat milk	60	25 ml	RT
Primary antibody	No primary	Overnight	6 ml	4°C
Secondary antibody	1:40000 NA931	120	6 ml	RT
ECL reagent	RPN2232	2	2 ml	RT

v.

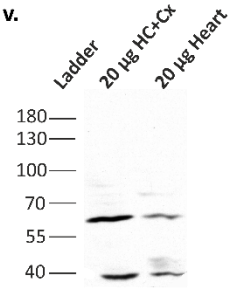

vi.

Western Blot Parameters	Solutions/Reagents	Time (min)	Volume (per membrane)	Temp
Blocking	5% RPN2125	60	25 ml	RT
Primary antibody	1:4000 sc-514298	Overnight	6 ml	4°C
Secondary antibody	1:40000 NA931	120	6 ml	RT
ECL reagent	RPN2232	2	2 ml	RT

vii.

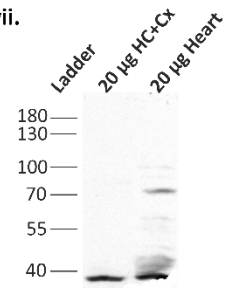

viii.

Western Blot Parameters	Solutions/Reagents	Time (min)	Volume (per membrane)	Temp
Blocking	5% RPN2125	60	25 ml	RT
Primary antibody	No primary	Overnight	6 ml	4°C
Secondary antibody	1:40000 NA931	120	6 ml	RT
ECL reagent	RPN2232	2	2 ml	RT

Figure 4.20 Results of the western blots probed against Zbtb14 with sc-514298 antibody using the standard protocol and the protocol to compare 5% nonfat milk and 5% RPN2125 as blocking agents. The anti-Zbtb14 antibody sc-514298 was utilised in the standard WB protocol **(A)** and WB protocol to compare 5% nonfat milk and 5% RPN2125 as blocking agents **(B)**. The standard

WB protocol **(A-ii and A-iv)** and the WB protocol to compare 5% nonfat milk and 5% RPN2125 as blocking agents **(B-ii, B-iv, B-vi, and B-viii)** are given in a table following the WB images. HC+Cx: hippocampus and cortex; Temp: temperature.

4.1.8.3. Evaluation of specificity of sc-514298

Dot blotting was performed to assess the specificity of the sc-514298 primary antibody to the Zbtb14 protein. The dot blot image indicates that sc-514298 recognises the full-length recombinant ZF5 protein but not the MBD3 peptide, which was used as a negative control. APREST73794 is a partial recombinant ZF5 peptide produced using amino acid sequences from 81 to 173 of the full-length protein at the N-terminus. The sc-514298 antibody is raised against amino acid sequences from 150 to 449 of the full-length protein at the C-terminus. The Zbtb14 antibody sc-514298 did not recognise the APREST73794 peptide because there are only 23 amino acids overlapping the sequence that is produced against, and it was not enough to recognise the sequence (Figure 4.21).

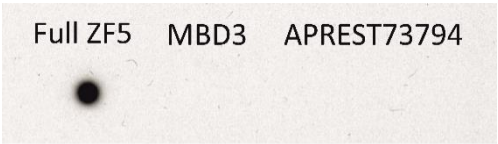

IB: sc-514298, anti-Zbtb14

Figure 4.21 Image of the membrane spotted with the full-length ZF5 ORF, MBD3 peptide, and APREST73794 peptide (partial ZF5 peptide) and probed against Zbtb14 with sc-514298.

4.1.9 Atlas antibodies, #HPA050758, anti-ZBTB14 antibody produced in rabbit

HPA050758 is a rabbit polyclonal antibody produced with a recombinant protein epitope signature tag (PrEST) antigen sequence: LRSDIFEEVLNYMYTAKISVKKEDVNLMM SSGQILGIRFLDKLCSQKRDVSSPDENNGQSKSKYCLKINRPIGDAADTQDDDVEEIGDQDDSP (https://www.atlasantibodies.com/products/antibodies/primary-antibodies/triple-a-polyclonals/zbtb14-antibody-hpa050758/).

4.1.9.1 Immunofluorescence

For the standard staining protocol, the primary antibody against Zbtb14 HPA050758 was diluted to 1:200 in PBST and incubated overnight at 4°C. The biotinylated anti-mouse secondary antibody BA-1000 was diluted to 1:500 in PBST and incubated for 2 hours at

room temperature. The sections were incubated with fluorescein Avidin D A-2001 at a 1:500 dilution in PBST for 20 minutes (Figure 4.22 A-iv). The standard staining with HPA050758 shows that the cells in the CA1 and CA3 pyramidal cell layer and granular cell layers of dentate gyrus have cytoplasmic staining and morphologically resemble neurons. Some cells also had nuclear staining. For example, the hilar cells have nuclear and cytoplasmic staining (Figure 4.22 A-i-iii).

To distinguish the Zbtb14 signal from the unspecific signal, the recombinant protein used for antibody production was used as a sponge in the primary antibody solution. The anti-Zbtb14 antibody HPA050758 and recombinant Zbtb14 protein APREST73794 were incubated together to observe the disappearance of the Zbtb14 signal on the staining (Figure 4.22 B-ii, B-iv, B-vi, and B-viii). The staining with recombinant protein after two hours of incubation shows that the staining patterns in Zbtb14+RecPro+FITC and Zbtb14+FITC are similar. The staining pattern is not as straightforward as in the standard protocol images, most likely due to two hours of storage period of the solutions. Both RecPro+FITC and FITC images do not have specific staining. This means that the staining pattern I observed in Zbtb14+RecPro+FITC and Zbtb14+FITC images is due to the anti-Zbtb14 antibody HPA050758 but not the secondary antibody (Figure 4.22 B-i, B-iii, B-v, and B-vii).

A. Standard Staining Protocol

i.

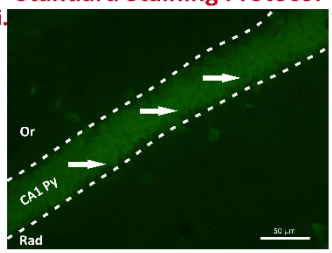

ii.

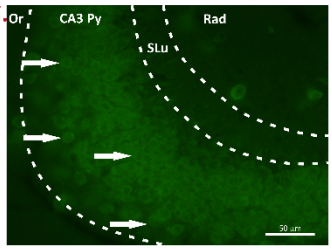

iii.

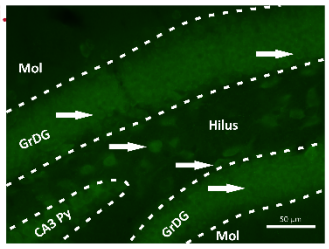

iv.

Steps	Solutions/Reagents	Time (min)	Volume (per well)	Temp
Wash	PBST	15 x 3	500 µl	RT
Blocking	10% NGS	120	300 µl	RT
Primary antibody	1:200 HPA050758	Overnight	300 µl	4°C
Wash	PBST	15 x 3	500 µl	RT
Secondary antibody	1:500 BA-1000	120	300 µl	RT
Wash	PBST	15 x 3	500 µl	RT
Fluorescein Avidin D	1:500 A-2001	20	300 µl	RT
Wash	PB	15 x 3	500 µl	RT

B. The Staining Protocol with Recombinant Protein for Two Hours

i.

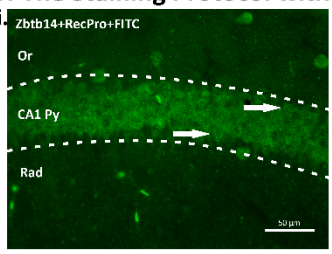

ii.

Steps	Solutions/Reagents		Time (min)	Volume (per well)	Temp
Wash	PBST		15 x 3	500 µl	RT
Blocking	10% NGS		120	300 µl	RT
Primary antibody	+HPA050758 +APREST73794 2 hours incubation	1:500 HPA050758 and 1:500 APREST73794 prepared and stored for two hours at 4°C before the overnight incubation with sections	Overnight	300 µl	4°C
Wash	PBST		15 x 3	500 µl	RT
Secondary antibody	1:1000 FI-1000		120	300 µl	RT
Wash	PB		15 x 3	500 µl	RT

iii.

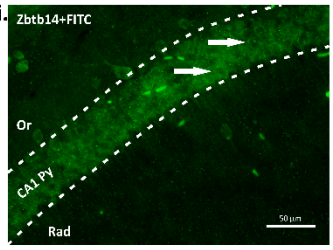

iv.

Steps	Solutions/Reagents		Time (min)	Volume (per well)	Temp
Wash	PBST		15 x 3	500 µl	RT
Blocking	10% NGS		120	300 µl	RT
Primary antibody	+HPA050758 -APREST73794 2 hours incubation	1:500 HPA050758 was prepared and stored for two hours at 4°C before the overnight incubation with the sections	Overnight	300 µl	4°C
Wash	PBST		15 x 3	500 µl	RT
Secondary antibody	1:1000 FI-1000		120	300 µl	RT
Wash	PB		15 x 3	500 µl	RT

v.

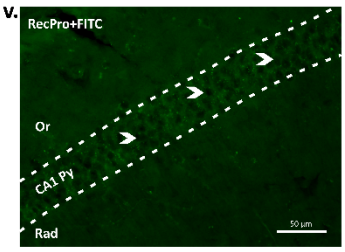

vi.

Steps	Solutions/Reagents		Time (min)	Volume (per well)	Temp
Wash	PBST		15 x 3	500 µl	RT
Blocking	10% NGS		120	300 µl	RT
Primary antibody	-HPA050758 +APREST73794 2 hours incubation	1:500 APREST73794 was prepared and stored for two hours at 4°C before the overnight incubation with the sections	Overnight	300 µl	4°C
Wash	PBST		15 x 3	500 µl	RT
Secondary antibody	1:1000 FI-1000		120	300 µl	RT
Wash	PB		15 x 3	500 µl	RT

vii.

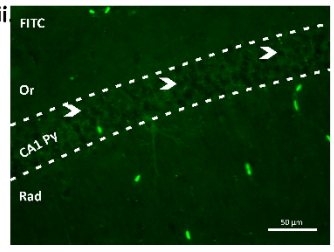

viii.

Steps	Solutions/Reagents		Time (min)	Volume (per well)	Temp
Wash	PBST		15 x 3	500 µl	RT
Blocking	10% NGS		120	300 µl	RT
Primary antibody	-HPA050758 -APREST73794	Sections are incubated with PBST 2 hours	Overnight	300 µl	4°C
Wash	PBST		15 x 3	500 µl	RT
Secondary antibody	1:1000 FI-1000		120	300 µl	RT
Wash	PB		15 x 3	500 µl	RT

Figure 4.22 Images of the hippocampal sections after the standard staining protocol, the staining protocol with recombinant protein for two hours using anti-Zbtb14 antibody, HPA050758. The CA1 **(A-i)**, CA3 **(A-ii),** and DG **(A-iii)** of the hippocampus are shown with a standard staining protocol. The standard staining protocol is a table under the images **(A-iv)**. The CA1 subfield of the hippocampus is shown with the staining protocol with recombinant protein for two hours **(B-i, B-iii, B-v, and B-vii)**. The staining protocols with recombinant protein for two hours are

given as a table next to the images **(B-ii, B-iv, B-vi, and B-viii)**. The white arrows indicate Zbtb14-positive cells. The white arrowheads indicate the empty nuclei of the primary cells. CA1 Py, pyramidal layer of CA1 field; CA3 Py, pyramidal layer of CA3 field; GrDG, granular layer of the dentate gyrus; Mol, molecular layer of the dentate gyrus; Or, oriens layer of the hippocampus; Rad, stratum radiatum of the hippocampus; SLu, stratum lucidum.

For the staining protocols with recombinant protein overnight (Figure 4.23 B-ii, B-iv, B-vi, and B-viii), the staining patterns in Zbtb14+RecPro+FITC and Zbtb14+FITC were fainter than the staining with recombinant protein after two hours of incubation. The staining pattern is not as straightforward as in the standard protocol images, most likely due to the overnight storage of the solutions. Both RecPro+FITC and FITC images did not have specific staining (Figure 4.23 B-i, B-iii, B-v, and B-vii).

A. Standard Staining Protocol

i.

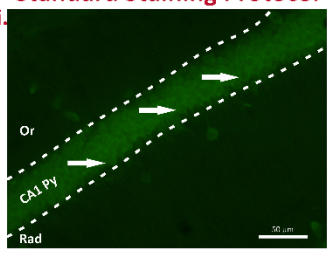

ii.

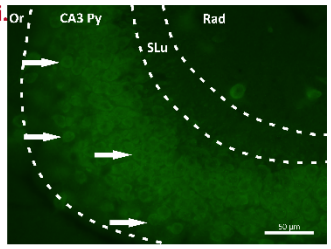

iii.

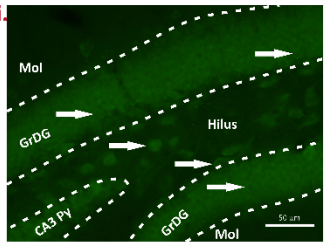

iv.

Steps	Solutions/Reagents	Time (min)	Volume (per well)	Temp
Wash	PBST	15 x 3	500 µl	RT
Blocking	10% NGS	120	300 µl	RT
Primary antibody	1:200 HPA050758	Overnight	300 µl	4°C
Wash	PBST	15 x 3	500 µl	RT
Secondary antibody	1:500 BA-1000	120	300 µl	RT
Wash	PBST	15 x 3	500 µl	RT
Fluorescein Avidin D	1:500 A-2001	20	300 µl	RT
Wash	PB	15 x 3	500 µl	RT

B. The Staining Protocol with Recombinant Protein for Overnight

i.

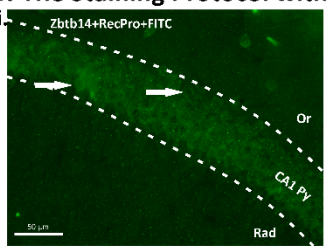

ii.

Steps	Solutions/Reagents		Time (min)	Volume (per well)	Temp
Wash	PBST		15 x 3	500 µl	RT
Blocking	10% NGS		120	300 µl	RT
Primary antibody	+HPA050758 +APREST73794 Overnight incubation	1:500 HPA050758 and 1:500 APREST73794 was prepared and stored overnight before the overnight incubation with sections	Overnight	300 µl	4°C
Wash	PBST		15 x 3	500 µl	RT
Secondary antibody	1:1000 FI-1000		120	300 µl	RT
Wash	PB		15 x 3	500 µl	RT

iii.

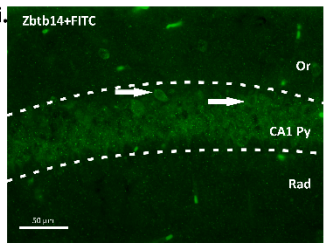

iv.

Steps	Solutions/Reagents		Time (min)	Volume (per well)	Temp
Wash	PBST		15 x 3	500 µl	RT
Blocking	10% NGS		120	300 µl	RT
Primary antibody	+HPA050758 -APREST73794 Overnight incubation	1:500 HPA050758 was prepared and stored overnight before the overnight incubation with the sections	Overnight	300 µl	4°C
Wash	PBST		15 x 3	500 µl	RT
Secondary antibody	1:1000 FI-1000		120	300 µl	RT
Wash	PB		15 x 3	500 µl	RT

v.

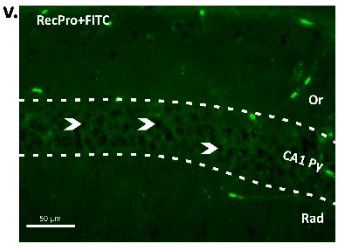

vi.

Steps	Solutions/Reagents		Time (min)	Volume (per well)	Temp
Wash	PBST		15 x 3	500 µl	RT
Blocking	10% NGS		120	300 µl	RT
Primary antibody	-HPA050758 +APREST73794 Overnight incubation	1:500 APREST73794 was prepared and stored overnight before the overnight incubation with the sections	Overnight	300 µl	4°C
Wash	PBST		15 x 3	500 µl	RT
Secondary antibody	1:1000 FI-1000		120	300 µl	RT
Wash	PB		15 x 3	500 µl	RT

vii.

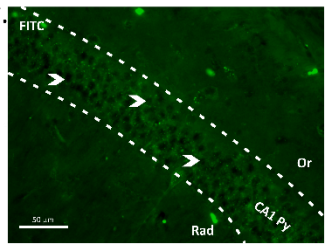

viii.

Steps	Solutions/Reagents		Time (min)	Volume (per well)	Temp
Wash	PBST		15 x 3	500 µl	RT
Blocking	10% NGS		120	300 µl	RT
Primary antibody	-HPA050758 -APREST73794	Sections are incubated with PBST overnight	Overnight	300 µl	4°C
Wash	PBST		15 x 3	500 µl	RT
Secondary antibody	1:1000 FI-1000		120	300 µl	RT
Wash	PB		15 x 3	500 µl	RT

Figure 4.23 Images of the hippocampal sections after the standard staining protocol, the staining protocol with recombinant protein overnight using anti-Zbtb14 antibody, HPA050758. The CA1 **(A-i)**, CA3 **(A-ii)** and DG **(A-iii)** of the hippocampus are shown with a standard staining protocol. The standard staining protocol is a table under the images **(A-iv)**. The CA1 subfield of the hippocampus is shown with the staining protocol with recombinant protein overnight **(B-i, B-iii, B-v, and B-vii)**. The staining protocols with recombinant protein overnight are given as a table next to the images **(B-ii, B-iv, B-vi, and B-viii)**. The white arrows indicate Zbtb14-positive cells.

The white arrowheads indicate the empty nuclei of the principal cells. CA1 Py, pyramidal layer of CA1 field; CA3 Py, pyramidal layer of CA3 field; GrDG, granular layer of the dentate gyrus; Mol, molecular layer of the dentate gyrus; Or, oriens layer of the hippocampus; Rad, stratum radiatum of the hippocampus; SLu, stratum lucidum.

For the staining protocol with fresh tissue following acetone fixation, the sections were fixed with ice-cold acetone for 10 minutes and blocked with 5% NGS in PBST for 90 minutes on microscope slides. The primary antibody against Zbtb14 HPA050758 was diluted to 1:100 in PBST and incubated overnight at 4°C. The biotinylated anti-rabbit secondary antibody BA-1000 was diluted to 1:200 in PBST and incubated for 2 hours at room temperature. The sections were incubated with fluorescein Avidin D A-2001 at a 1:100 dilution in PBST for 20 minutes (Figure 4.24 C-iv). The fresh frozen tissue staining images have nuclear staining with HPA050758 contrary to standard staining (Figure 4.24 C-i-iii). I concluded that the previous cytoplasmic-only staining pattern was due to paraformaldehyde fixation of the tissue. When the staining protocol changed to the acetone fixation protocol, I observed nuclear staining with anti-Zbtb14 antibodies, HPA050758 and sc-5142987.

A. Standard Staining Protocol

i.

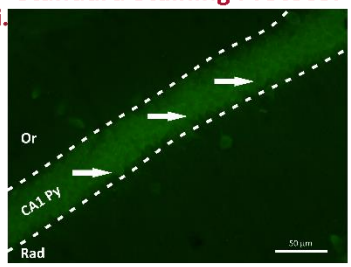

ii.

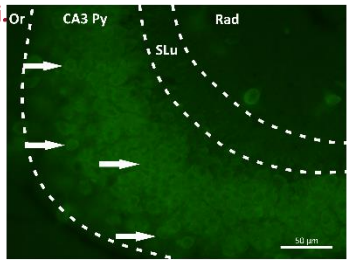

iii.

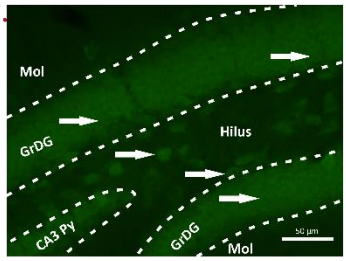

iv.

Steps	Solutions/Reagents	Time (min)	Volume (per well)	Temp
Wash	PBST	15 x 3	500 µl	RT
Blocking	10% NGS	120	300 µl	RT
Primary antibody	1:200 HPA050758	Overnight	300 µl	4°C
Wash	PBST	15 x 3	500 µl	RT
Secondary antibody	1:500 BA-1000	120	300 µl	RT
Wash	PBST	15 x 3	500 µl	RT
Fluorescein Avidin D	1:500 A-2001	20	300 µl	RT
Wash	PB	15 x 3	500 µl	RT

B. The Staining Protocol with Fresh Tissue Following Acetone Fixation

i.

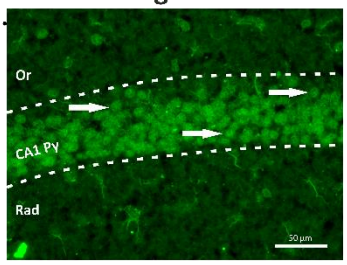

ii.

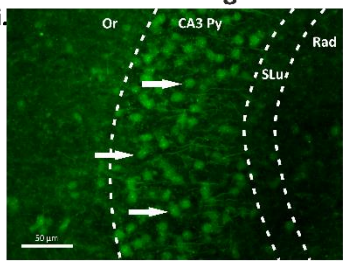

iii.

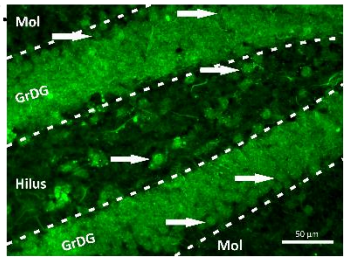

iv.

Steps	Solutions/Reagents	Time (min)	Volume (per slide)	Temp
Fixation	Acetone pure	10	-	4°C
Wash	PBST	5 x 3	-	RT
Blocking	5% NGS	90	200 µl	RT
Primary antibody	1:100 HPA050758	Overnight	200 µl	4°C
Wash	PBST	5 x 3	-	RT
Secondary antibody	1:200 BA-1000	120	200 µl	RT
Wash	PBST	5 x 3	-	RT
Fluorescein Avidin D	1:100 A-2001	20	200 µl	RT
Wash	PBS	5 x 3	-	RT

Figure 4.24 Images of the hippocampal sections after the standard staining protocol and the staining protocol with fresh tissue following acetone fixation using the anti-Zbtb14 antibody HPA050758. The CA1 **(A-i)**, CA3 **(A-ii)** and DG **(A-iii)** of the hippocampus are shown with a standard staining protocol. The standard staining protocol is a table under the images **(A-iv)**. The CA1 **(B-i)**, CA3 **(B-ii)** and DG **(B-iii)** of the hippocampus are shown with the staining protocol with fresh tissue following acetone fixation. The staining protocol with fresh tissue following acetone fixation is given as a table under the images **(B-iv)**. The white arrows indicate Zbtb14-positive cells. CA1 Py, pyramidal layer of CA1 field; CA3 Py, pyramidal layer of CA3 field; GrDG, granular layer of the dentate gyrus; Mol, molecular layer of the dentate gyrus; Or, oriens layer of the hippocampus; Rad, stratum radiatum of the hippocampus; SLu, stratum lucidum.

4.1.9.2. Western blot

For the standard WB protocol (Figure 4.25 A-ii), the membrane image shows that in the brain extracts, several bands were observed, but the most significant band is at the level

of 55 kDa, and in the heart extracts, no bands were detected. The image of the primary antibody-omitted membrane is clear; this means that any bands on the right-hand side image are associated with the primary antibody HPA050758 (Figure 4.25 A-i).

To distinguish the Zbtb14 band from unspecific bands, the recombinant protein used for antibody production was used as a sponge in primary antibody solution. The anti-Zbtb14 antibody HPA050758 and recombinant Zbtb14 protein APREST73794 were incubated together before incubation with the membrane. Next, the identical membranes were incubated with (Figure 4.25 B-ii, B-iv, B-vi, and B-viii):

i. only recombinant Zbtb14 protein, 1:500 APREST73794,

ii. only with anti-Zbtb14 antibody, 1:500 HPA050758,

iii. 1:500 HPA050758 and 1:500 APREST73794 incubated together for 2 hours, and

iv. HPA050758 (1:500) and APREST73794 (1:500) were incubated together overnight.

The aim was to observe the disappearance of the Zbtb14 protein band on the membrane. However, I identified that membranes that were incubated with both HPA050758 and APREST73794 and the membrane that was only incubated with HPA050758 had the same band pattern. I concluded that incubation with recombinant protein did not bind HPA050758 antibody as expected, and there was no apparent disappearance of a band (Figure 4.25 B-i, B-iii, B-v, and B-vii).

A. Standard WB Protocol

i.

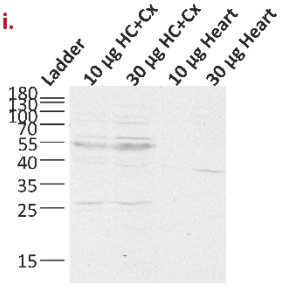

ii.

Western Blot Parameters	Solutions/Reagents	Time (min)	Volume (per membrane)	Temp
Blocking	5% nonfat milk	60	25 ml	RT
Primary antibody	1:500 HPA050758	Overnight	6 ml	4°C
Secondary antibody	1:5000 AP132P	120	6 ml	RT
ECL reagent	RPN2108	2	2 ml	RT

B. WB Protocols with Recombinant Protein

i.

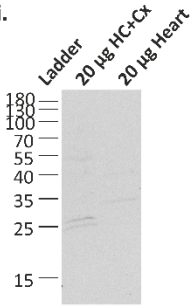

ii.

Western Blot Parameters	Solutions/Reagents		Time (min)	Volume (per membrane)	Temp
Blocking	5% nonfat milk		60	25 ml	RT
Primary antibody	+ HPA050758 + APREST73794 2 hours incubation	1:500 HPA050758 and 1:500 APREST73794 was incubated together for two hours at 4°C before the overnight incubation with membrane	Overnight	6 ml	4°C
Secondary antibody	1:5000 AP132P		120	6 ml	RT
ECL reagent	RPN2108		2	2 ml	RT

iii.

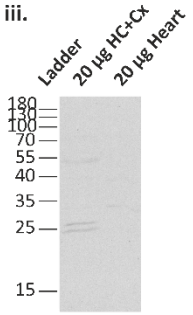

iv.

Western Blot Parameters	Solutions/Reagents		Time (min)	Volume (per membrane)	Temp
Blocking	5% nonfat milk		60	25 ml	RT
Primary antibody	+ HPA050758 + APREST73794 Overnight incubation	1:500HPA050758 and 1:500 APREST73794 were incubated together overnight before the overnight incubation with the membrane	Overnight	6 ml	4°C
Secondary antibody	1:5000 AP132P		120	6 ml	RT
ECL reagent	RPN2108		2	2 ml	RT

v.

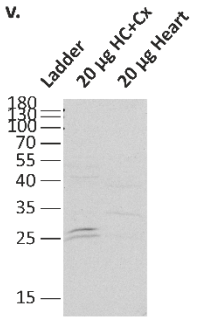

vi.

Western Blot Parameters	Solutions/Reagents		Time (min)	Volume (per membrane)	Temp
Blocking	5% nonfat milk		60	25 ml	RT
Primary antibody	+ HPA050758 - APREST73794 Overnight incubation	1:500 HPA050758 kept at 4°C overnight before the overnight incubation with the membrane	Overnight	6 ml	4°C
Secondary antibody	1:5000 AP132P		120	6 ml	RT
ECL reagent	RPN2108		2	2 ml	RT

vii.

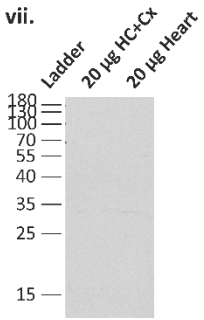

viii.

Western Blot Parameters	Solutions/Reagents		Time (min)	Volume (per membrane)	Temp
Blocking	5% nonfat milk		60	25 ml	RT
Primary antibody	- HPA050758 + APREST73794 Overnight incubation	1:500APREST73794 was kept at 4°C overnight before the overnight incubation with the membrane	Overnight	6 ml	4°C
Secondary antibody	1:5000 AP132P		120	6 ml	RT
ECL reagent	RPN2108		2	2 ml	RT

Figure 4.25 Results of the western blots probed against Zbtb14 with HPA050758 antibody using a standard protocol and protocols with recombinant protein. The anti-Zbtb14 antibody HPA050758 was utilised in the standard WB protocol **(A)** and WB protocol with recombinant protein APREST73794 as a competitor **(B)**. The standard WB protocol **(A-ii)** and the WB protocols

with recombinant protein **(B-ii, B-iv, B-vi, and B-viii)** are given as a table next to the images. HC+Cx: hippocampus and cortex; Temp: temperature.

The ECL reagent RPN2232 has increased sensitivity when using higher antibody dilutions, according to the manufacturer's manual. Hence, I reduced the antibody concentration by four times for primary and secondary antibody solutions compared to the standard WB protocol. The primary antibody dilution was increased to 1:2000 in TBS-T, and the secondary antibody dilution was increased to 1:20000 in TBS-T (Figure 4.26 B-i). The image has the same ~55 kDa band in the brain extracts but not in the heart extracts. The same ~55 kDa band was observed in the brain extracts with three times less sample and four times increased dilution in antibody solution using RPN2232 (Figure 4.26 B-ii).

A. Standard WB Protocol

i.

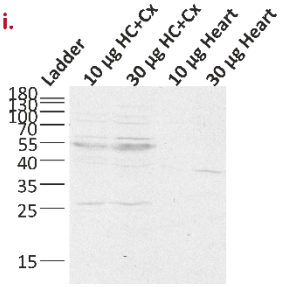

ii.

Western Blot Parameters	Solutions/Reagents	Time (min)	Volume (per membrane)	Temp
Blocking	5% nonfat milk	60	25 ml	RT
Primary antibody	1:500 HPA050758	Overnight	6 ml	4°C
Secondary antibody	1:5000 AP132P	120	6 ml	RT
ECL reagent	RPN2108	2	2 ml	RT

B. The WB Protocol with RPN2232 as ECL Reagent

i.

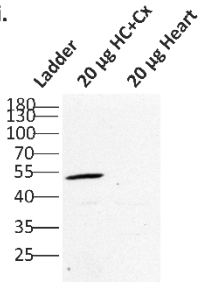

ii.

Western Blot Parameters	Solutions/Reagents	Time (min)	Volume (per membrane)	Temp
Blocking	5% nonfat milk	60	25 ml	RT
Primary antibody	1:2000 HPA050758	Overnight	6 ml	4°C
Secondary antibody	1:20000 NA934	120	6 ml	RT
ECL reagent	RPN2232	2	2 ml	RT

Figure 4.26 Results of the western blots probed against Zbtb14 with HPA050758 antibody using the standard protocol and protocols with RPN2232 as the ECL reagent. The anti-Zbtb14 antibody HPA050758 was utilised in the standard WB protocol **(A)** and WB protocol with RPN2232 and ECL reagent **(B)**. The standard WB protocol **(A-ii)** and the WB protocols with RPN2232 as and ECL reagent **(B-ii)** are given as a table next to the images. HC+Cx: hippocampus and cortex; Temp: temperature.

3.1.9.3. Evaluation of the specificity of HPA050758

Dot blotting was performed to assess the specificity of the HPA050758 primary antibody to the Zbtb14 protein. The dot blot image indicates that HPA050758 can recognise the full-length recombinant ZF5 protein and that APREST73794 is a partial recombinant ZF5 peptide but not the MBD3 peptide that has been used as a negative control. APREST73794 is a partial recombinant ZF5 peptide, and the antibody HPA050758 was raised against this peptide. The APREST73794 peptide was used as a positive control in this dot blot. Taken together with the WB results of HPA050758, these results show that both HPA050758 antibodies can also bind the full-length ZF5 protein (Figure 4.27).

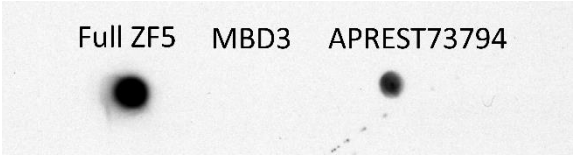

IB: HPA050758, anti-Zbtb14

Figure 4.27 Image of the membrane spotted with the full-length ZF5 ORF, MBD3 peptide, and APREST73794 peptide (partial ZF5 peptide) and probed against Zbtb14 with HPA050758.

4.2 Immunoprecipitation Validation

For each immunoprecipitation, one experimental and four control columns were labelled with the following name in the results below:

1. With primary antibody and with protein isolate = Sample
2. With isotype control antibody and with protein isolate = Control Ab
3. With primary antibody immobilised on control resin and with protein isolate = Control Resin
4. Without primary antibody and with protein isolate = +HC -Ab
5. With primary antibody and without protein isolate = -HC +Ab

The labels frequently used are listed below to increase clarity and avoid repetitiveness:

- Protein: 20 µg protein isolate of hippocampi used for IP

- ELU1: first elution
- ELU3: third elution
- Control Ab: isotype control antibody
- HC: hippocampus

Total protein isolation was performed from hippocampi pooled from six mice. Each column had 0.8 mg protein isolate except the –HC +Ab column. The eluates from IP were used for western blotting.

Control samples of ELU1 and ELU3 do not have any bands. The control antibody and resin did not precipitate the Zbtb14 protein. In addition, the +HC-Ab and –HC+Ab columns show that without one another, either antibody or protein does not result in an unspecific band(s). The ELU1 sample lane has the same ~55 kDa I observed in our previous blot images. However, the protein lane did not have the Zbtb14 protein band. This could be due to the relatively low amount of Zbtb14 protein compared to the overall protein amount. Nevertheless, when taken together, these results also indicate that sc-514298 successfully detects the Zbtb14 protein (Figure 4.28). Overall, I immunoprecipitated the Zbtb14 protein using sc-514298 and confirmed the precipitation with WB with sc-514298.

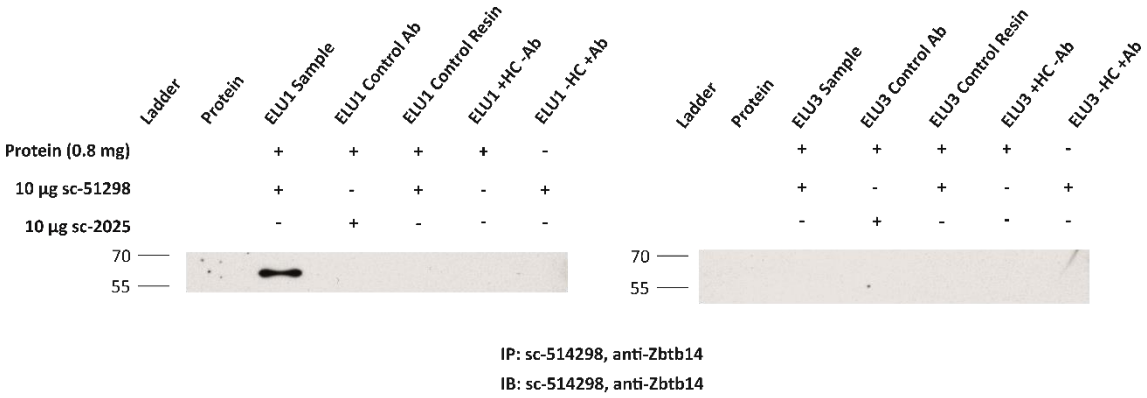

Figure 4.28 Western blot images of immunoprecipitation of Zbtb14 with sc-514298.

After reprobing the IP membranes with the HPA050758 antibody, the control samples of ELU1 and ELU3 had no bands. The control antibody and resin did not precipitate the

Zbtb14 protein. In addition, +HC-Ab and –HC+Ab columns show that without one another, either antibody or protein does not result in an unspecific band(s). Protein and ELU1 sample lanes have the same ~55 kDa I observed in our previous IP blot image (Figure 4.28). This western blot indicates that sc-514298 successfully precipitated the Zbtb14 protein, and HPA050758 detected the same band detected by sc-514298. These results validate that both the sc-514298 and HPA050758 antibodies detect the same protein, Zbtb14 (Figure 4.29).

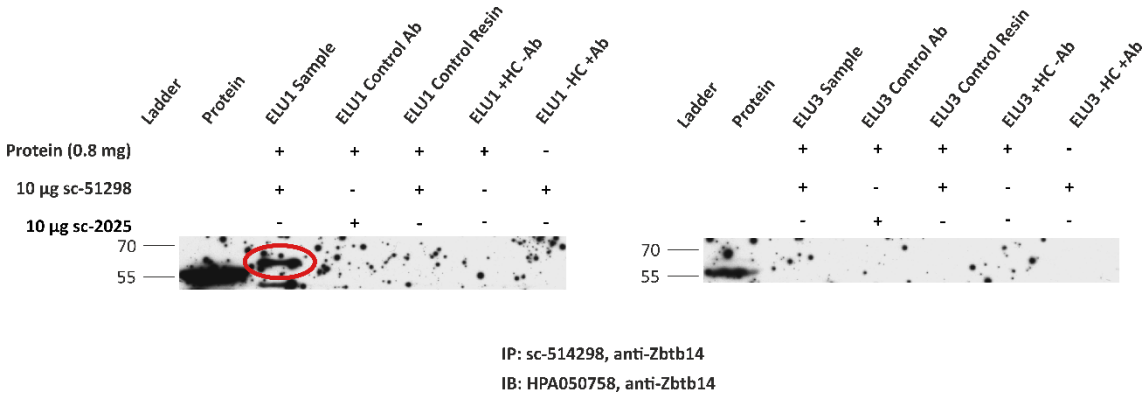

Figure 4.29 Western blot images of immunoprecipitation of Zbtb14 with HPA050758.

4.3 Circadian Rhythm Experiments

After setting up our methods, I aimed to identify:

i. What type of cell does the Zbtb14 express in the brain?

ii. Does subcellular localisation of the Zbtb14 protein change over the circadian cycle?

iii. Does the Zbtb14 protein oscillate over the circadian cycle?

iv. If the Zbtb14 protein oscillates over the circadian cycle, is the expression of Zbtb14 perturbed by epilepsy pathology?

I will answer these questions in the subsections below.

4.3.1 Localisation of Zbtb14 immunofluorescence

To investigate the localisation of Zbtb14 immunofluorescence, double staining of fresh tissue following acetone fixation was performed with the anti-Zbtb14 antibody

HPA050758 and the anti-NeuN antibody ABN91 over the circadian cycle. The images show that all Zbtb14-positive cells are also NeuN-positive (Figure 4.30).

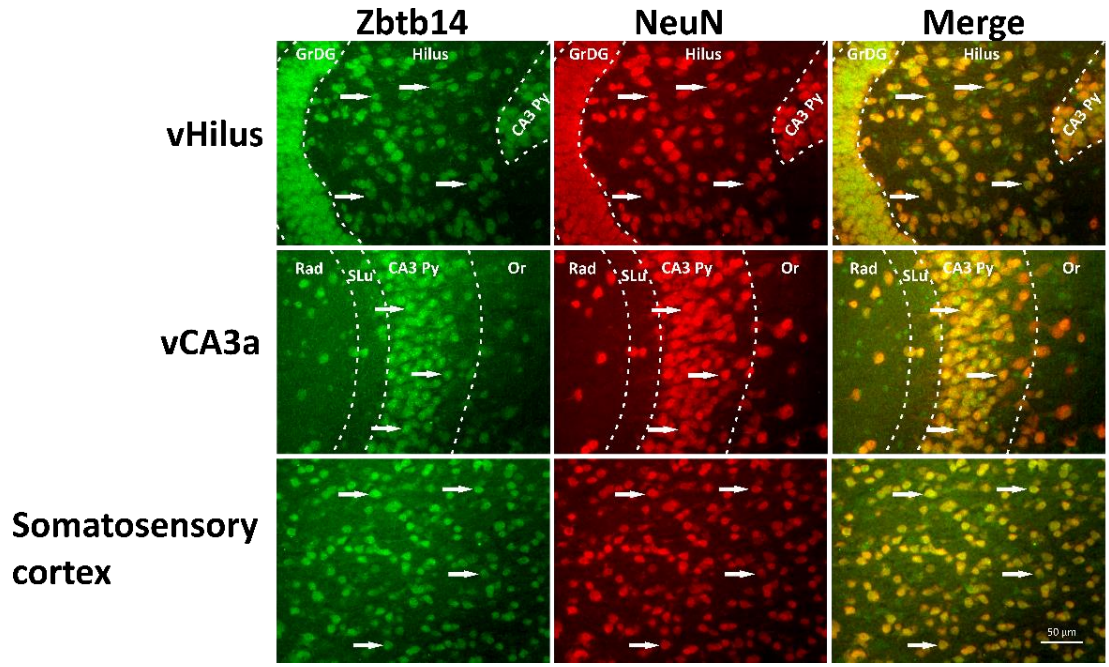

Figure 4.30 Images of the hippocampal and somatosensory cortex sections after double staining of fresh tissue following acetone fixation using anti-Zbtb14, HPA050758, and anti-NeuN antibodies. Representative images of the ventral hilus, ventral CA3a, and somatosensory layer III of naïve mice at 3 PM. The white arrows indicate Zbtb14-positive nuclei. CA3 Py, pyramidal layer of CA3 field; GrDG, granular layer of the dentate gyrus; Or, oriens layer of the hippocampus; Rad, stratum radiatum of the hippocampus; SLu, stratum lucidum.

To cross-check the validity of neuron-specific staining of Zbtb14, I performed another double staining with Zbtb14 and GFAP antibodies using a fresh frozen tissue staining protocol over the circadian cycle. Zbtb14-positive cells do not colocalise with GFAP-positive cells. This confirms that the Zbtb14 protein was not expressed in GFAP-positive astrocytes (Figure 4.31).

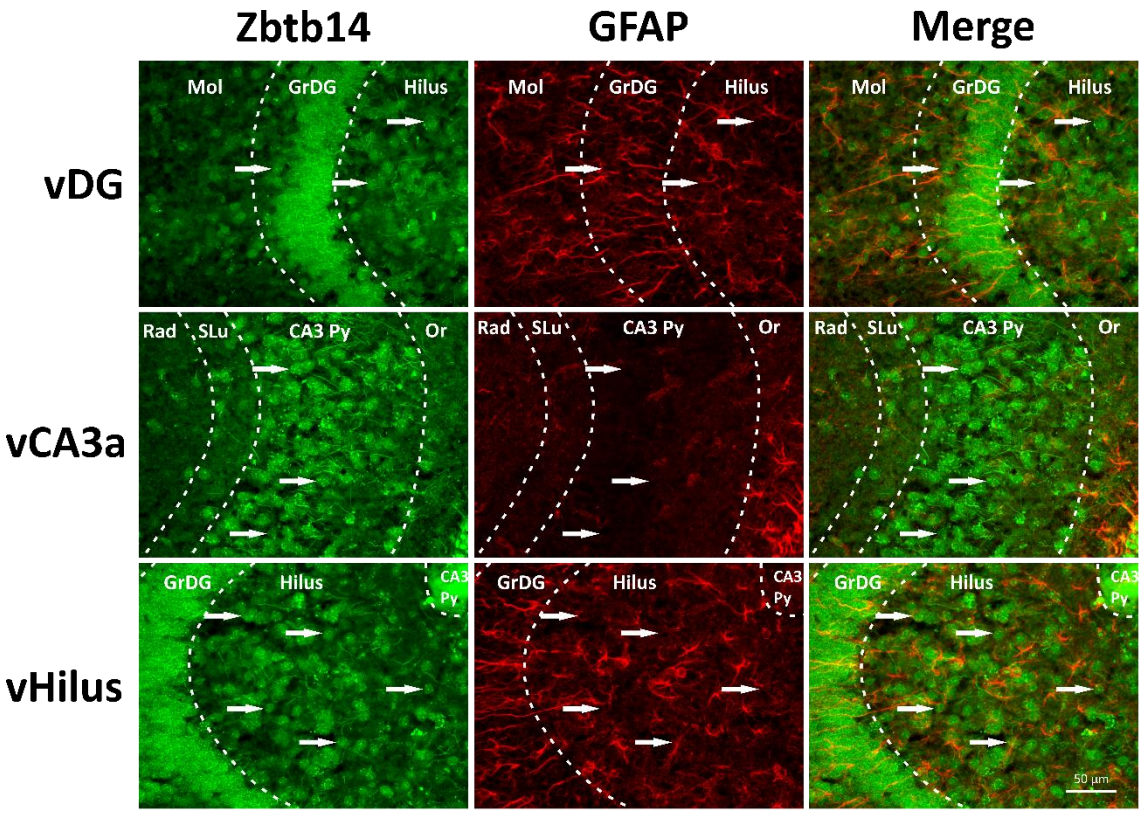

Figure 4.31 Images of the hippocampal sections after double staining of acetone fixed using anti-Zbtb14, HPA050758 and anti-GFAP antibodies. Representative images of the ventral DG, ventral CA3a and ventral hilus of naïve mice at the 3 AM time point. The white arrows indicate Zbtb14-positive nuclei. CA3 Py, pyramidal layer of CA3 field; GrDG, granular layer of the dentate gyrus; Mol, molecular layer of the dentate gyrus; Or, oriens layer of the hippocampus; Rad, stratum radiatum of the hippocampus; SLu, stratum lucidum.

4.3.2 Alterations in numbers of Zbtb14-positive cells in the hippocampus and somatosensory cortex over the circadian cycle

After establishing the localisation of the Zbtb14 protein, I focused on the circadian dynamics of Zbtb14-expressing cells in the hippocampus. The circadian dynamics of Zbtb14-expressing cell densities were evaluated in the dorsal hilus (n=5 at 11 PM and n=6 at the other time points) and ventral hilus (n=5 at 7 AM and n=6 at the other time points), the dorsal CA3a (n=4 at 11 PM and n=6 at the other time points) and ventral CA3a (n=4 at 11 PM and n=6 at the other time points) of the hippocampus, and individual layers of the somatosensory cortex [layer II/III (n=6 per time point), layer IV (n=6 per time point), layer V (n=6 per time point), and layer VI (n=6 per time point) by immunofluorescence (Figure 4.32). The data are presented in Figure 4.32 starting from when the light was turned on, i.e., 11 AM.

The densities of Zbtb14-positive cells did not change at the observed time points in the dorsal hilus, dorsal CA3a, and somatosensory cortex (Figure 4.32 a, c, e-h). In contrast, the density of Zbtb14-positive cells revealed significant differences throughout the circadian cycle in the ventral hilus and CA3a areas (Figure 4.32 b and d). The mean density of Zbtb14-positive cells in the ventral hilus at 11 AM, the first time point after the light was on, was 43.01±4.88 cells/mm^2. It increased significantly at 3 PM to 81.85±8.88 cells/mm^2 ($p<0.01$ compared to 11 AM). Then, it decreased steadily, reaching 64.35±2.22 cells/mm^2 at 7 PM and 28.68±5.31 cells/mm^2 at 11 PM ($p<0.001$ compared to 3 PM and $p<0.01$ compared to 7 PM). Next, the density of Zbtb14-positive cells increased again and was 73.74±8.25 cells/mm^2 at 3 AM ($p<0.001$ compared to 11 PM; $p<0.05$ compared to 11 AM) and 86.40±4.14 at 7 AM ($p<0.001$ compared to 11 PM; $p<0.001$ higher compared to 11 AM).

The mean density of the Zbtb14-positive cells in the ventral CA3a at 11 AM was 191.6±8.91 cells/mm^2 and remained unchanged at 3 PM, 188.1±5.73 cells/mm^2, and at 7 PM, 218.9 ±10.26 cells/mm^2. During the light-off phase, the Zbtb14-positive cell density first decreased to 141.4±8.83 cells/mm^2 at 11 PM ($p<0.001$ compared to 7 PM; $p<0.01$ compared to 11 AM and 3 PM) and then started to increase to 153.0± 5.65 cells/mm^2 at 3 AM ($p<0.001$ compared to 7 PM; $p<0.05$ compared to 11 AM and 3 PM) and to 192.7±7.47 cells/mm^2 at 7 AM ($p<0.01$ compared to 11 PM; $p<0.05$ compared to 3 AM), which was not different from the density at 11 AM.

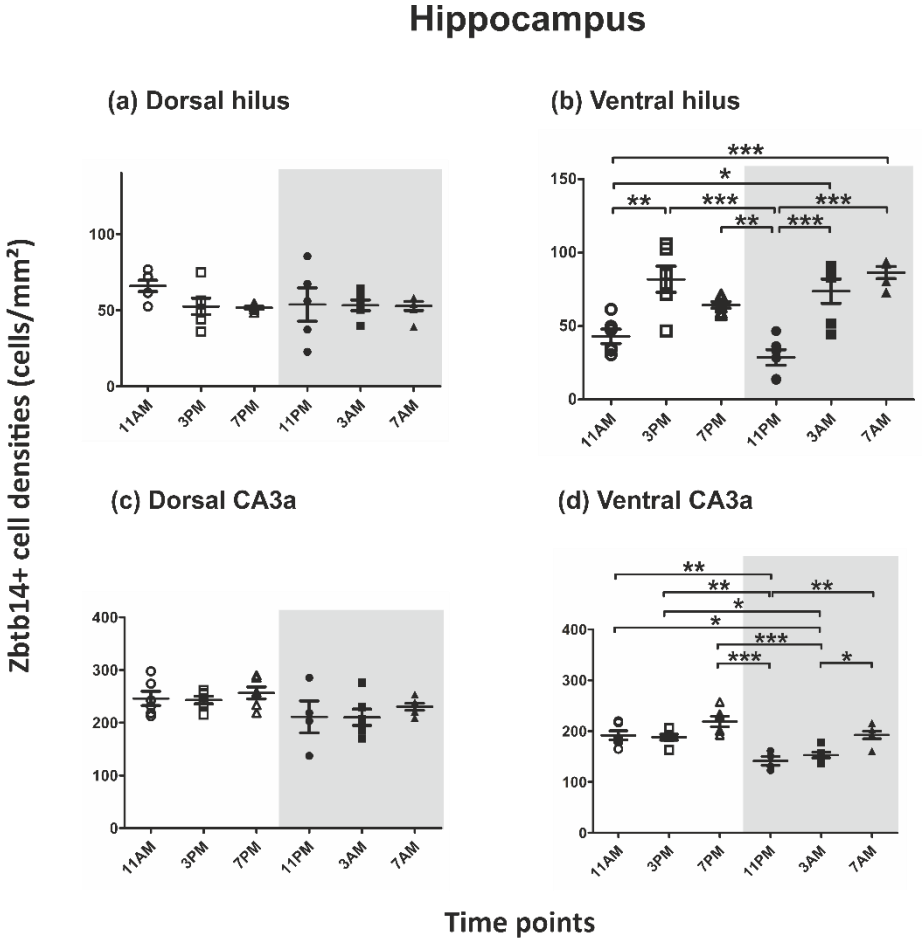
Hippocampus
(a) Dorsal hilus
(b) Ventral hilus
(c) Dorsal CA3a
(d) Ventral CA3a
Zbtb14+ cell densities (cells/mm²)
11AM
3PM
7PM
11PM
3AM
7AM
Time points

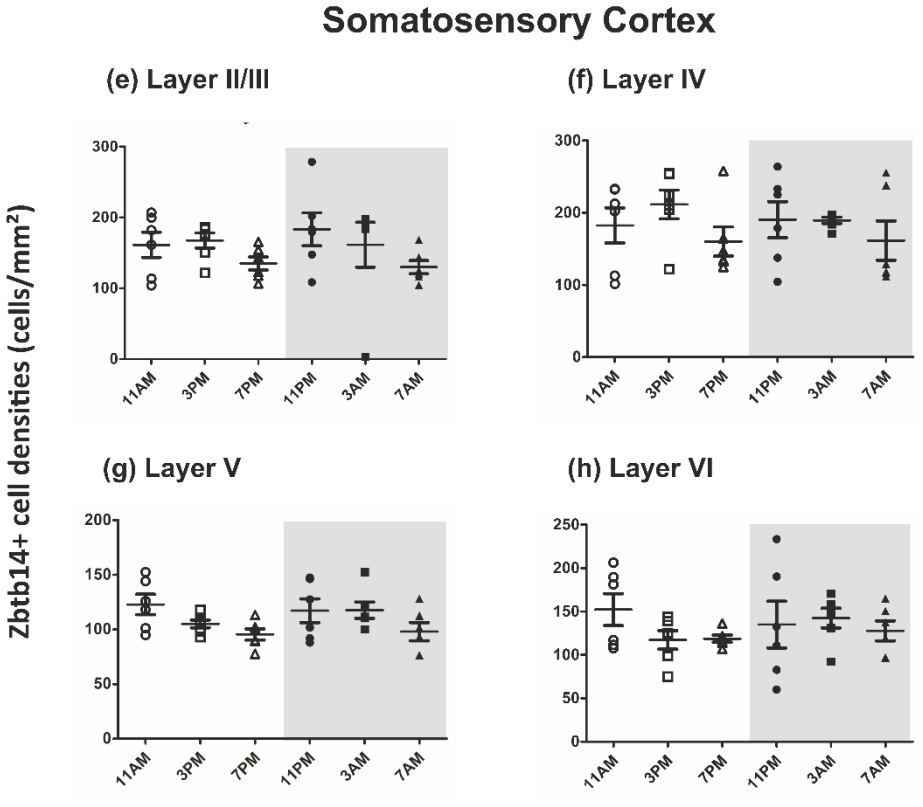
Somatosensory Cortex
(e) Layer II/III
(f) Layer IV
(g) Layer V
(h) Layer VI
Zbtb14+ cell densities (cells/mm²)
11AM
3PM
7PM
11PM
3AM
7AM
Time points

Figure 4.32 Zbtb14-positive cell densities in the dorsal hilus and CA3a and the ventral hilus and CA3a of the hippocampus and the somatosensory cortex. The density of Zbtb14-positive cells was counted in **(a)** dorsal hilus, **(b)** ventral hilus, **(c)** dorsal CA3a, **(d)** ventral CA3a, **(e)** layer II/III, **(f)** layer IV, **(g)** layer V, and **(h)** layer VI. Values are represented as the mean number of cells/mm^2 ± SEM. Data were analysed by one-way ANOVA with Tukey's multiple comparison post hoc test (*p<0.05, **p<0.01, ***p<0.001).

Representative images of the Zbtb14 staining pattern at 3 PM, 11 PM, and 3 AM are presented in Figure 4.33.

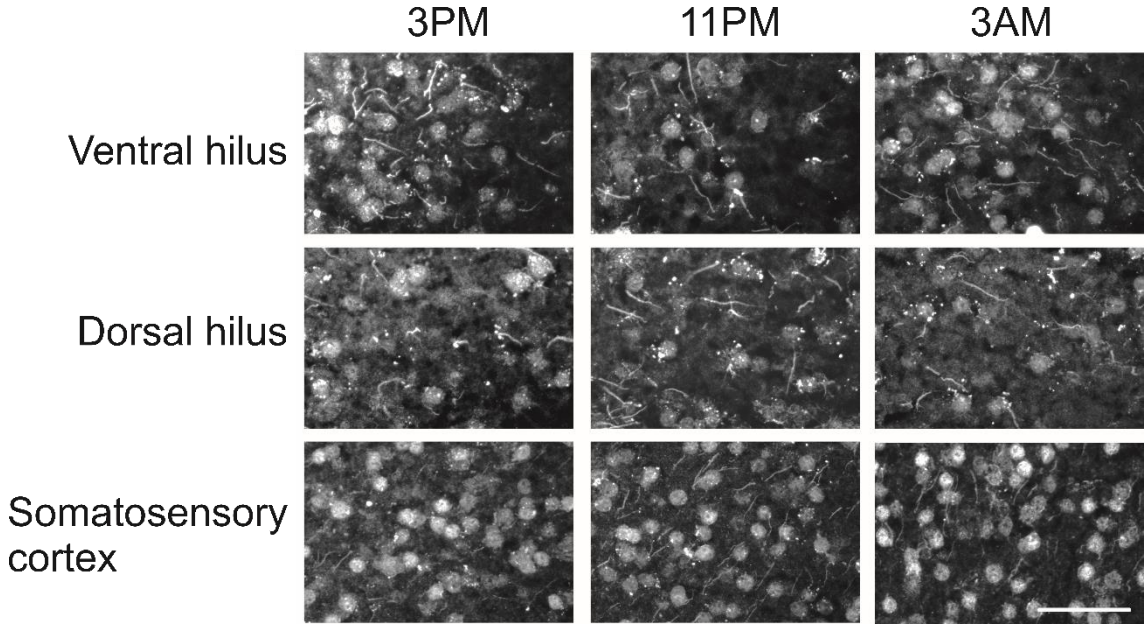

Figure 4.33 Fresh frozen tissue staining images of the anti-Zbtb14 antibody HPA050758 on the ventral and dorsal hilus and the somatosensory cortex at three time points: 3 PM, 11 PM, and 3 AM. Scale bar: 50 µm.

4.3.3 Circadian dynamics of the Zbtb14 protein in cytoplasmic and nuclear extracts

The Zbtb14 protein levels throughout the circadian cycle were assessed separately in the cytoplasmic and nuclear extracts. Data are presented as multiples of the first time after the light was turned on, i.e., 11 AM (Figure 4.34). In the cytoplasm, the Zbtb14 protein level increased by 1.45±0.05 at 3 PM compared to 11 AM ($p<0.05$) and then gradually decreased to 1.13±0.11 at 7 PM, 0.84±0.08 at 11 PM ($p<0.01$ compared to 3 PM), 0.73±0.11 3 AM ($p<0.001$ compared to 3 PM), and 0.54±0.16 at 7 AM ($p<0.05$ compared to 11 AM; $p<0.001$ compared to 3 PM; and $p<0.01$ compared to 7 PM). No

significant differences were observed in the Zbtb14 protein level in the cytoplasm within the light-off phase.

Different dynamics were observed in the Zbtb14 protein levels of the nuclear extracts. During the light-on phase, the level of Zbtb14 was not different from the level at 11 AM and was 2.76±0.96 at 3 PM and 2.61±0.75 at 7 PM. At 11 PM, the level of Zbtb14 was 6.07±1.48-fold higher than that at 11 AM ($p<0.01$). Then, it gradually decreased to 3.57±1.05 at 3 AM and then to 1.98±0.43 at 7 AM, significantly lower than at 11 PM ($p<0.05$).

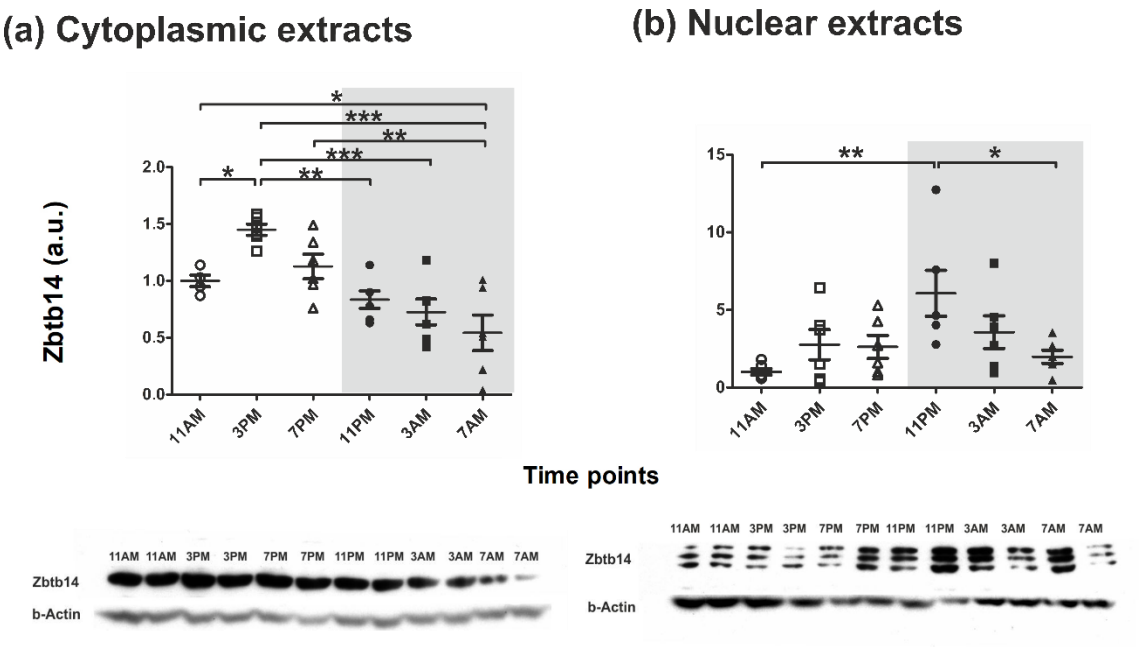

Figure 4.34 Relative levels of the Zbtb14 protein in the cytoplasm and nuclei in the hippocampus throughout the circadian cycle and the representative western blot images of the cytoplasmic and nuclear extracts of the hippocampus over the circadian cycle. The data are expressed as multiples of the relative ratios at 11 AM in the cytoplasmic **(a)** or nuclear **(b)** extracts. The relative ratios of Zbtb14 to β-actin are represented as the mean ± SEM (n=6, *p<0.05, **p<0.01, ***p<0.001, one-way ANOVA with Tukey's multiple comparison post hoc test). a.u., arbitrary unit.

4.3.4 Epileptiform discharges *in vitro* affect the expression of genes containing the ZF5 motif in their promoters

The RNAseq data set containing gene expression profiles 24 hours after induction of epileptiform discharges in rat primary cortical neurons *in vitro* was used for functional enrichment analysis via gProfiler. *In silico* analysis revealed the overrepresentation of

the ZF5 motif in the promoters of genes that were differentially expressed. The ZF5 motif was present only in the promoters of downregulated genes and was detected in the promoters of 21 out of 24 downregulated genes, which is significantly different (p_{adj} = 7.233x 10^{-4}) than expected (Table 3.85).

Table 4.1 Presence of the ZF5 motif (GSGCGCGR; TF: M00716_1) in the promoters of genes with the expression level altered in an *in vitro* model of epileptiform discharges.

Official Gene Symbol	Full Name	Fold Change	ZF5
Downregulation			
Adamts15	ADAM metallopeptidase with thrombospondin type 1 motif, 15	-5.951588472	+
Adamts8	ADAM metallopeptidase with thrombospondin type 1 motif, 8	-3.159296244	+
Bola1	bolA family member 1	-0.946936945	+
Camkk1	calcium/calmodulin-dependent protein kinase kinase 1	-0.849109925	+
Drp2	dystrophin related protein 2	-1.095477261	-
Emc9	ER membrane protein complex subunit 9	-1.430967314	+
Galntl6	polypeptide N-acetylgalactosaminyltransferase-like 6	-2.786664408	-
Grik1	glutamate ionotropic receptor kainate type subunit 1	-3.391188431	+
Hctr1	hypocretin receptor 1	-3.798795218	+
Ifit1bl	interferon-induced protein with tetratricopeptide repeats 1B-like	-2.917247163	-
Inha	inhibin subunit alpha	-1.157343502	+
Kcnab2	potassium voltage-gated channel subfamily A regulatory beta subunit 2	-1.470790413	+
Lrrc24	leucine rich repeat containing 24	-0.883549539	+
Polr3k	RNA polymerase III subunit K	-0.560025598	+
Ppp1r3e	protein phosphatase 1, regulatory subunit 3E	-1.472834238	+
RGD1562229	similar to hypothetical protein FLJ40298	-5.716667009	+
RT1-DMa	Rt1 class II, locus Dma	-1.124408168	+
Rtl6	retrotransposon Gag like 6	-0.462762635	+
Rxrg	retinoid X receptor gamma	-2.449907867	+
Sh3rf3	Sh3 domain containing ring finger 3	-1.344191437	+
Slc7a4	solute carrier family 7, member 4	-1.540354421	+
Synpr	synaptoporin	-1.710370056	+
1700030J22Rik	RIKEN cDNA 1700030J22 gene	-1.336028724	+
AABR07001519.1	parkin RBR E3 ubiquitin protein ligase	-1.392497667	+
Upregulation			
Giot1	gonadotropin inducible ovarian transcription factor 1	3.24517695	-

$p_{adj} = 7.233 \times 10^{-4}$

4.3.5 Expression Zbtb14 protein in the temporal lobe epilepsy

Zbtb14 protein level in the epileptic hippocampus was investigated in a pilocarpine model of epilepsy in mice. Tissues were collected at two selected time points: 3 PM and 11 PM (Figure 4.35). No difference was observed in protein levels between control and epileptic animals at 3 PM (1.64±0.62 vs. 2.84±0.61 a.u., respectively). In contrast, at 11 PM, expression of the Zbtb14 protein was significantly higher in epileptic animals than in controls (19.95±2.24 vs. 3.73 ±1.16 a.u., respectively, $p<0.001$). The expression of the Zbtb14 protein in epileptic animals was significantly higher at 11 PM than at 3 PM ($p<0.001$).

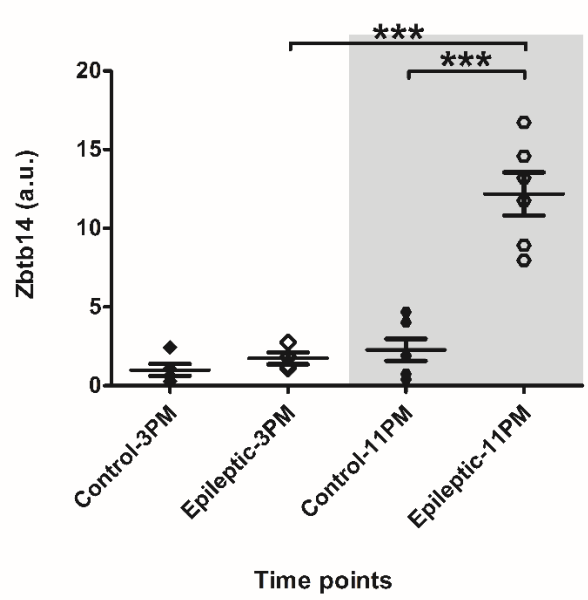

Figure 4.35 Zbtb14 protein level in the hippocampus of epileptic mice. The relative ratios of Zbtb14 to β-actin are represented as the mean ± SEM (n=5 for Control-3 PM, n=4 for Epileptic-3 PM, and n=6 for Control- and Epileptic-11 PM; *p<0.05, **p<0.01, ***p<0.001, one-way ANOVA with Bonferroni's multiple comparison post hoc test). a.u.: arbitrary unit.

CHAPTER 5

DISCUSSION

In this study, I established the following:

i. The Zbtb14 protein is expressed exclusively in neurons in the mammalian brain,

ii. The Zbtb14 protein oscillates through a circadian cycle in the ventral hippocampus only but not in the dorsal hippocampus nor in the somatosensory cortex,

iii. The oscillation of the Zbtb14 protein occurs in both the cytoplasm and nucleus but in a different pattern,

iv. The genes that are downregulated in the *in vitro* model of epileptiform discharges have a ZF5 motif in their promoters, and these downregulated genes that are potentially regulated by the Zbtb14 transcription factor mostly play a role in synaptic plasticity and transmission and

v. The circadian dynamics of the Zbtb14 protein are perturbed by epilepsy pathology in an *in vivo* model of epilepsy.

5.1 Nucleocytoplasmic transport

Although the Zbtb14 protein has been known for over three decades (Numoto et al., 1993), its specific expression within the brain, including the types of cells it is expressed in, remains unknown. My research showed that it is exclusively expressed in neurons

and found in the cell's cytosol and nucleus. Furthermore, our findings indicated that the expression of the Zbtb14 protein follows distinct circadian patterns in these two cellular compartments. In the cytoplasm, the highest Zbtb14 protein level was observed at 3 pm, and the lowest levels were observed during the light-off phase. In the nucleus, the Zbtb14 level peaks at 11 pm and then gradually decreases during the dark period. This suggests that the transport of the Zbtb14 protein into the nucleus might preferentially occur at the beginning of the dark period. As a transcription factor, being in the nucleus is essential for the role of the Zbtb14 protein; regulating of its transport from the cytoplasm to the nucleus might be a way to control its function in a time-dependent manner.

Protein nucleocytoplasmic shuttling requires several complex steps from and to the nucleus or cytoplasm. First, a nuclear import/export receptor recognises a localisation signal, for example, a nuclear localisation signal (NLS), and these receptors transport proteins or RNA through the nuclear pore complex (NPC). Next, the transported molecule is released, and the import/export receptors are recycled for future translocations (Bednenko et al., 2003; Fabbro & Henderson, 2003). The regulation of nucleocytoplasmic trafficking is crucial for the role of nuclear proteins or RNAs; any disorganisation in the transport of a protein or RNA may develop into mislocalisation or perturb the downstream effects of the protein or RNA in question (Fabbro & Henderson, 2003).

Although the Zbtb protein family is one of the largest protein families in mammals, its nuclear localisation signals, the proteins that interact, and the nucleocytoplasmic shuttling mechanisms of many Zbtb proteins are unknown. A review by Tamanini et al. (2005) reports that small proteins that have a molecular weight of approximately 50 kDa and less can be translocated from and to the nucleus spontaneously. The Zbtb14 protein has a predicted molecular weight of 51 kDa and an observed molecular weight of ~55 kDa. As a small protein, Zbtb14 might be transported in and out of the nucleus immediately, which can explain why we did not observe a time point that had no Zbtb14 protein within the nucleus at the observed time points. The UniProt database suggests a domain between 50 and 66 amino acid sequences that can act as a nuclear localisation

signal (NLS) of the Zbtb14 protein (https://www.uniprot.org/uniprotkb/O43829/entry#family_and_domains).

My data show that the Zbtb14 protein can cross nuclear envelope but there is no literature on how the Zbtb14 protein is being shuttled into the nucleus when there is a signal for it to be reallocated. From the literature on other Zbtb proteins and core clock proteins, we can speculate that it may be transported via (i) importin receptors, (ii) piggy-backing other proteins that cross the NPC, and (iii) spontaneous crossing (Donaldson et al., 2007; Rodríguez et al., 2010; Tamanini et al., 2005). Transportation of the Zbtb14 protein might be controlled at the level of translation, posttranslational modifications, time-controlled accumulation at the nuclear membrane border and/or protein degradation, similar to other Zbtb proteins (Tamanini et al., 2005; Tamaru et al., 2003). When we consider the dynamic environment within the cell, we can assume that many of these processes play a role in the outcome.

5.2 Dorsal-ventral axis of the hippocampus

The analysis of Zbtb14-positive cell densities along the longitudinal axis of the hippocampus and in the somatosensory cortex revealed that Zbtb14 protein level is dynamically regulated over the circadian cycle only in the ventral hippocampus.

Historically, the hippocampus has been known for its relation to memory (e.g., declarative and spatial memory) (Klinzing et al., 2019; Scoville & Milner, 1957). Nevertheless, later studies on the hippocampus revealed that the hippocampus also plays a vital role in mood regulation and emotional memory (Komorowski et al., 2013; Sokolov & Vinogradova, 1975; Yoshida, 1984). Regardless of half a century of research on the hippocampus, there is no consensus even on its basic function (Fanselow & Dong, 2010). However, the recent literature shows that the ventral hippocampus is different in connectivity, gene expression pattern, neurochemical pattern, and function from the dorsal hippocampus in rodents, which corresponds to the human anterior and posterior hippocampus, respectively (Bienkowski et al., 2018; Lothmann et al., 2021; O'Leary & Cryan, 2014). The latest consensus associates the dorsal hippocampus with spatial memory and learning and the ventral hippocampus with context- and emotion-based memory (Brancati et al., 2021).

Current research on the hippocampus has shown that it has three compartments that control different aspects of hippocampal function: dorsal, intermediate, and ventral. The study that Bienkowski et al. (2018) published on gene expression and connectivity of the hippocampus established that the hippocampal network and gene expression gradually change dorsoventrally. They found that the dorsal CA1 and the dorsoventral subiculum play a crucial part in spatial orientation and send output to the visual and spatial brain areas (i.e., ventral retrosplenial cortex, medial mammillary nucleus, and postsubicilum). Meanwhile, the CA2, the dorsocaudal CA1, the prosubiculum and intermediate CA1, the ventral CA1 and the ventral subiculum networks perform as modulators of social behaviour such as aggression (Bienkowski et al., 2018). Another study on neurochemical receptor densities associated with anatomical segmentation revealed distinct regional differences between dorsal, intermediate, and ventral hippocampal structures. While high AMPA expression was observed in the dorsal and intermediate CA1 and the intermediate and ventral CA3, the rest of the hippocampal structures showed significantly lower expression. Kainate and NMDA receptors were higher in the dorsal DG than in the ventral DG. The dorsoventral pattern of kainate expression increased significantly in CA1, while NMDA expression displayed a reverse expression pattern. $GABA_B$ receptors did not show any changes depending on the anatomical sections in the hippocampus. $GABA_A$ receptors presented a significant increase between the ventral DG and the dorsal DG. CA1 displayed a significant gradual decrease from the dorsal axis to the ventral axis. The catecholaminergic receptor α_2 showed significantly higher expression in the ventral DG than in the dorsal DG and in the intermediate CA1 than in the dorsal and ventral CA1 and a significant gradual increase from dorsal to ventral CA3 (Lothmann et al., 2021). Brancati and colleagues (2021) showed that energy metabolism was altered along the dorsoventral axis of the hippocampus over a circadian cycle. They suggested that the energy production differences in the dorsal and ventral hippocampus might originate from their role. They proposed that the higher GABA and glutamate release in the ventral hippocampus might require higher energy (Brancati et al., 2021). As these studies emphasise, the hippocampal formation is extremely complex neurochemically, transcriptionally, metabolically and structurally. My study supports the literature on the heterogeneity of the hippocampus over the longitudinal axis.

5.3 Enriched ZF5 Motif in the Promoters of Downregulated Genes with the Induction of Epileptiform Discharges *In Vitro*

The functional enrichment analysis on RNAseq data of the *in vitro* model of epileptiform discharge revealed that many of the downregulated genes have the GC-rich consensus binding site of the ZF5 motif – 5'-GSGCGCGR-3' (R represents A or G, and S represents G or C) (Bozek et al., 2009; Obata et al., 1999). Further analysis with the DAVID database (https://david.ncifcrf.gov/home.jsp) showed that 11 of the 21 downregulated genes that have ZF5 motifs in their promoters are also expressed in the mouse brain: Adamts15, Bola1, Camkk1, Grik1, Kcnab2, Lrrc24, Ppp1r3e, Sh3rf3, Slc7a4, Synpr, and 1700030J22Rik. An additional six genes were found to be present in the mammalian brain after a PubMed search: Adamts8 (Dunn et al., 2006; Rossier et al., 2015), Hcrtr1 (Li et al., 2018; Scott et al., 2011), Inha (Fujimura et al., 1999), Polr3k (Lata et al., 2021), Rtl6 (Irie et al., 2022), and Rxrg (McCullough et al., 2018). Adamts15 and Adamts8 are metalloprotease enzymes that reshape perineuronal nets (Rossier et al., 2015). Kcnab2 is a subunit of voltage-gated potassium channel complexes such as Kv1 that play an essential part in neuronal excitability (Yee et al., 2022). Synpr is a component of synaptic vesicle membranes and a part of the synaptophysin superfamily (Knaus et al., 1990). Grik1 encodes an ionotropic glutamate receptor subunit known as GluK1 and is involved in synaptic transmission and plasticity (Valbuena et al., 2019). Taken together, the Zbtb14 protein seemingly regulates the genes associated with synaptic activity, transmission and plasticity.

Hcrtr1 stands for hypocretin/orexin receptor 1 and can induce neurotransmitter release both post- and pre-synaptically. Hcrtr1 is known to play a great array of roles and triggers several signalling cascades depending on the context, including the sleep-wake cycle and mood. Hcrtr1 antagonists have been shown to decrease epileptic seizures and alleviate anxiety-like behaviours (Kordi Jaz et al., 2017; Li et al., 2018; Scott et al., 2011). Within the context of the *in vitro* epileptiform discharge experiment, downregulation of Hcrtr1 expression 24 hours after the induction of epileptiform activity might be in response to recovery from epileptiform discharges by reducing epileptic seizures.

Grik1 is a subunit of the ionotropic glutamate receptor kainate 1 (GluK1) and regulates a subset of GABAergic neurons, i.e., parvalbumin- and somatostatin-positive cells. Grik1

inactivation in the lateral amygdala is associated with an increase in neuronal excitability, anxiety-like behaviour and long-term potentiation (Englund et al., 2021). Additionally, Grik1 overexpression, due to triplication of the gene in a Down syndrome mouse model, resulted in spatial memory deficits. The authors showed that overinhibition of CA1 pyramidal cells via dysfunctional GABA release is responsible for disruption in spatial navigation (Valbuena et al., 2019). The downregulation of Grik1 can explain affective disorders and memory issues that are observed in epileptic patients.

Retinoid X receptor gamma (Rxrg) is part of a nuclear receptor family and is activated by retinoic acid (https://www.genecards.org/cgi-bin/carddisp.pl?gene=DRD2). Its expression increases with fear conditioning in the central amygdala and is observed in Drd2-positive neurons. Drd2-expressing neurons are associated with learning and memory, especially within reward- and fear-based schemes (McCullough et al., 2018). Lee et al. (2004) reported that the Zbtb14 transcription factor is a positive regulator of the human dopamine transporter (hDAT). DAT and Drd2 interact with each other in the presynaptic compartment. They modulate the dopamine available in the synaptic cleft. Therapeutics that induce dopaminergic pathways, such as Parkinson's disease (PD) medications, are presumed to suppress epileptic seizures and have anti-epileptogenic properties (Bozzi & Borrelli, 2013). In an *in vitro* model of PD in primary ventral midbrain cells, it has been shown that the retinoid X receptor supports the survival of dopaminergic neurons (Friling et al., 2009). Taken together, downregulation of Rxrg might reduce the protective effect of Drd2-positive neurons, increase seizure susceptibility and play a role in the anxious behaviour phenotype in patients with epilepsy.

RNA polymerase III is a complex enzyme composed of 17 subunits, and Polr3k is one of the subunits. RNA polymerase III is not responsible for any protein-coding RNAs but navigates the transcription of small RNAs such as tRNAs and 5S RNA. Disruption in RNA polymerase III function due to mutations to its subunits, including Polr3k, results in a reduction in tRNA and 7SL RNA expression, which correlates with the incapacitation of global protein synthesis and stabilisation. Especially in neurons, decreased RNA polymerase III activity perturbs protein and neurotransmitter shuttling via the ER and affects synaptic plasticity in both axons and dendrites (Lata et al., 2021). Hypothetically, the downregulation of Polr3k via the Zbtb14 transcription factor in an *in vitro* model of

epileptiform discharges might explain the downregulation of other genes observed even without the direct involvement of Ztbt14.

Kcnab2 protein is studied in epilepsy as a risk factor (Kurosawa et al., 2005). Kcnab2 plays a crucial role in action potential modulation as a subunit of the potassium channel complex and affects neuronal excitability. Kcnab2 knockout mice had a decreased level of Kv1.2 channels and displayed increased excitability. Researchers have observed deficits in learning and memory in Kcnab2 knockout animals (Yee et al., 2022).

Synaptoporin (Synpr) is a widely used mossy fiber marker in the hippocampus (Cabrera et al., 2022). Although synaptoporin is highly expressed in dentate granular cell axons, it has also been shown to be expressed in the CA3 subfield. Synpr is an isoform of synaptophysin, a component of small synaptic vesicles. Synpr is located especially in mossy fiber boutons and thought to interact with the SNARE complex and modulate neurotransmitter release, such as synaptophysin (Singec et al., 2002). Synpr expression is decreased in patients with schizophrenia. Hence, it is considered a marker of disturbance in synaptic transmission (Ibi et al., 2020). The dentate gyrus is one of the special locations in the mammalian brain where adult neurogenesis takes place. After the initial insult that triggers epileptogenic events, neural stem cells in the subgranular zone (SGZ) increase the generation of new granular cells. However, these new granular cells do not always integrate into the neuronal network properly. The axons of the dentate granular cells are called mossy fiber axons, and the axons of these incorrectly integrated granular cells project into the CA3 pyramidal layer, similar to their properly engaged counterparts. Improper integration results in a hyperexcitable network (Hattiangady & Shetty, 2008). Neuronal loss due to the initial insult, incorrectly integrated neuronal network and disrupted synaptic transmission due to downregulation of Synpr might explain the complex picture we see in epilepsy pathology. Taken together, these results indicate that Synpr downregulation hinders transmitter regulation and synaptic connectivity strength.

Inhibin A (Inha) is a member of the transforming growth factor beta (TGFβ) family along with activins. Inha is expressed in adult astrocytes in the dentate gyrus of the hippocampus, among several other brain regions (Fujimura et al., 1999). Astrocytes play an essential role in the chemical arrangement of the synaptic cleft to modulate neuronal

signalling (Hastings et al., 2023). The Zbtb14 protein is not expressed in astrocytes, yet it is implicated with the genes that modify the extracellular matrix (Adamts8 and Adamts15); this might explain its indirect effect on Inha expression in mature astrocytes. A research on an ovarian cancer cell line (HEY) showed that when Inha expression was silenced via shRNA use, it increased the protein level of Adamts-1 by about 1.6 times (Horst et al., 2022). Therefore, it is probable that an insult to the brain might induce perineuronal net proteolysis by Adamts8 and Adamts15 (Chaunsali et al., 2021; Domingues et al., 2016). The literature on Activin A shows that it boosts oligodendrocyte differentiation and new myelin sheath production, and has neuroprotective effects after an insult to the brain, such as stroke. (Tumurgan et al., 2019; Tumurgan et al., 2020). The mechanism of action of Inha is yet to be elucidated, but it is assumed that it has an opposite role to Activin A (Ying et al., 1995). Based on the assumption that Inha has a reverse function compared to Activin A, downregulation of Inha in astrocytes would affect oligodendrocytes and myelination. Aberrant myelination might contribute to epileptic seizures because of changes in neuronal activity (Knowles et al., 2022).

Additionally, our previous transcriptomics data (Debski et al., 2020) from the ventral hippocampus of control and epileptic animals share three differentially expressed genes with the *in vitro* data: Adamts15, 1700030J22Rik, and Inha. The transcriptomic data (Debski et al., 2020) reported that Adamts15 and 1700030J22Rik did not have circadian oscillations in control animals but gained oscillatory patterns in pilocarpine-treated epileptic animals. This circadian dynamics change in Adamts15 might result in altered regulatory function on the extracellular matrix of Adamts15 that is triggered due to epilepsy pathology. Conversely, Inha oscillates throughout the circadian cycle in the control animals, but this rhythm is abolished in epileptic animals. The overlap of three genes –Adamts15, 1700030J22Rik and Inha– from two different data sets and the identification of the same transcription factor further strengthens the possibility of the involvement of the Zbtb14 transcription factor in the regulation of Adamts15, 1700030J22Rik and Inha.

5.4 Effect of epilepsy on the circadian dynamics of Zbtb14 protein level in the hippocampus

The comparison of Zbtb14 expression at two time points in the circadian cycle showed that Zbtb14 expression is perturbed in a time-specific manner. While comparison of control and epileptic animals at 3 pm showed no significant difference in Zbtb14 protein level, at 11 pm epileptic animals had almost six times higher expression of Zbtb14 protein than control pm animals. Bozek et al. (2009) reported that the same ZF5 motif that we identified in our *in vitro* data, among many circadian-regulated transcription factors with GC-rich motifs, had tissue- and time-point-specific patterns in an *in silico* analysis. The 11 pm time-point is the peak expression time-point of the Zbtb14 protein in my nuclear extracts. Although it is tempting, I cannot draw a direct conclusion because epileptic and control protein extracts were total protein extracts. However, we cannot exclude the idea that the higher expression of the Zbtb14 protein might be related to the contribution of the higher nuclear content.

A higher nuclear Zbtb14 content would correlate with higher transcriptional activity of Zbtb14. This would presumably conclude in the decreased expression of the genes identified in the *in vitro* experiment. Because my data showed that the Zbtb14 protein only has dynamic oscillations over circadian cycle in its expression in the ventral hippocampus. This suggests that all the genes that have ZF5 overrepresentation in their promoters from the *in vitro* experiment would be dysregulated only in the ventral hippocampus as a downstream effect of disrupted Zbtb14 protein level. Downregulation of many of these genes increases excitability in neurons and anxiety-related behaviour. Hence, it is not surprising to identify many genes that affect learning and memory that are associated with the hippocampus and anxiety-like behaviours that are implicated in the ventral hippocampus. Having higher Zbtb24 protein in the nuclear compartment can aggravate epilepsy by increasing seizure susceptibility and inducing common comorbidities such as mood and anxiety disorders (https://www.epilepsy.com/parents-and-caregivers/talking-kids-about-epilepsy/related-conditions).

5.5 Chronotherapy

The risk factors that jetlag and shiftwork created for cardiovascular disease, obesity, and several cancers showed that the circadian cycle affects and controls more than entrainment to the light cue for the sleep-wake cycle. Transcription of core clock genes and translocation of the core clock proteins/transcription factors triggers multiple pathways responsible for energy metabolism, DNA replication, and DNA damage and repair responses. Every peripheral organ and CNS are aligned with the circadian rhythm through the SCN via zeitgebers (Hetman et al., 2022). The entrainment signal from the SCN attunes every cell, generating an oscillatory pattern in every organ. Misaligned circadian rhythm has been shown to concur with many psychiatric, neuroinflammatory and neurodegenerative diseases as well as many metabolic diseases. The arrhythmic circadian cycle and disease pathology bidirectionally affect each other (Hetman et al., 2022; Leite Góes Gitai et al., 2019; Sun & Wang, 2023). A gene with dynamic oscillatory expression can lose its rhythmicity due to disease pathology, and vice versa; when a particular gene loses/gains rhythmicity due to disruption in the circadian cycle chronically, it may alter cell dynamics to create disease pathology. For example, melatonin is a pineal hormone that responds to darkness. It peaks at night, and its levels drop before wakefulness (Lavie, 1997; Zisapel, 2007, 2018). The release of melatonin is disrupted and decreased in shiftworkers such as security guards and healthcare workers. Chronic disruption of melatonin secretion results in a higher risk of sleep and mood disorders and certain types of cancer (Cipolla-Neto et al., 2014; Mancio et al., 2018; Razavi et al., 2019; Wright et al., 2013). In contrast, acute complications such as traumatic brain injury perturb the regular oscillatory pattern in the brain and periphery due to the injury. The desynchronised circadian cycle would transfer the perturbed activity to its downstream pathways, and depending on the time point of the injury, it can worsen or aid the outcome (Hetman et al., 2022).

Epilepsy is a neurological disease that is known to affect the circadian cycle (Brancati et al., 2021; Debski et al., 2020; Hofstra et al., 2009; Leite Góes Gitai et al., 2019; Sun & Wang, 2023). Remarkably, although epileptic seizures seem to arise spontaneously, clinical data, patient journals and research have shown that epileptic seizures occur more often and severely at certain times over the circadian cycle (Hofstra et al., 2009;

Karoly et al., 2021; Zhang et al., 2021). For example, patients who have neocortical temporal lobe epilepsy have epileptic seizures in the afternoon (Sun & Wang, 2023). Quigg and colleagues (2000) reported that a rat model of mesial temporal lobe epilepsy revealed that epileptic seizures in animals housed in total darkness continued to occur in the same pattern as the animals housed in light-dark conditions with 12-hour periods. However, they also demonstrated that light exposure affects the endogenous rhythm of rats and changes the amplitude of seizures and the distribution of seizure occurrence time (Quigg et al., 2000). Additionally, Re and colleagues (2020) stated that while generalised, atonic and myoclonic seizures are linked to the light phase of the day, automotor, tonic, and clonic seizures occur at the dark phase of the day.

Although the effect of epilepsy on the circadian rhythm is well established, the effect of the perturbed circadian rhythm on epilepsy remains largely unknown. In a study by Li et al. (2017), they performed transcriptomic analysis on human tissue samples of two focal epilepsies: focal cortical dysplasia and tuberous sclerosis complex. They revealed that the expression of the core clock gene *Clock* was reduced significantly in these two focal epilepsy samples. They investigated the molecular mechanisms by which the loss of *Clock* expression in excitatory neurons affects neuronal excitability and spine density in a Cre knockout mouse model. They reported that the Cre mouse model they used had a lower seizure threshold when injected with pentylenetetrazol and increased excitability due to malfunctioning inhibitory neurons or impaired synapses (Li et al., 2017). This study shows a direct connection between loss of a core clock gene and an increase in seizure susceptibility. Yue and colleagues (2020) used a pilocarpine mouse model and revealed that *Rev-Erbα* gene expression was reduced in an animal model and human tissue samples. The administration of an agonist of Rev-Erbα after SE diminished the inflammatory response and had a protective effect on principal neurons of the hippocampus. Another study found that a Rev-Erbα antagonist had an anticonvulsant effect in different models of epilepsy, and the best administration time window was between ZT6 and ZT10 (Zhang et al., 2021). The two studies on the disruption of *Rev-Erbα* gene expression have seemingly opposite effects. However, both studies claimed that manipulating *Rev-Erbα* gene expression might be a therapeutic target to reduce seizure susceptibility and reduce the inflammatory response. However, more research

is needed to inspect the changes in the molecular mechanisms over the circadian cycle and how the changes in circadian regulated genes affect epileptogenesis and epileptic seizures.

In another approach, Zhang et al. (2018) showed that the disadvantage of having a “leaky” blood–brain barrier in epileptic patients might be turned into an advantage. In naïve *Drosophila melanogaster*, Zhang and colleagues (2018) presented that blood–brain barrier permeability is not stable and that the rate of efflux changes depending on the time of day. Additionally, they used a *Drosophila* mutant that is prone to seizure and induced seizure via mechanical shock. They administered an anticonvulsant drug – phenytoin – at different time points over the circadian cycle to observe how it affected the recovery time. Authors revealed that night time administration of phenytoin was more efficacious in mutant flies than at other time points (Zhang et al., 2018). Taken together, it is clear that circadian arrhythmia and epilepsy pathology cannot be separated, and the portrait that we see in epileptic patients is a mixture of these factors. Circadian cycle studies can be used in multiple ways to increase the quality of life, reduce or eliminate seizures and/or alleviate the side effects of the drugs administered to the patient while maximising the beneficial effects.

The investigation of cycles from circadian to circannual has been a popular direction recently due to the prospect of chronotherapy – the administration of active ingredients when they are most effective. The effect of circadian and multidian (multiple days) cycles on epilepsy was known as early as 1881 thanks to the observations of Sir William Richard Gowers, who identified three different groups of patients based on the time-of-day of the seizures: 45% diurnal, 33% mixed, and 22% nocturnal (Karoly et al., 2021). The circadian rhythm within the brain and periphery regulates the sleep-wake cycle, body temperature, and daily hormonal cycles. The effects of zeitgebers are integrated into every single aspect of our lives (Hastings et al., 2018). Hence, it is not inconceivable that circadian rhythmicity can and would affect the timing of epileptic seizures to some extent.

Our study aimed to identify and characterise a transcription factor that plays an important role by potentially regulating the genes altered by epilepsy pathology. While "fixing" the domino effect that the Zbtb14 protein created in epilepsy via chronotherapy

approach is not going to cure epilepsy, our goal with chronotherapy studies is to improve the overall quality of life of the patients (Hetman et al., 2022; Karoly et al., 2021). Therefore, my results offer another focus point for circadian studies in epilepsy: the transcription factor Zbtb14.

CHAPTER 6

CONCLUSION AND LIMITATIONS

6.1 Conclusion

The data presented in this thesis emphasise the importance of circadian studies within the context of epilepsy. Circadian oscillations of the Zbtb14 transcription factor only in the ventral hippocampus is an exciting and vital finding of my study as the ventral hippocampus is the most ictogenic site in temporal lobe epilepsy patients and rodent models of TLE. The different oscillatory dynamics of the Zbtb14 protein in cytoplasmic and nuclear compartments throughout the circadian cycle highlight the prominence of nucleocytoplasmic transportation for the controlling of the role of Zbtb14. The *in vitro* data revealed 21 downregulated genes with ZF5 motifs on their promoters, and the nuclear-present Zbtb14 protein is probably responsible for these alterations. Lastly, my *in vivo* data presented that the expression of Zbtb14 protein is dysregulated in a time-specific manner in temporal lobe epileptic animals.

6.2 Limitations

In this study, we only used male animals to reduce the complexity included with the female estrous cycle. However, I recognise the need to include female animals in future studies as several epidemiological studies are emphasising the sexual dimorphism in epilepsy, including the differences in the types of epilepsy females inclined to have,

seizure threshold, and epileptogenesis (Hophing et al., 2022; McHugh & Delanty, 2008; Reddy, 2020; Reddy et al., 2021).

My results and the literature reiterate the heterogeneity along the dorsal-ventral axis of the hippocampus (Bienkowski et al., 2018; Lothmann et al., 2021; O'Leary & Cryan, 2014). Moreover, the ventral hippocampus has also been shown to be the primary ictal onset and epileptogenic site in rodent models of temporal lobe epilepsy (Buckmaster et al., 2022; Wyeth et al., 2020) and human temporal lobe epilepsy (King et al., 1997). Our preliminary study (Debski et al., 2020) identified the ZF5 motif on the promoters of several differentially expressed genes in the ventral hippocampus of epileptic animals. Hence, it would be beneficial to see how Zbtb14-positive cell densities are affected along the longitudinal axis of the hippocampus by epilepsy in future studies.

I observed different circadian dynamics of cytoplasmic and nuclear content of the Zbtb14 protein in naïve animals. However, the epileptic animal protein extracts were total protein extracts. Therefore, we do not know the subcellular dynamics of the Zbtb14 protein within these two cellular compartments in epileptic animals. Given that the epilepsy pathology changed the Zbtb14 protein level in time-point dependent, how much nuclear fraction contributes to the outcome would be an interesting point to investigate in future studies.

BIBLIOGRAPHY

Amaral, D., Scharfman, H., & Lavenex, P. (2007). The dentate gyrus: fundamental neuroanatomical organization (dentate gyrus for dummies) [Review]. *Dentate Gyrus: a Comphrehensive Guide To Structure, Function, and Clinical Implications*, *163*, 3-+. https://doi.org/10.1016/S0079-6123(07)63001-5

Aronica, E., & Gorter, J. (2007). Gene expression profile in temporal lobe epilepsy [Article]. *Neuroscientist*, *13*(2), 100-108. https://doi.org/10.1177/1073858406295832

Barr, J. L., Bray, B., & Forster, G. L. (2017). The Hippocampus as a Neural Link between Negative Affect and Vulnerability for Psychostimulant Relapse. In S. Ales (Ed.), *The Hippocampus*. IntechOpen. https://doi.org/10.5772/intechopen.70854

Bednenko, J., Cingolani, G., & Gerace, L. (2003). Nucleocytoplasmic transport: navigating the channel. *Traffic*, *4*(3), 127-135. https://doi.org/10.1034/j.1600-0854.2003.00109.x

Bienkowski, M. S., Bowman, I., Song, M. Y., Gou, L., Ard, T., Cotter, K., . . . Dong, H. W. (2018). Integration of gene expression and brain-wide connectivity reveals the multiscale organization of mouse hippocampal networks. *Nat Neurosci*, *21*(11), 1628-1643. https://doi.org/10.1038/s41593-018-0241-y

Bileck, A., Mayer, R. L., Kreutz, D., Weiss, T., Taschner-Mandl, S., Meier, S. M., . . . Gerner, C. (2017). Evaluation of inflammation-related signaling events covering phosphorylation and nuclear translocation of proteins based on mass spectrometry data. *J Proteomics*, *152*, 161-171. https://doi.org/10.1016/j.jprot.2016.11.008

Bozek, K., Relógio, A., Kielbasa, S. M., Heine, M., Dame, C., Kramer, A., & Herzel, H. (2009). Regulation of clock-controlled genes in mammals. *PLoS One*, *4*(3), e4882. https://doi.org/10.1371/journal.pone.0004882

Bozzi, Y., & Borrelli, E. (2013). The role of dopamine signaling in epileptogenesis. *Front Cell Neurosci*, *7*, 157. https://doi.org/10.3389/fncel.2013.00157

Brancati, G. E., Rawas, C., Ghestem, A., Bernard, C., & Ivanov, A. I. (2021). Spatio-temporal heterogeneity in hippocampal metabolism in control and epilepsy conditions. *Proc Natl Acad Sci U S A*, *118*(11). https://doi.org/10.1073/pnas.2013972118

Buckmaster, P. S., Reyes, B., Kahn, T., & Wyeth, M. (2022). Ventral hippocampal formation is the primary epileptogenic zone in a rat model of temporal lobe epilepsy. *J Neurosci*, *42*(39), 7482-7495. https://doi.org/10.1523/JNEUROSCI.0429-22.2022

Cabrera, O. H., Useinovic, N., Maksimovic, S., Near, M., Quillinan, N., Todorovic, S. M., & Jevtovic-Todorovic, V. (2022). Neonatal ketamine exposure impairs infrapyramidal bundle pruning and causes lasting increase in excitatory synaptic transmission in hippocampal CA3 neurons. *Neurobiol Dis*, *175*, 105923. https://doi.org/10.1016/j.nbd.2022.105923

Chatzikonstantinou, A. (2014). Epilepsy and the hippocampus. *Front Neurol Neurosci*, *34*, 121-142. https://doi.org/10.1159/000356435

Chaunsali, L., Tewari, B. P., & Sontheimer, H. (2021). Perineuronal Net Dynamics in the Pathophysiology of Epilepsy. *Epilepsy Curr*, *21*(4), 273-281. https://doi.org/10.1177/15357597211018688

Cipolla-Neto, J., Amaral, F. G., Afeche, S. C., Tan, D. X., & Reiter, R. J. (2014). Melatonin, energy metabolism, and obesity: a review. *J Pineal Res*, *56*(4), 371-381. https://doi.org/10.1111/jpi.12137

Debski, K., Ceglia, N., Ghestem, A., Ivanov, A., Brancati, G., Broer, S., . . . Bernard, C. (2020). The circadian dynamics of the hippocampal transcriptome and proteome is altered in experimental temporal lobe epilepsy [Article]. *Science Advances*, *6*(41), Article ARTN eaat5979. https://doi.org/10.1126/sciadv.aat5979

Deng, Y., Wang, H., Liu, X., Yuan, H., Xu, J., de Thé, H., . . . Zhu, J. (2022). Zbtb14 regulates monocyte and macrophage development through inhibiting. *Elife*, *11*. https://doi.org/10.7554/eLife.80760

Dobin, A., Davis, C. A., Schlesinger, F., Drenkow, J., Zaleski, C., Jha, S., . . . Gingeras, T. R. (2013). STAR: ultrafast universal RNA-seq aligner. *Bioinformatics*, *29*(1), 15-21. https://doi.org/10.1093/bioinformatics/bts635

Domingues, H. S., Portugal, C. C., Socodato, R., & Relvas, J. B. (2016). Oligodendrocyte, Astrocyte, and Microglia Crosstalk in Myelin Development, Damage, and Repair. *Front Cell Dev Biol*, *4*, 71. https://doi.org/10.3389/fcell.2016.00071

Donaldson, N. S., Daniel, Y., Kelly, K. F., Graham, M., & Daniel, J. M. (2007). Nuclear trafficking of the POZ-ZF protein Znf131. *Biochim Biophys Acta*, *1773*(4), 546-555. https://doi.org/10.1016/j.bbamcr.2006.12.005

Dunn, J. R., Reed, J. E., du Plessis, D. G., Shaw, E. J., Reeves, P., Gee, A. L., . . . Walker, C. (2006). Expression of ADAMTS-8, a secreted protease with antiangiogenic properties, is downregulated in brain tumours. *Br J Cancer*, *94*(8), 1186-1193. https://doi.org/10.1038/sj.bjc.6603006

Edgar, R. S., Stangherlin, A., Nagy, A. D., Nicoll, M. P., Efstathiou, S., O'Neill, J. S., & Reddy, A. B. (2016). Cell autonomous regulation of herpes and influenza virus infection by the circadian clock. *Proc Natl Acad Sci U S A*, *113*(36), 10085-10090. https://doi.org/10.1073/pnas.1601895113

Englund, J., Haikonen, J., Shteinikov, V., Amarilla, S. P., Atanasova, T., Shintyapina, A., . . . Lauri, S. E. (2021). Downregulation of kainate receptors regulating GABAergic transmission in amygdala after early life stress is associated with anxiety-like behavior in rodents. *Transl Psychiatry*, *11*(1), 538. https://doi.org/10.1038/s41398-021-01654-7

Eun, B., Kim, H. J., Kim, S. Y., Kim, T. W., Hong, S. T., Choi, K. M., . . . Sun, W. (2011). Induction of Per1 expression following an experimentally induced epilepsy in the mouse hippocampus. *Neurosci Lett*, *498*(2), 110-113. https://doi.org/10.1016/j.neulet.2011.03.039

Fabbro, M., & Henderson, B. R. (2003). Regulation of tumor suppressors by nuclear-cytoplasmic shuttling. *Exp Cell Res*, *282*(2), 59-69. https://doi.org/10.1016/s0014-4827(02)00019-8

Fanselow, M. S., & Dong, H. W. (2010). Are the dorsal and ventral hippocampus functionally distinct structures? *Neuron*, *65*(1), 7-19. https://doi.org/10.1016/j.neuron.2009.11.031

Franklin, K. B. J., & Paxinos, G. (2008). *The mouse brain in stereotaxic coordinates*. Elsevier.

Friling, S., Bergsland, M., & Kjellander, S. (2009). Activation of Retinoid X Receptor increases dopamine cell survival in models for Parkinson's disease. *BMC Neurosci*, *10*, 146. https://doi.org/10.1186/1471-2202-10-146

Fujimura, H., Ohsawa, K., Funaba, M., Murata, T., Murata, E., Takahashi, M., . . . Torii, K. (1999). Immunological localization and ontogenetic development of inhibin alpha subunit in rat brain. *J Neuroendocrinol*, *11*(3), 157-163. https://doi.org/10.1046/j.1365-2826.1999.00310.x

Gerstner, J. R., Smith, G. G., Lenz, O., Perron, I. J., Buono, R. J., & Ferraro, T. N. (2014). BMAL1 controls the diurnal rhythm and set point for electrical seizure threshold in mice. *Front Syst Neurosci*, *8*, 121. https://doi.org/10.3389/fnsys.2014.00121

Gigli, G. L., Calia, E., Marciani, M. G., Mazza, S., Mennuni, G., Diomedi, M., . . . Janz, D. (1992). Sleep microstructure and EEG epileptiform activity in patients with juvenile myoclonic

epilepsy. *Epilepsia*, *33*(5), 799-804. https://doi.org/10.1111/j.1528-1157.1992.tb02184.x

Goosens, K. A. (2011). Hippocampal regulation of aversive memories. *Curr Opin Neurobiol*, *21*(3), 460-466. https://doi.org/10.1016/j.conb.2011.04.003

Grabowska, A., Sas-Nowosielska, H., Wojtas, B., Holm-Kaczmarek, D., Januszewicz, E., Yushkevich, Y., . . . Magalska, A. (2022). Activation-induced chromatin reorganization in neurons depends on HDAC1 activity. *Cell Rep*, *38*(7), 110352. https://doi.org/10.1016/j.celrep.2022.110352

Grigg-Damberger, M., & Foldvary-Schaefer, N. (2021). Bidirectional relationships of sleep and epilepsy in adults with epilepsy. *Epilepsy Behav*, *116*, 107735. https://doi.org/10.1016/j.yebeh.2020.107735

Gulyy, P. V., Orlov, S. V., Dizhe, E. B., Kuteikin-Teplyakov, K. B., Ignatovich, I. A., Zhuk, S. V., & Perevozchikov, A. P. (2010). Roles of ZF5 and CGGBP-20 transcription factors in regulating expression of human FMR1 gene responsible for fragile X-syndrome. *Cell and Tissue Biology*, *4*(1), 54-62. https://doi.org/10.1134/S1990519X10010050

Hastings, M. H., Brancaccio, M., Gonzalez-Aponte, M. F., & Herzog, E. D. (2023). Circadian Rhythms and Astrocytes: The Good, the Bad, and the Ugly. *Annu Rev Neurosci*, *46*, 123-143. https://doi.org/10.1146/annurev-neuro-100322-112249

Hastings, M. H., Maywood, E. S., & Brancaccio, M. (2018). Generation of circadian rhythms in the suprachiasmatic nucleus. *Nat Rev Neurosci*, *19*(8), 453-469. https://doi.org/10.1038/s41583-018-0026-z

Hattiangady, B., & Shetty, A. K. (2008). Implications of decreased hippocampal neurogenesis in chronic temporal lobe epilepsy. *Epilepsia*, *49 Suppl 5*(0 5), 26-41. https://doi.org/10.1111/j.1528-1167.2008.01635.x

Herman, J. P., Cullinan, W. E., Morano, M. I., Akil, H., & Watson, S. J. (1995). Contribution of the ventral subiculum to inhibitory regulation of the hypothalamo-pituitary-adrenocortical axis. *J Neuroendocrinol*, *7*(6), 475-482. https://doi.org/10.1111/j.1365-2826.1995.tb00784.x

Hetman, M., Slomnicki, L. P., Hodges, E. R., Saraswat Ohri, S., & Whittemore, S. R. (2022). Role of circadian rhythms in pathogenesis of acute CNS injuries: Insights from experimental studies. *Exp Neurol*, *353*, 114080. https://doi.org/10.1016/j.expneurol.2022.114080

Hirano, A., Shi, G., Jones, C. R., Lipzen, A., Pennacchio, L. A., Xu, Y., . . . Fu, Y. H. (2016). A Cryptochrome 2 mutation yields advanced sleep phase in humans. *Elife*, *5*. https://doi.org/10.7554/eLife.16695

Hofstra, W. A., Spetgens, W. P., Leijten, F. S., van Rijen, P. C., Gosselaar, P., van der Palen, J., & de Weerd, A. W. (2009). Diurnal rhythms in seizures detected by intracranial electrocorticographic monitoring: an observational study. *Epilepsy Behav*, *14*(4), 617-621. https://doi.org/10.1016/j.yebeh.2009.01.020

Holth, J. K., Fritschi, S. K., Wang, C., Pedersen, N. P., Cirrito, J. R., Mahan, T. E., . . . Holtzman, D. M. (2019). The sleep-wake cycle regulates brain interstitial fluid tau in mice and CSF tau in humans. *Science*, *363*(6429), 880-884. https://doi.org/10.1126/science.aav2546

Hophing, L., Kyriakopoulos, P., & Bui, E. (2022). Chapter Seven - Sex and gender differences in epilepsy. In E. Moro, G. Arabia, M. C. Tartaglia, & M. T. Ferretti (Eds.), *International Review of Neurobiology* (Vol. 164, pp. 235-276). Academic Press. https://doi.org/https://doi.org/10.1016/bs.irn.2022.06.012

Horst, B., Pradhan, S., Chaudhary, R., Listik, E., Quintero-Macias, L., Choi, A. S., . . . Mythreye, K. (2022). Hypoxia-induced inhibin promotes tumor growth and vascular permeability in ovarian cancers. *Commun Biol*, *5*(1), 536. https://doi.org/10.1038/s42003-022-03495-6

Ibi, D., Nakasai, G., Koide, N., Sawahata, M., Kohno, T., Takaba, R., . . . Hiramatsu, M. (2020). Reelin Supplementation Into the Hippocampus Rescues Abnormal Behavior in a Mouse Model of Neurodevelopmental Disorders. *Front Cell Neurosci*, *14*, 285. https://doi.org/10.3389/fncel.2020.00285

Irie, M., Itoh, J., Matsuzawa, A., Ikawa, M., Kiyonari, H., Kihara, M., . . . Kaneko-Ishino, T. (2022). Retrovirus-derived RTL5 and RTL6 genes are novel constituents of the innate immune system in the eutherian brain. *Development*, *149*(18). https://doi.org/10.1242/dev.200976

Jardim, A. P., Duarte, J. T. C., Lancellotti, C. L. P., Carrete, H., Centeno, R. S., Scorza, C. A., . . . Yacubian, E. M. T. (2021). Granule cell dispersion is associated with hippocampal neuronal cell loss, initial precipitating injury, and other clinical features in mesial temporal lobe epilepsy and hippocampal sclerosis. *Seizure*, *90*, 60-66. https://doi.org/10.1016/j.seizure.2021.05.024

Jiang, Q., Wu, Y., Wang, J., Wu, X., Qin, J., & Jiang, Y. (2010). Characterization of developing rat cortical neurons after epileptiform discharges. *Int J Dev Neurosci*, *28*(6), 455-463. https://doi.org/10.1016/j.ijdevneu.2010.06.006

Kaplan, J., & Calame, K. (1997). The ZiN/POZ domain of ZF5 is required for both transcriptional activation and repression. *Nucleic Acids Res*, *25*(6), 1108-1116. https://doi.org/10.1093/nar/25.6.1108

Karoly, P. J., Goldenholz, D. M., Freestone, D. R., Moss, R. E., Grayden, D. B., Theodore, W. H., & Cook, M. J. (2018). Circadian and circaseptan rhythms in human epilepsy: a retrospective cohort study. *Lancet Neurol*, *17*(11), 977-985. https://doi.org/10.1016/S1474-4422(18)30274-6

Karoly, P. J., Rao, V. R., Gregg, N. M., Worrell, G. A., Bernard, C., Cook, M. J., & Baud, M. O. (2021). Cycles in epilepsy. *Nat Rev Neurol*, *17*(5), 267-284. https://doi.org/10.1038/s41582-021-00464-1

Kiessling, S., Dubeau-Laramée, G., Ohm, H., Labrecque, N., Olivier, M., & Cermakian, N. (2017). The circadian clock in immune cells controls the magnitude of Leishmania parasite infection. *Sci Rep*, *7*(1), 10892. https://doi.org/10.1038/s41598-017-11297-8

Kim, W., Zhao, F., Wu, R., Qin, S., Nowsheen, S., Huang, J., . . . Yuan, J. (2019). ZFP161 regulates replication fork stability and maintenance of genomic stability by recruiting the ATR/ATRIP complex. *Nat Commun*, *10*(1), 5304. https://doi.org/10.1038/s41467-019-13321-z

King, D., Bronen, R. A., Spencer, D. D., & Spencer, S. S. (1997). Topographic distribution of seizure onset and hippocampal atrophy: relationship between MRI and depth EEG. *Electroencephalogr Clin Neurophysiol*, *103*(6), 692-697. https://doi.org/10.1016/s0013-4694(97)00090-4

Klinzing, J. G., Niethard, N., & Born, J. (2019). Mechanisms of systems memory consolidation during sleep. *Nat Neurosci*, *22*(10), 1598-1610. https://doi.org/10.1038/s41593-019-0467-3

Knaus, P., Marquèze-Pouey, B., Scherer, H., & Betz, H. (1990). Synaptoporin, a novel putative channel protein of synaptic vesicles. *Neuron*, *5*(4), 453-462. https://doi.org/10.1016/0896-6273(90)90084-s

Knowles, J. K., Xu, H., Soane, C., Batra, A., Saucedo, T., Frost, E., . . . Monje, M. (2022). Maladaptive myelination promotes generalized epilepsy progression. *Nat Neurosci*, *25*(5), 596-606. https://doi.org/10.1038/s41593-022-01052-2

Komorowski, R. W., Garcia, C. G., Wilson, A., Hattori, S., Howard, M. W., & Eichenbaum, H. (2013). Ventral hippocampal neurons are shaped by experience to represent behaviorally relevant contexts. *J Neurosci*, *33*(18), 8079-8087. https://doi.org/10.1523/JNEUROSCI.5458-12.2013

Kordi Jaz, E., Moghimi, A., Fereidoni, M., Asadi, S., Shamsizadeh, A., & Roohbakhsh, A. (2017). SB-334867, an orexin receptor 1 antagonist, decreased seizure and anxiety in pentylenetetrazol-kindled rats. *Fundam Clin Pharmacol*, *31*(2), 201-207. https://doi.org/10.1111/fcp.12249

Kossoff, E. H., Al-Macki, N., Cervenka, M. C., Kim, H. D., Liao, J., Megaw, K., . . . Zupec-Kania, B. A. (2015). What are the minimum requirements for ketogenic diet services in resource-

limited regions? Recommendations from the International League Against Epilepsy Task Force for Dietary Therapy. *Epilepsia*, *56*(9), 1337-1342. https://doi.org/10.1111/epi.13039

Kurosawa, K., Kawame, H., Okamoto, N., Ochiai, Y., Akatsuka, A., Kobayashi, M., . . . Kuroki, Y. (2005). Epilepsy and neurological findings in 11 individuals with 1p36 deletion syndrome. *Brain Dev*, *27*(5), 378-382. https://doi.org/10.1016/j.braindev.2005.02.004

Lata, E., Choquet, K., Sagliocco, F., Brais, B., Bernard, G., & Teichmann, M. (2021). RNA Polymerase III Subunit Mutations in Genetic Diseases. *Front Mol Biosci*, *8*, 696438. https://doi.org/10.3389/fmolb.2021.696438

Lavie, P. (1997). Melatonin: role in gating nocturnal rise in sleep propensity. *J Biol Rhythms*, *12*(6), 657-665. https://doi.org/10.1177/074873049701200622

Lee, K. H., Kwak, Y. D., Kim, D. H., Chang, M. Y., & Lee, Y. S. (2004). Human zinc finger protein 161, a novel transcriptional activator of the dopamine transporter. *Biochem Biophys Res Commun*, *313*(4), 969-976. https://doi.org/10.1016/j.bbrc.2003.11.183

Leite Góes Gitai, D., de Andrade, T. G., Dos Santos, Y. D. R., Attaluri, S., & Shetty, A. K. (2019). Chronobiology of limbic seizures: Potential mechanisms and prospects of chronotherapy for mesial temporal lobe epilepsy. *Neurosci Biobehav Rev*, *98*, 122-134. https://doi.org/10.1016/j.neubiorev.2019.01.004

Li, P., Fu, X., Smith, N. A., Ziobro, J., Curiel, J., Tenga, M. J., . . . Liu, J. S. (2017). Loss of CLOCK Results in Dysfunction of Brain Circuits Underlying Focal Epilepsy. *Neuron*, *96*(2), 387-401.e386. https://doi.org/10.1016/j.neuron.2017.09.044

Li, S., Franken, P., & Vassalli, A. (2018). Bidirectional and context-dependent changes in theta and gamma oscillatory brain activity in noradrenergic cell-specific Hypocretin/Orexin receptor 1-KO mice. *Sci Rep*, *8*(1), 15474. https://doi.org/10.1038/s41598-018-33069-8

Li, S., Zhai, J., Chu, W., Geng, X., Chen, Z. J., & Du, Y. (2020). Altered circadian clock as a novel therapeutic target for constant darkness-induced insulin resistance and hyperandrogenism of polycystic ovary syndrome. *Transl Res*, *219*, 13-29. https://doi.org/10.1016/j.trsl.2020.02.003

Liao, Y., Smyth, G. K., & Shi, W. (2014). featureCounts: an efficient general purpose program for assigning sequence reads to genomic features. *Bioinformatics*, *30*(7), 923-930. https://doi.org/10.1093/bioinformatics/btt656

Liu, Q., Yao, F., Wang, M., Zhou, B., Cheng, H., Wang, W., . . . Wang, J. C. (2011). Novel human BTB/POZ domain-containing zinc finger protein ZBTB1 inhibits transcriptional activities of CRE. *Mol Cell Biochem*, *357*(1-2), 405-414. https://doi.org/10.1007/s11010-011-0911-5

Lothmann, K., Deitersen, J., Zilles, K., Amunts, K., & Herold, C. (2021). New boundaries and dissociation of the mouse hippocampus along the dorsal-ventral axis based on glutamatergic, GABAergic and catecholaminergic receptor densities. *Hippocampus*, *31*(1), 56-78. https://doi.org/10.1002/hipo.23262

Love, M. I., Huber, W., & Anders, S. (2014). Moderated estimation of fold change and dispersion for RNA-seq data with DESeq2. *Genome Biol*, *15*(12), 550. https://doi.org/10.1186/s13059-014-0550-8

Mancio, J., Leal, C., Ferreira, M., Norton, P., & Lunet, N. (2018). Does the association of prostate cancer with night-shift work differ according to rotating vs. fixed schedule? A systematic review and meta-analysis. *Prostate Cancer Prostatic Dis*, *21*(3), 337-344. https://doi.org/10.1038/s41391-018-0040-2

McCullough, K. M., Daskalakis, N. P., Gafford, G., Morrison, F. G., & Ressler, K. J. (2018). Cell-type-specific interrogation of CeA Drd2 neurons to identify targets for pharmacological modulation of fear extinction. *Transl Psychiatry*, *8*(1), 164. https://doi.org/10.1038/s41398-018-0190-y

McHugh, J. C., & Delanty, N. (2008). Epidemiology and classification of epilepsy: gender comparisons. *Int Rev Neurobiol*, *83*, 11-26. https://doi.org/10.1016/s0074-7742(08)00002-0

Moore, J. L., Carvalho, D. Z., St Louis, E. K., & Bazil, C. (2021). Sleep and Epilepsy: a Focused Review of Pathophysiology, Clinical Syndromes, Co-morbidities, and Therapy. *Neurotherapeutics*, *18*(1), 170-180. https://doi.org/10.1007/s13311-021-01021-w

Morris, G. L., Gloss, D., Buchhalter, J., Mack, K. J., Nickels, K., & Harden, C. (2013). Evidence-based guideline update: vagus nerve stimulation for the treatment of epilepsy: report of the Guideline Development Subcommittee of the American Academy of Neurology. *Neurology*, *81*(16), 1453-1459. https://doi.org/10.1212/WNL.0b013e3182a393d1

Moser, M. B., & Moser, E. I. (1998). Functional differentiation in the hippocampus. *Hippocampus*, *8*(6), 608-619. https://doi.org/10.1002/(SICI)1098-1063(1998)8:6<608::AID-HIPO3>3.0.CO;2-7

Mure, L. S., Le, H. D., Benegiamo, G., Chang, M. W., Rios, L., Jillani, N., . . . Panda, S. (2018). Diurnal transcriptome atlas of a primate across major neural and peripheral tissues. *Science*, *359*(6381). https://doi.org/10.1126/science.aao0318

Nizińska, K., Olszewski, M., Binias, S., Nowicka, D., Szydłowska, K., Wojtas, B., & Łukasiuk, K. *The role of Methyl-CpG binding domain 3 (Mbd3) in epileptogenesis*.

Noebels, J. L., Avoli, M., Rogawski, M. A., Olsen, R. W., & Delgado-Escueta, A. V. (2012). Jasper's Basic Mechanisms of the Epilepsies. In. https://doi.org/NBK98174

Numoto, M., Niwa, O., Kaplan, J., Wong, K. K., Merrell, K., Kamiya, K., . . . Calame, K. (1993). Transcriptional repressor ZF5 identifies a new conserved domain in zinc finger proteins. *Nucleic Acids Res*, *21*(16), 3767-3775. https://doi.org/10.1093/nar/21.16.3767

Numoto, M., Yokoro, K., & Koshi, J. (1999). ZF5, which is a Kruppel-type transcriptional repressor, requires the zinc finger domain for self-association. *Biochem Biophys Res Commun*, *256*(3), 573-578. https://doi.org/10.1006/bbrc.1999.0375

Numoto, M., Yokoro, K., Yasuda, S., Yanagihara, K., & Niwa, O. (1997). Detection of mouse skeletal muscle-specific product, which includes ZF5 zinc fingers and a VP16 acidic domain, by reverse transcriptase PCR. *Biochem Biophys Res Commun*, *236*(1), 20-25. https://doi.org/10.1006/bbrc.1997.6769

Nylén, C., Aoi, W., Abdelmoez, A. M., Lassiter, D. G., Lundell, L. S., Wallberg-Henriksson, H., . . . Krook, A. (2018). IL6 and LIF mRNA expression in skeletal muscle is regulated by AMPK and the transcription factors NFYC, ZBTB14, and SP1. *Am J Physiol Endocrinol Metab*, *315*(5), E995-E1004. https://doi.org/10.1152/ajpendo.00398.2017

O'Leary, O. F., & Cryan, J. F. (2014). A ventral view on antidepressant action: roles for adult hippocampal neurogenesis along the dorsoventral axis. *Trends Pharmacol Sci*, *35*(12), 675-687. https://doi.org/10.1016/j.tips.2014.09.011

Obata, T., Yanagidani, A., Yokoro, K., Numoto, M., & Yamamoto, S. (1999). Analysis of the consensus binding sequence and the DNA-binding domain of ZF5. *Biochem Biophys Res Commun*, *255*(2), 528-534. https://doi.org/10.1006/bbrc.1998.9970

Orlov, S. V., Kuteykin-Teplyakov, K. B., Ignatovich, I. A., Dizhe, E. B., Mirgorodskaya, O. A., Grishin, A. V., . . . Perevozchikov, A. P. (2007). Novel repressor of the human FMR1 gene - identification of p56 human (GCC)(n)-binding protein as a Krüppel-like transcription factor ZF5. *FEBS J*, *274*(18), 4848-4862. https://doi.org/10.1111/j.1742-4658.2007.06006.x

Patke, A., Murphy, P. J., Onat, O. E., Krieger, A. C., Özçelik, T., Campbell, S. S., & Young, M. W. (2017). Mutation of the Human Circadian Clock Gene CRY1 in Familial Delayed Sleep Phase Disorder. *Cell*, *169*(2), 203-215.e213. https://doi.org/10.1016/j.cell.2017.03.027

Pluta, R. (2021). Cerebral Ischemia. In. https://doi.org/NBK575732

Quigg, M., Clayburn, H., Straume, M., Menaker, M., & Bertram III, E. H. (2000). Effects of Circadian Regulation and Rest—Activity State on Spontaneous Seizures in a Rat Model

of Limbic Epilepsy. *Epilepsia*, *41*(5), 502-509. https://doi.org/https://doi.org/10.1111/j.1528-1157.2000.tb00202.x

Razavi, P., Devore, E. E., Bajaj, A., Lockley, S. W., Figueiro, M. G., Ricchiuti, V., . . . Schernhammer, E. S. (2019). Shift Work, Chronotype, and Melatonin Rhythm in Nurses. *Cancer Epidemiol Biomarkers Prev*, *28*(7), 1177-1186. https://doi.org/10.1158/1055-9965.EPI-18-1018

Re, C. J., Batterman, A. I., Gerstner, J. R., Buono, R. J., & Ferraro, T. N. (2020). The Molecular Genetic Interaction Between Circadian Rhythms and Susceptibility to Seizures and Epilepsy. *Front Neurol*, *11*, 520. https://doi.org/10.3389/fneur.2020.00520

Reddy, D. S. (2020). Brain structural and neuroendocrine basis of sex differences in epilepsy. *Handb Clin Neurol*, *175*, 223-233. https://doi.org/10.1016/B978-0-444-64123-6.00016-3

Reddy, D. S., Thompson, W., & Calderara, G. (2021). Molecular mechanisms of sex differences in epilepsy and seizure susceptibility in chemical, genetic and acquired epileptogenesis. *Neuroscience Letters*, *750*, 135753. https://doi.org/https://doi.org/10.1016/j.neulet.2021.135753

Redfern, P. H., Waterhouse, J. M., & Minors, D. S. (1991). Circadian rhythms: principles and measurement. *Pharmacol Ther*, *49*(3), 311-327. https://doi.org/10.1016/0163-7258(91)90061-p

Rocha, A. K., de Lima, E., do Amaral, F. G., Peres, R., Cipolla-Neto, J., & Amado, D. (2016). Pilocarpine-induced epilepsy alters the expression and daily variation of the nuclear receptor RORα in the hippocampus of rats. *Epilepsy Behav*, *55*, 38-46. https://doi.org/10.1016/j.yebeh.2015.11.026

Rodríguez, E., Aburjania, N., Priedigkeit, N. M., DiFeo, A., & Martignetti, J. A. (2010). Nucleo-cytoplasmic localization domains regulate Krüppel-like factor 6 (KLF6) protein stability and tumor suppressor function. *PLoS One*, *5*(9). https://doi.org/10.1371/journal.pone.0012639

Roliz, A. H., & Kothare, S. (2022). The Interaction Between Sleep and Epilepsy. *Curr Neurol Neurosci Rep*, *22*(9), 551-563. https://doi.org/10.1007/s11910-022-01219-1

Rossier, J., Bernard, A., Cabungcal, J. H., Perrenoud, Q., Savoye, A., Gallopin, T., . . . Lein, E. S. (2015). Cortical fast-spiking parvalbumin interneurons enwrapped in the perineuronal net express the metallopeptidases Adamts8, Adamts15 and Neprilysin. *Mol Psychiatry*, *20*(2), 154-161. https://doi.org/10.1038/mp.2014.162

Rugg-Gunn, F., Miserocchi, A., & McEvoy, A. (2020). Epilepsy surgery. *Pract Neurol*, *20*(1), 4-14. https://doi.org/10.1136/practneurol-2019-002192

Schurhoff, N., & Toborek, M. (2023). Circadian rhythms in the blood-brain barrier: impact on neurological disorders and stress responses. *Mol Brain*, *16*(1), 5. https://doi.org/10.1186/s13041-023-00997-0

Scott, M. M., Marcus, J. N., Pettersen, A., Birnbaum, S. G., Mochizuki, T., Scammell, T. E., . . . Lutter, M. (2011). Hcrtr1 and 2 signaling differentially regulates depression-like behaviors. *Behav Brain Res*, *222*(2), 289-294. https://doi.org/10.1016/j.bbr.2011.02.044

Scoville, W. B., & Milner, B. (1957). Loss of recent memory after bilateral hippocampal lesions. *J Neurol Neurosurg Psychiatry*, *20*(1), 11-21. https://doi.org/10.1136/jnnp.20.1.11

Singec, I., Knoth, R., Ditter, M., Hagemeyer, C. E., Rosenbrock, H., Frotscher, M., & Volk, B. (2002). Synaptic vesicle protein synaptoporin is differently expressed by subpopulations of mouse hippocampal neurons. *J Comp Neurol*, *452*(2), 139-153. https://doi.org/10.1002/cne.10371

Sobek-Klocke, I., Disqué-Kochem, C., Ronsiek, M., Klocke, R., Jockusch, H., Breuning, A., . . . Eichenlaub-Ritter, U. (1997). The human gene ZFP161 on 18p11.21-pter encodes a putative c-myc repressor and is homologous to murine Zfp161 (Chr 17) and Zfp161-rs1 (X Chr). *Genomics*, *43*(2), 156-164. https://doi.org/10.1006/geno.1997.4784

Sokolov, E. N., & Vinogradova, O. S. (1975). *Neuronal Mechanisms of the Orienting Reflex*. L. Erlbaum Associates.

Spencer, R. L., & Bland, S. T. (2019). Chapter 5 - Hippocampus and Hippocampal Neurons∗. In F. George (Ed.), *Stress: Physiology, Biochemistry, and Pathology* (pp. 57-68). Academic Press. https://doi.org/https://doi.org/10.1016/B978-0-12-813146-6.00005-9

StatPearls. (2023). In. https://doi.org/NBK482171

Stevanovic, K., Yunus, A., Joly-Amado, A., Gordon, M., Morgan, D., Gulick, D., & Gamsby, J. (2017). Disruption of normal circadian clock function in a mouse model of tauopathy. *Exp Neurol*, *294*, 58-67. https://doi.org/10.1016/j.expneurol.2017.04.015

Sugiura, K., Muro, Y., Nagai, Y., Kamimoto, T., Wakabayashi, T., Ohashi, M., & Hagiwara, M. (1997). Expression cloning and intracellular localization of a human ZF5 homologue. *Biochim Biophys Acta*, *1352*(1), 23-26. https://doi.org/10.1016/s0167-4781(97)00045-6

Sun, S., & Wang, H. (2023). Reprogramming the Circadian Dynamics of Epileptic Genes in Mouse Temporal Lobe Epilepsy. *Int J Mol Sci*, *24*(7). https://doi.org/10.3390/ijms24076400

Takebayashi-Suzuki, K., Konishi, H., Miyamoto, T., Nagata, T., Uchida, M., & Suzuki, A. (2018). Coordinated regulation of the dorsal-ventral and anterior-posterior patterning of Xenopus embryos by the BTB/POZ zinc finger protein Zbtb14. *Dev Growth Differ*, *60*(3), 158-173. https://doi.org/10.1111/dgd.12431

Takebayashi-Suzuki, K., Uchida, M., & Suzuki, A. (2022). Zbtb21 is required for the anterior-posterior patterning of neural tissue in the early Xenopus embryo. *Biochem Biophys Res Commun*, *630*, 190-197. https://doi.org/10.1016/j.bbrc.2022.09.048

Tamanini, F., Yagita, K., Okamura, H., & van der Horst, G. T. (2005). Nucleocytoplasmic shuttling of clock proteins. *Methods Enzymol*, *393*, 418-435. https://doi.org/10.1016/S0076-6879(05)93020-6

Tamaru, T., Isojima, Y., van der Horst, G. T., Takei, K., Nagai, K., & Takamatsu, K. (2003). Nucleocytoplasmic shuttling and phosphorylation of BMAL1 are regulated by circadian clock in cultured fibroblasts. *Genes Cells*, *8*(12), 973-983. https://doi.org/10.1046/j.1365-2443.2003.00686.x

Toyoda, I., Bower, M. R., Leyva, F., & Buckmaster, P. S. (2013). Early activation of ventral hippocampus and subiculum during spontaneous seizures in a rat model of temporal lobe epilepsy. *J Neurosci*, *33*(27), 11100-11115. https://doi.org/10.1523/JNEUROSCI.0472-13.2013

Tumurgan, Z., Kanasaki, H., Tumurbaatar, T., Oride, A., Okada, H., Hara, T., & Kyo, S. (2019). Role of activin, follistatin, and inhibin in the regulation of Kiss-1 gene expression in hypothalamic cell models†. *Biol Reprod*, *101*(2), 405-415. https://doi.org/10.1093/biolre/ioz094

Tumurgan, Z., Kanasaki, H., Tumurbaatar, T., Oride, A., Okada, H., & Kyo, S. (2020). Roles of intracerebral activin, inhibin, and follistatin in the regulation of Kiss-1 gene expression: Studies using primary cultures of fetal rat neuronal cells. *Biochem Biophys Rep*, *23*, 100785. https://doi.org/10.1016/j.bbrep.2020.100785

Valbuena, S., García, Á., Mazier, W., Paternain, A. V., & Lerma, J. (2019). Unbalanced dendritic inhibition of CA1 neurons drives spatial-memory deficits in the Ts2Cje Down syndrome model. *Nat Commun*, *10*(1), 4991. https://doi.org/10.1038/s41467-019-13004-9

Vitaterna, M. H., Takahashi, J. S., & Turek, F. W. (2001). Overview of circadian rhythms. *Alcohol Res Health*, *25*(2), 85-93.

von Gall, C. (2022). The Effects of Light and the Circadian System on Rhythmic Brain Function. *Int J Mol Sci*, *23*(5). https://doi.org/10.3390/ijms23052778

Wang, J., Kudoh, J., Takayanagi, A., & Shimizu, N. (2005). Novel human BTB/POZ domain-containing zinc finger protein ZNF295 is directly associated with ZFP161. *Biochem Biophys Res Commun*, *327*(2), 615-627. https://doi.org/10.1016/j.bbrc.2004.12.048

Wright, K. P., Bogan, R. K., & Wyatt, J. K. (2013). Shift work and the assessment and management of shift work disorder (SWD). *Sleep Med Rev*, *17*(1), 41-54. https://doi.org/10.1016/j.smrv.2012.02.002

Wu, J., Li, Y., Feng, D., Yu, Y., Long, H., Hu, Z., . . . Zhao, M. (2023). Integrated analysis of ATAC-seq and RNA-seq reveals the transcriptional regulation network in SLE. *Int Immunopharmacol*, *116*, 109803. https://doi.org/10.1016/j.intimp.2023.109803

Wyeth, M., Nagendran, M., & Buckmaster, P. S. (2020). Ictal onset sites and γ-aminobutyric acidergic neuron loss in epileptic pilocarpine-treated rats. *Epilepsia*, *61*(5), 856-867. https://doi.org/10.1111/epi.16490

Xu, S. Y., Wu, Y. M., Ji, Z., Gao, X. Y., & Pan, S. Y. (2012). A modified technique for culturing primary fetal rat cortical neurons. *J Biomed Biotechnol*, *2012*, 803930. https://doi.org/10.1155/2012/803930

Yanagidani, A., Matsuoka, M., Yokoro, K., Tanaka, H., & Numoto, M. (2000). Identification of human autoantibodies to the transcriptional repressor ZF5. *J Autoimmun*, *15*(1), 75-80. https://doi.org/10.1006/jaut.2000.0385

Yee, J. X., Rastani, A., & Soden, M. E. (2022). The potassium channel auxiliary subunit Kvβ2 (*J Neurophysiol*, *128*(1), 62-72. https://doi.org/10.1152/jn.00194.2022

Ying, S. Y., Li, S. Q., & Zhang, Z. (1995). Expression and localization of inhibin alpha-subunit in rat retinal photoreceptor cells. *Life Sci*, *57*(1), 45-52. https://doi.org/10.1016/0024-3205(95)00241-w

Yokoro, K., Yanagidani, A., Obata, T., Yamamoto, S., & Numoto, M. (1998). Genomic cloning and characterization of the mouse POZ/zinc-finger protein ZF5. *Biochem Biophys Res Commun*, *246*(3), 668-674. https://doi.org/10.1006/bbrc.1998.8675

Yoshida, K. (1984). Influences of bilateral hippocampal lesions upon kindled amygdaloid convulsive seizure in rats. *Physiol Behav*, *32*(1), 123-126. https://doi.org/10.1016/0031-9384(84)90082-9

Yu, G., Wang, L. G., Han, Y., & He, Q. Y. (2012). clusterProfiler: an R package for comparing biological themes among gene clusters. *OMICS*, *16*(5), 284-287. https://doi.org/10.1089/omi.2011.0118

Yue, J., He, J., Wei, Y., Shen, K., Wu, K., Yang, X., . . . Yang, H. (2020). Decreased expression of Rev-Erbα in the epileptic foci of temporal lobe epilepsy and activation of Rev-Erbα have anti-inflammatory and neuroprotective effects in the pilocarpine model. *Journal of Neuroinflammation*, *17*(1), 43. https://doi.org/10.1186/s12974-020-1718-7

Zeidler, Z., Brandt-Fontaine, M., Leintz, C., Krook-Magnuson, C., Netoff, T., & Krook-Magnuson, E. (2018). Targeting the Mouse Ventral Hippocampus in the Intrahippocampal Kainic Acid Model of Temporal Lobe Epilepsy. *eNeuro*, *5*(4). https://doi.org/10.1523/ENEURO.0158-18.2018

Zhang, S. L., Yue, Z., Arnold, D. M., Artiushin, G., & Sehgal, A. (2018). A Circadian Clock in the Blood-Brain Barrier Regulates Xenobiotic Efflux. *Cell*, *173*(1), 130-139.e110. https://doi.org/10.1016/j.cell.2018.02.017

Zhang, T., Yu, F., Xu, H., Chen, M., Chen, X., Guo, L., . . . Wu, B. (2021). Dysregulation of REV-ERBα impairs GABAergic function and promotes epileptic seizures in preclinical models. *Nat Commun*, *12*(1), 1216. https://doi.org/10.1038/s41467-021-21477-w

Zisapel, N. (2007). Sleep and sleep disturbances: biological basis and clinical implications. *Cell Mol Life Sci*, *64*(10), 1174-1186. https://doi.org/10.1007/s00018-007-6529-9

Zisapel, N. (2018). New perspectives on the role of melatonin in human sleep, circadian rhythms and their regulation. *Br J Pharmacol*, *175*(16), 3190-3199. https://doi.org/10.1111/bph.14116